DOT/FAA/TC-13/32

Federal Aviation Administration
William J. Hughes Technical Center
Aviation Research Division
Atlantic City International Airport
New Jersey 08405

Focused Investigation for the Application of Sonic IR NDE Methods for the Detection of Service-Induced Defects on Critical Rotating Components

October 2013

Final Report

This document is available to the U.S. public through the National Technical Information Services (NTIS), Springfield, Virginia 22161.

This document is also available from the Federal Aviation Administration William J. Hughes Technical Center at actlibrary.tc.faa.gov.

U.S. Department of Transportation
Federal Aviation Administration

NOTICE

This document is disseminated under the sponsorship of the U.S. Department of Transportation in the interest of information exchange. The U.S. Government assumes no liability for the contents or use thereof. The U.S. Government does not endorse products or manufacturers. Trade or manufacturers' names appear herein solely because they are considered essential to the objective of this report. The findings and conclusions in this report are those of the author(s) and do not necessarily represent the views of the funding agency. This document does not constitute FAA policy. Consult the FAA sponsoring organization listed on the Technical Documentation page as to its use.

This report is available at the Federal Aviation Administration William J. Hughes Technical Center's Full-Text Technical Reports page: actlibrary.tc.faa.gov in Adobe Acrobat portable document format (PDF).

Technical Report Documentation Page

1. Report No. DOT/FAA/TC-13/32	2. Government Accession No.	3. Recipient's Catalog No.
4. Title and Subtitle FOCUSED INVESTIGATION FOR THE APPLICATION OF SONIC IR NDE METHODS FOR THE DETECTION OF SERVICE-INDUCED DEFECTS ON CRITICAL ROTATING COMPONENTS		5. Report Date October 2013 6. Performing Organization Code
7. Author(s) Forrest Ruhge[1], Ian Doran[1], Shail Derashri[1], Michel D Bode[2]		8. Performing Organization Report No.
9. Performing Organization Name and Address [1]Siemens Energy 4400 Alafaya Trail Orlando, FL 32826 [2]Sandia National Laboratories FAA Airworthiness Assurance NDI Validation Center Airworthiness Assurance Nondestructive 3260 Spirit Dr. SE Albuquerque, NM 87112		10. Work Unit No. (TRAIS) 11. Contract or Grant No.
12. Sponsoring Agency Name and Address U.S. Department of Transportation Federal Aviation Administration New England Region—Aircraft Certification Service Engine and Propeller Directorate FAA New England Regional Office 12 New England Executive Park Burlington, MA 01803		13. Type of Report and Period Covered Final Report 14. Sponsoring Agency Code ANE-110

15. Supplementary Notes

The Federal Aviation Administration William J. Hughes Technical Center Aviation Research Division COR was Cu Nguyen.

16. Abstract

Siemens Power Generation, Inc. (SPG) conducted a 2-year, cost-reimbursable contract to demonstrate to the Federal Aviation Administration (FAA) the applicability of the Siemens Acoustic Thermography (SIEMAT®) nondestructive evaluation (NDE) technology. The SIEMAT is SPG's version of the sonic infrared acoustic thermography inspection technique. SPG teamed up with Delta Air Lines, Inc. and Rolls-Royce plc, both of whom provided commercially relevant engine test parts and data from standard validated NDE parts inspections. Florida Turbine Technologies (FTT) participated on this team as the preferred candidate for the development of commercially available SIEMAT-based equipment and services, as cost-effective improvements to the aircraft industry's existing NDE options.

During this program, FTT performed an evaluation of commercial engines to determine which type of engine disks the program should focus on. Delta and Rolls Royce contributed engine disks and expert opinion from the industry on the inspection technology. This program also investigated the use of cracks in shim stock to act as an artificial defect for the evaluation of the technique capability. Acquired parts were analyzed using finite element modeling and experiments to determine the best fixtures and excitation method. The SIEMAT system was then modified for the parts inspection. New fixtures were made for specific parts, interface materials were developed to protect parts, and defect documentation was added to the software interface. An inspection procedure was developed and a design of experiments parameter optimization was executed for the inspection of disks with the SIEMAT system. Several acquired disks were inspected with the system, which was demonstrated in a double-blind study at the FAA Airworthiness Assurance Nondesdructive Inspection Validation Center at Sandia National Laboratories. Training of industry partners was also provided at this event. A commercialization plan was developed with input from industry partners and is included in this report. This program has demonstrated the capabilities of the SIEMAT system for reliability improvement of NDE applications on commercial aircraft engine disks.

17. Key Words Damage tolerance, Crack growth damage tolerance, Fatigue, Fatigue crack growth, Finite element modeling analysis, Laser-generated crack-like features	18. Distribution Statement This document is available to the U.S. public through the National Technical Information Service (NTIS), Springfield, Virginia 22161. This document is also available from the Federal Aviation Administration William J. Hughes Technical Center at actlibrary.tc.faa.gov.

19. Security Classif. (of this report) Unclassified	20. Security Classif. (of this page) Unclassified	21. No. of Pages 128	22. Price

Form DOT F 1700.7 (8-72) Reproduction of completed page authorized

TABLE OF CONTENTS

EXECUTIVE SUMMARY xiii

1. INTRODUCTION 1

2. BACKGROUND 1

2.1 History and Typical Setup 1
2.2 Interaction of Acoustic Wave With Defects 2
2.3 Initial Test With Engine Disk Component 2

3. SURVEY OF DISKS TO BE INCLUDED IN STUDY 4

4. ARTIFICIAL CRACK DEFECT DEVELOPMENT 7

4.1 Introduction 7
4.2 Defect Fabrication Methods 8
4.3 Defect Attachment Methods 9
4.4 Test Results 11
4.5 Comparison of Artificial Defect Response to Confirmed Cracks 12
4.6 Next Steps 16

5. ACOUSTIC ANALYSIS OF PARTS 18

5.1 Proposed Testing Setup 18
5.2 The FEM Analysis 21
5.3 Experimental Investigation 24
5.4 Summary 30

6. MODIFICATION OF THE SIEMAT SYSTEM 31

6.1 Fixture Development 31
6.2 Evaluation of Interface Materials 33

6.2.1 Introduction 33
6.2.2 Test Setup and Procedure 33
6.2.3 Data Analysis 35
6.2.4 Summary and Conclusions 38

6.3 Automatic Defect Detection 38

7. INSPECTION OF SELECTED DISKS 41

7.1 Inspection Procedure 41

7.1.1 Start-up Process 42
7.1.2 Inspection Process 42
7.1.3 Shutdown Process 43
7.1.4 Horn-Down Process 43

7.2 Optimization of Test System for Disks 43

7.2.1 Amplitude 44
7.2.2 Horn Contact Force 45
7.2.3 Horn/Disk Contact Area 47
7.2.4 Clamping Torque 48
7.2.5 Ambient Temperature 49
7.2.6 Multiple Linear Regression 50

7.3 Testing Results of Selected Disks 52

7.3.1 United States Air Force Disk Inspection 52
7.3.2 Results From Acquired Disk 60

7.4 Demonstration of the SIEMAT System at the Airworthiness Assurance Nondestructive Inspection Validation Center 78

7.4.1 Equipment Setup and Operation 79
7.4.2 Inspections of P&W JT8D Second-Stage Turbine Disks 81
7.4.3 Inspections of HW APU Second-Stage Turbine Disks 87
7.4.4 Inspections of USAF Turbine Disk Anti-Rotation Tangs 92
7.4.5 Inspections of Allied Signal TFE731 Fan Disk 95
7.4.6 Conclusions 95

8. DEVELOPMENT AND COMMERCIALIZATION PLAN 97

9. TRAINING OF INDUSTRY PARTNERS 100

10. CONCLUSION 101

11. REFERENCES 103

APPENDICES

A—Inspection Procedure Flowcharts
B—Horn Contact Angle Test Results
C—Auxiliary Power Unit Disk Inspection Results

LIST OF FIGURES

Figure		Page
1	Experimental Setup for the Inspection of the Cracked Disk Piece	3
2	Pulse Phase Result for the Inspection of the Cracked Disk Piece	3
3	Digital Microscope Images of the Two Indications Observed by Acoustic Thermography	4
4	Number of In-Service Turbine Engines by Engine and Manufacturer	5
5	The CAD Models of Parts Created From Measurements Made at the Delta Repair Facility in Atlanta	6
6	Overhead Chain Hoists Used to Transport Disks and Disk Transport Fixtures	7
7	Resulting Defect Created by the Diagonal Pliers-Initiated Tear Method	8
8	Resulting Defect in 0.006" Fatigue Specimen	9
9	Completed Bar Sample With Attached Shim Stock Samples	10
10	Acoustic Thermography Inspection Setup for the Evaluation of Adhesives	10
11	Pulse Phase Results From Acoustic Thermography Test of Different Adhesives	11
12	Temperature vs. Time Plot for Each Adhesive and Crack Emission	12
13	Thermal Signal From All Defects Just After the One-Second Excitation	14
14	Temperature vs. Time Plot for the Power Strip, Sample Crack, and Fatigue Crack During the Test	15
15	Normalized Temperature vs. Time Plot for the Three Defects Tested	16
16	Experiment 1: Do the Artificial Defects Represent Real Crack Amplitude?	17
17	Experiment 2: Do the Artificial Defects Represent Real Crack Temp vs. Time?	17
18	Experiment 3: First Approximation of How Small of An Indication We Can See	18
19	General Excitation Methods for Cylindrical Aircraft Engine Disks: Radial Excitation and Axial Excitation	19

20	Demonstration of the Variation in the Number of Contact Locations for Radial Excitation	20
21	Demonstration of the Number and Orientation of Constraints That Can be Used in Axial Excitation	20
22	Real Disk Model and Simplified Disk Model	21
23	Excitation and Support Positions for FEM Analysis	22
24	Average Deformation Amplitude as a Function of Axial Excitation Configuration	23
25	Average Deformation Amplitude as a Function of Radial Excitation Configuration	24
26	Inspection Setup for the Radial Inspection Methods	25
27	Inspection Setup for the Axial Inspection Methods	26
28	Results of the Excitation Method and Setup Experiments	27
29	Average Pixel Values From the Brightest Frame in the Video Sequence That Fall Within the Orange ROI	28
30	Nonuniformity of the Surface Excitation of the JTS Disk Excited by the Automatic Adjustment Frequency Method Using the Radial Excitation Setup	29
31	Radial Signal as a Function of ROI Arranged From Disk OD to ID	30
32	Lathe Chuck Fixture for Horizontal Excitation Setup Used to Inspect Aero Turbine Disks	32
33	Fixture for Axial Disk Excitation Setup Used to Inspect Aero Turbine Disks	33
34	Test Setup Used for Interface Material Testing	34
35	Example of Photo Documentation of Interface Material Before and After Excitation	35
36	Excitation Energy at Failure for Various Interface Materials	36
37	Energy Levels for Which Failure Occurs for Each Material	37
38	Pulse-Phase Result From Which Inspectors Make Interpretations of the Indication Types and Relevancy	39
39	Steps Necessary for the Training of the Classifiers	40

40	Updated Version of SInE^2 Showing the Ability to Digitally Document Indications	41
41	Power Strip Used to Optimize the Acoustic Thermography System	44
42	Scatter Plot of Power Strip Signal Strength vs. Amplitude	45
43	Schematic of the Horn Assembly	46
44	Scatter Plot of Power Strip Signal vs. Horn Contact Force	47
45	Setup Used to Determine the Horn Contact Area	48
46	Scatter Plot of Power Strip Signal vs. Contact Area	48
47	Scatter Plot of Power Strip Signal vs. Clamping Torque	49
48	Scatter Plot of Power Strip Signal vs. Ambient Temperature	50
49	Overview of Acoustic Thermography Testing Setup for the Inspection of the USAF Disks	53
50	Detailed View of the Acoustic Thermography Test Setup Showing How the Fixture, Part, and Actuator Are Oriented	54
51	Setup for the Digital Microscope Verification of Marked Indications	54
52	Indication 1b on Disk AF1 Observed by Digital Microscopy	55
53	Indication 1b on Disk AF2 Observed by Digital Microscopy	55
54	Indication #2 on Disk AF3 Observed by Acoustic Thermography and Digital Microscopy	56
55	Indication #4 on Disk AF3 Observed by Digital Microscopy	56
56	Indication #5 on Disk AF3 Observed by Digital Microscopy	57
57	Disk AF4 Anti-Rotation Indication	57
58	Indication #1 on Disk AF4 Observed by Digital Microscopy	58
59	Indication #4 on Disk AF4 Observed by Digital Microscopy	58
60	Indication #13 on Disk AF4 Observed by Digital Microscopy	59

61 The USAF Disk AF4 Indication on Blade Attachment Point 59

62 Acoustic Thermography Performed With the Camera Placed at an Oblique Angle to the Disk and Placed Above the Disk Using a Mirror to See the Edge of the Disk 61

63 Use of the Mirror in the Horizontal Mount Setup for Viewing the Edge and Top of the Disk at the Same Time 61

64 Top and Bottom of the Solid Head Disk Provided by Rolls-Royce 62

65 Locations of Observed Indications in Zones 23 and 24 on the Rolls-Royce Solid Head Disk 63

66 Locations of Observed Indications in Zones 1 and 2 on the Rolls-Royce Solid Head Disk 64

67 Thirteen Indications Observed by FPI at Siemens 65

68 Types of Indications Observed on the Solid Head Disk 65

69 The P&W Second Stage Compressor Disk 67

70 Representative Acoustic Thermography Results for the P&W Second Stage Compressor Disk 67

71 The P&W Eighth Stage Compressor Disk 68

72 Representative Acoustic Thermography Results for the P&W Eighth Stage Compressor Disk 68

73 The FPI Observation of a Linear Indication and Indication as Observed Under White Light Illumination 69

74 The P&W Seventh Stage Compressor Disk 70

75 Linear Indication on BENCAL3598 at the 2:00 Position on Side A 70

76 Linear Indication on BENCAL3598 at the 10:30 Position on Side A Propagated From Initial Indication in Impact Location 71

77 Pieces of the Disk SN: BENCAL3598 That Fell off Because of Crack Propagation: Fit; Fracture Surface 71

78 The FPI Indication and Subsequent Visual Indication 72

79	The P&W Eleventh Stage Compressor Disk	72
80	Representative Acoustic Thermography Results for Disk SN: BENCAN4671	73
81	The FPI Indication Related to a Surface Scratch	73
82	The P&W Tenth Stage Compressor Disk	73
83	Representative Acoustic Thermography Results for Disk SN: BENCAR6446	74
84	The P&W Seventh Stage Compressor Disk	74
85	The FPI Indication and Microscope Verification Image for the First Indication Observed on Disk SN: BENCAR9734	75
86	First Acoustic Thermography Indication Observed on Disk SN: BENCAR9734	75
87	Second Indication Observed by FPI and the Corresponding Microscope Observation	75
88	The P&W First Stage Compressor Fan Disk	76
89	Representative Acoustic Thermography Results for Disk SN: M8320	76
90	The P&W Seventh Stage Compressor Fan Disk Stage Compressor Disk	77
91	Representative Acoustic Thermography Results for Disk SN: T04834	77
92	Modified Horn for Radial Excitation and SIEMAT System Configuration for Inspecting JT8D Disks	80
93	Loading Device and Apparatus Used to Grow Cracks in P&W JT8D Second-Stage Turbine Disks	81
94	Natural Discontinuity on Disk BLDLA34987 Tang 54 Slot 1 Viewed During FPI From the Top Side	82
95	Natural Discontinuity on Disk BLDLA34341 Tang 47 Slot 1 Viewed During FPI From the Top Side	82
96	Engineered Discontinuity on Disk BLDLA34598 Tang 5 Slot 1 Viewed During FPI From the Top Side in the Leading and Trailing Directions	83
97	A POD Curve for SIEMAT Inspection of P&W JT8D Second-Stage Turbine Disks for Grown Cracks in Fir Tree Slots	85

98 Example of a Large Crack and Its Measurement in an HW APU Fir Tree Slot After Etch Taken With 50x Optical Microscope 89

99 Crack Length Distribution for HW APU Disks as Determined by Etching and 50x Optimal Microscopy 89

100 The POD Curve for SIEMAT Acoustic Thermography Detection of Cracks in Fir Tree Slots of HW APU Disks on Front Side Only 90

101 The SIEMAT IR Image for a Screening Inspection of an Entire Disk 91

102 Anti-Rotation Tang and Associated SIEMAT Acoustic Thermography Inspection 93

103 An HW TFE731 Titanium Engine Fan Disk With Cracks That Propagated During Extreme Ultrasonic Excitation and the SIEMAT IR Inspection Image 95

LIST OF TABLES

1	General Information and Dimensions Collected From Parts at the Delta Repair Facility	6
2	Adhesive That Was Used to Attach Shim Stock Sample to Each Bar Sample	9
3	Acoustic Thermography Parameters for the Adhesive Study	11
4	Test Parameters Used to Compare Artificial Defect to a Crack Created by Three-Point Bending in a Titanium Bar	13
5	Test Parameters for Testing of the Different Excitation Methods	27
6	Reasons for Discrepancy Between FEM Results and Experimental Results	31
7	Place Number Assigned to Each Material in the Excitation Energy and Power Strip Signal Analysis and the Overall Score and Preference Place of Each Material	38
8	Multiple Linear Regression Results	51
9	Summary of Acoustic Thermography Results for USAF Disks	60
10	Type of Indication Observed by Digital Microscopy for Each Observed Penetrant Indication	66
11	Summary of the Observed Indications and Methods by Which They Were Detected	78
12	Discontinuity Characterization for Three P&W JT8D Second-Stage Turbine Disks	84
13	SIEMAT Inspection Results Sorted by Hit/Miss Value, Then FPI Size of Leading and Top Discontinuities	86
14	False Call Data for SIEMAT Inspections of P&W JT8D Second-Stage Turbine Disks—Also Showing Examples of Natural and Engineered Crack Locations	87
15	False Call Rates on the Back Side of HW APU Disks	91
16	Crack Truth Data for Screening Inspection of an Entire Disk	92
17	The SIEMAT Acoustic Thermography Inspection Results Showing Hits, Misses, and False Calls on USAF Nickel-Based Turbine Disk Anti-Rotation Tangs	94

LIST OF ABBREVIATIONS, SYMBOLS, AND ACRONYMS

MIL HDBK	Military Handbook
SIEMAT®	Siemens acoustic thermography
2D	Two-dimensional
3D	Three-dimensional
AANC	Airworthiness Assurance Nondestructive Inspection Validation Center
APU	Auxiliary power unit
CAD	Computer-aided design
CCA	Catalyzed Cyanoacrylate
EDM	Electrical discharge machining
FAA	Federal Aviation Administration
FEM	Finite element modeling
FPI	Fluorescent penetrant inspection
HW	Honeywell
ID	Inner diameter
IR	Infrared
MCP	Moisture-cured polyurethane
NDE	Nondestructive evaluation
NDI	Nondestructive inspection
NDT	Nondestructive testing
OD	Outer diameter
P&W	Pratt & Whitney
POD	Probability of detection
ROI	Region of interest
SPG	Siemens Power Generation, Inc.
USAF	United States Air Force

EXECUTIVE SUMMARY

Siemens Power Generation, Inc. (SPG) conducted a 2-year, cost-reimbursable contract to demonstrate to the Federal Aviation Administration (FAA) the applicability of the Siemens acoustic thermography (SIEMAT®) nondestructive evaluation (NDE) technology. The SIEMAT is SPG's version of the sonic infrared acoustic thermography inspection technique. The SPG will team with Delta Air Lines, Inc. and Rolls-Royce plc, who will provide commercially relevant engine test parts, data from standard validated NDE inspections of the parts, and information and guidance needed on the aircraft industry's requirements to fully validate SIEMAT as a commercial NDE process. Delta Air Lines, Inc. and Rolls-Royce plc will provide feedback in the development of a Product Requirement Specification for scoping and planning subsequent development and validation of SIEMAT for NDE processes on commercial aircraft engine parts. Florida Turbine Technologies (FTT) will participate in this team as the preferred candidate for development of commercially available SIEMAT-based equipment and services as cost-effective improvements to the aircraft industry's existing NDE options.

The results of the proposed work will provide a plan to commercialize sonic infrared (IR) NDE technology that could help achieve significant solutions towards the challenges identified in the FAA 5-year plan. The objectives of the project in the first year are to: (1) select five to ten turbine disks of a high priority engine model and perform laboratory tests using SIEMAT excitation methods, fixtures, and inspection procedures optimized for these selected parts; (2) compare the results with data from existing, validated NDE inspections to assess the readiness of SIEMAT technology; and (3) develop an implementation and technology transfer plan for use in a production environment. This plan will provide a complete roadmap to the steps to be taken to implement sonic IR in the aviation industry and to update the development objectives for the second year.

This project's second-year objectives are to: (1) investigate the use of advanced image-processing algorithms for automated defect detection; (2) train industry partner's NDE personnel in the use of the SIEMAT system; (3) assess the capability of the SIEMAT system developed for the inspection of aircraft engine disks based on a large set of actual service exposed turbine discs; and (4) update the implementation and technology transfer plans.

The potential impact of the project is the demonstration of the capabilities of the SIEMAT system for reliability improvement of NDE applications on commercial aircraft engine disks, by improved probability of detection compared with existing NDE methods. Also, the validation and commercialization of acoustic thermography as a substitute for dye penetrant methods will lead to meeting the aircraft industry's strategic objectives of reducing impact on the environment by eliminating the need to dispose of consumable materials. The transfer of technology from the power generation industry will provide additional commercial options for the aircraft industry and will expand the service offerings of SPG and FTT.

1. INTRODUCTION.

The process of acoustic thermography is a unique nondestructive evaluation (NDE) technique for the detection of cracks, kissing bonds, and delaminations in parts. This very new technology has several unique attributes that augment the historic NDE practices:

- The ability to excite a component that has low acoustic damping from any location and to detect flaws anywhere that can be viewed by the infrared (IR) camera.
- High sensitivity to tight defect interfaces typical of service-propagated cracks and disbonds.
- The ability to detect defects through coatings and on internal surfaces for thin wall components.
- The fast and highly intuitive two-dimensional (2D) or three-dimensional (3D) result that is computer-aided design (CAD) linkable and plays an important role in bridging the NDE/Engineering gap.
- The ability to inspect components with minimal preparation; no acid etching, no special cleaning, no coating removal.

Acoustic thermography is a nondestructive testing (NDT) technique by which a part under examination is exposed to ultrasonic energy to induce heating of crack facets as the part moves in response to the ultrasonic stimulus. For acoustic thermography to be a viable NDE technique, two crack facets must be in contact and generate heat when subjected to acoustic excitation. This basic operating principle may cause acoustic thermography to return a smaller-than-expected signal for large open cracks. This is because thermal energy is generated only at interacting crack facets. While larger, wide-open cracks have a larger internal surface area, not all of it interacts. This is why a visual inspection of the part is often recommended in conjunction with the acoustic thermography inspection for the detection of large cracks. With historical NDE practices, the probability of detection (POD) of small, tight cracks is low.

2. BACKGROUND.

2.1 HISTORY AND TYPICAL SETUP.

Siemens acoustic thermography (SIEMAT®) is a further development of the vibro-thermography technique [1]. This NDE method was designed to find and localize surface and subsurface cracks by means of energizing the part under test with high-power ultrasonic energy. Typically, systems based on ultrasonic welding systems (20 kHz @ 3 kW) are used with a standard booster/horn combination to contact the part.

A step change improvement in IR cameras (i.e., high frame rate and high thermal sensitivity) boosted the technique from the early stages in the 1970s to the applicable NDE technique of the current day. High-power ultrasonic welders are available, which further eased the building of systems. A typical acoustic thermography setup consists of an ultrasonic excitation source

(usually a high frequency, 20 kHz or greater amplifier and piezoelectric crystal) and an IR camera. Today's systems also incorporate computer control and postprocessing functions.

Since the damping of 20 kHz acoustic waves is very low in metals, the wave may penetrate the entire part at the speed of sound (typically in the order of km/s). Therefore, the technique is also suitable for large parts or parts with complex geometries. The whole test cycle typically takes only seconds.

2.2 INTERACTION OF ACOUSTIC WAVE WITH DEFECTS.

If the part under test contains defects with separated faces like cracks or delaminations, the acoustic wave leads to a local differential movement of these faces. If the separation is not larger than the displacement amplitude, this movement results in heat generation. Intensive studies were carried out to understand the mechanism of heat generation in a greater depth to allow for an optimization of the technique ([2-5]). Independent of the exact mechanism, it is clear that wide-open cracks may only be detected close to the tip where the separation of the faces is small enough to allow them to touch. This is not a principal issue in the determination of crack length because the length of a crack is obviously determined by its tips. If a portion of the crack in the middle does not show up, it can easily be interpolated. Other separated areas may also produce heat (e.g., intermittent welds or delaminations).

2.3 INITIAL TEST WITH ENGINE DISK COMPONENT.

While Siemens has a good background in applying acoustic thermography to gas turbine components like blades and veins, there has been comparatively little research done on aircraft critical rotation components, such as disks. To determine the capability of acoustic thermography, Rolls-Royce provided a test piece having a crack in it for some initial acoustic thermography testing. This test piece was cut from a full disk. Figure 1 shows the experimental setup for the inspection of the test piece. The IR camera is positioned so as to inspect inside the slot of the piece.

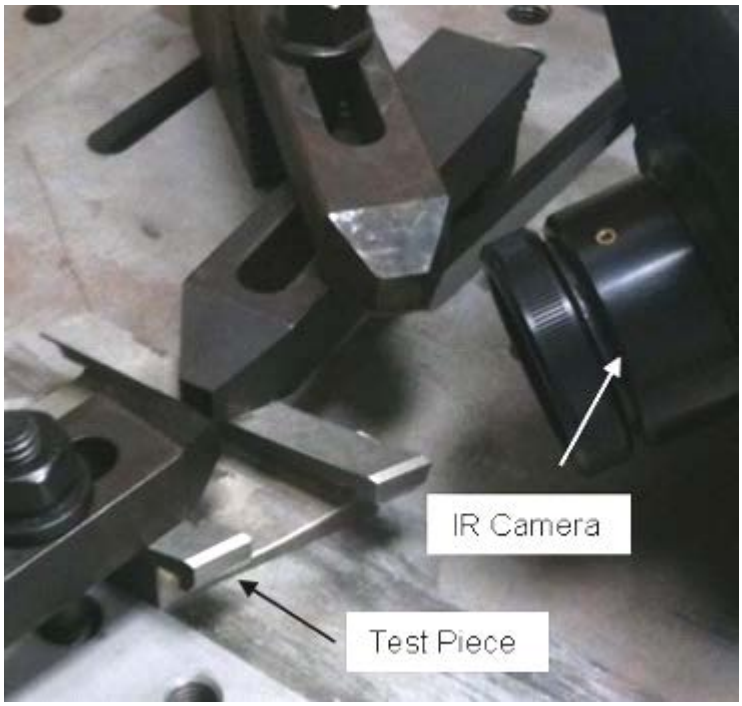

Figure 1. Experimental Setup for the Inspection of the Cracked Disk Piece

The acoustic thermography pulse phase result is displayed in figure 2 where two indications are shown. The indications were further investigated with the use of a digital microscope. A 3D representation of each indication was measured and is shown in figure 3. Because crack-like indications are clearly visible in the digital microscope images taken in the regions where the acoustic thermography indications were observed, it can be deduced that acoustic thermography may provide a viable method for the inspection of aircraft engine disks. This study further explores the use of acoustic thermography for the inspection of aircraft engine disks.

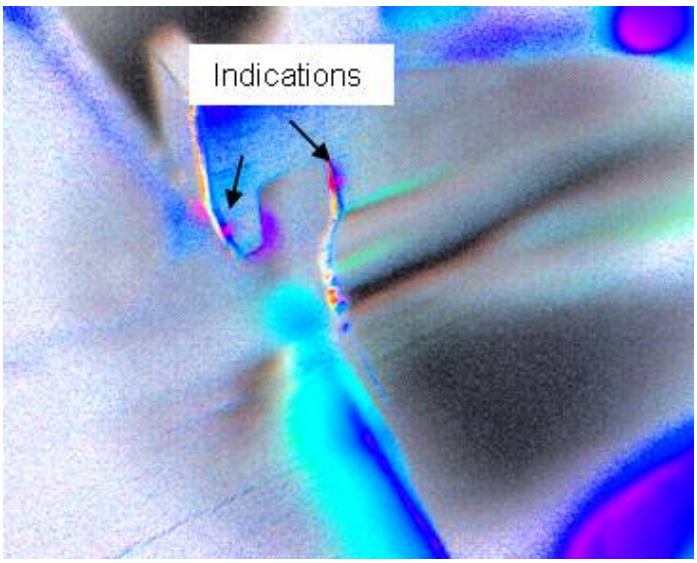

Figure 2. Pulse Phase Result for the Inspection of the Cracked Disk Piece

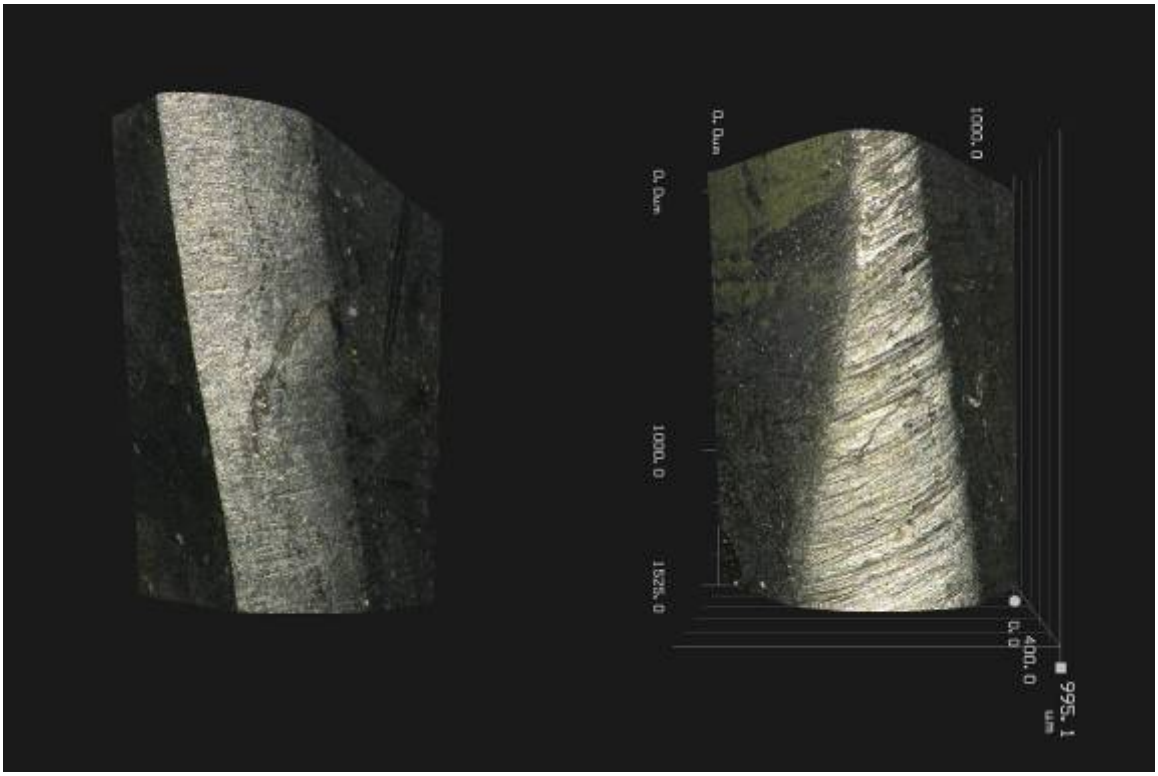

Figure 3. Digital Microscope Images of the Two Indications Observed by Acoustic Thermography

3. SURVEY OF DISKS TO BE INCLUDED IN STUDY.

An assessment of the variation in aircraft disks was completed to determine which disk geometries the acoustic thermography fixturing would need to accommodate. This assessment is expected to identify the most common disks that are in service and may be inspected by the acoustic thermography system. A summary of this information, collected from the engine industry, is shown in figure 4 for three major engine manufacturers.

Figure 4 shows that the Pratt and Whitney (P&W) JT8D engine is currently the most widely used engine, with approximately 14,000 engines in service. This is followed by the General Electric CFM 56, with 10,000 engines in service. Therefore, it was determined that disks from these two engines be acquired if possible and the acoustic thermography system be designed to inspect components from these engines.

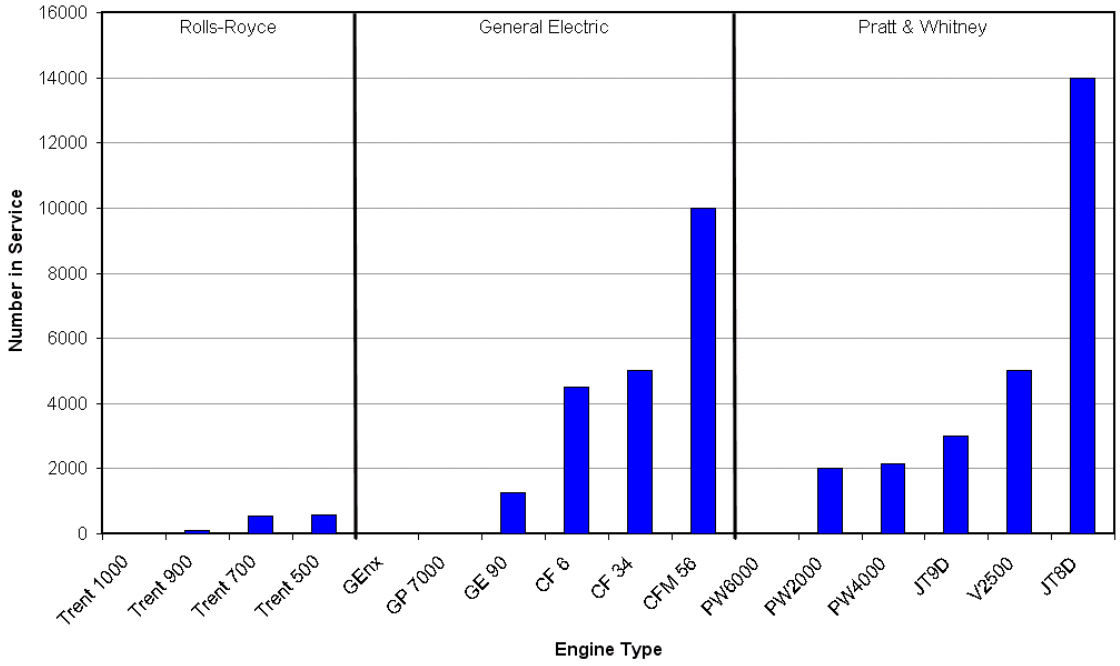

Figure 4. Number of In-Service Turbine Engines by Engine and Manufacturer

To gather more data on the size, weight, and geometry of disks from these engines, the manufacturers were contacted. This program was not successful at obtaining information about the disks from the manufacturers. Therefore, it was determined that a trip needed to be made to the Delta Inspection and Repair Facility in Atlanta, Georgia to measure applicable dimensions of several disks for the design of acoustic thermography fixtures and finite element modeling (FEM) analysis. This visit resulted in the generation of four CAD models of parts (figure 5), and a table of general information about parts that can be referred to when designing the breadboard acoustic thermography system for the inspection of aircraft engine disks (table 1).

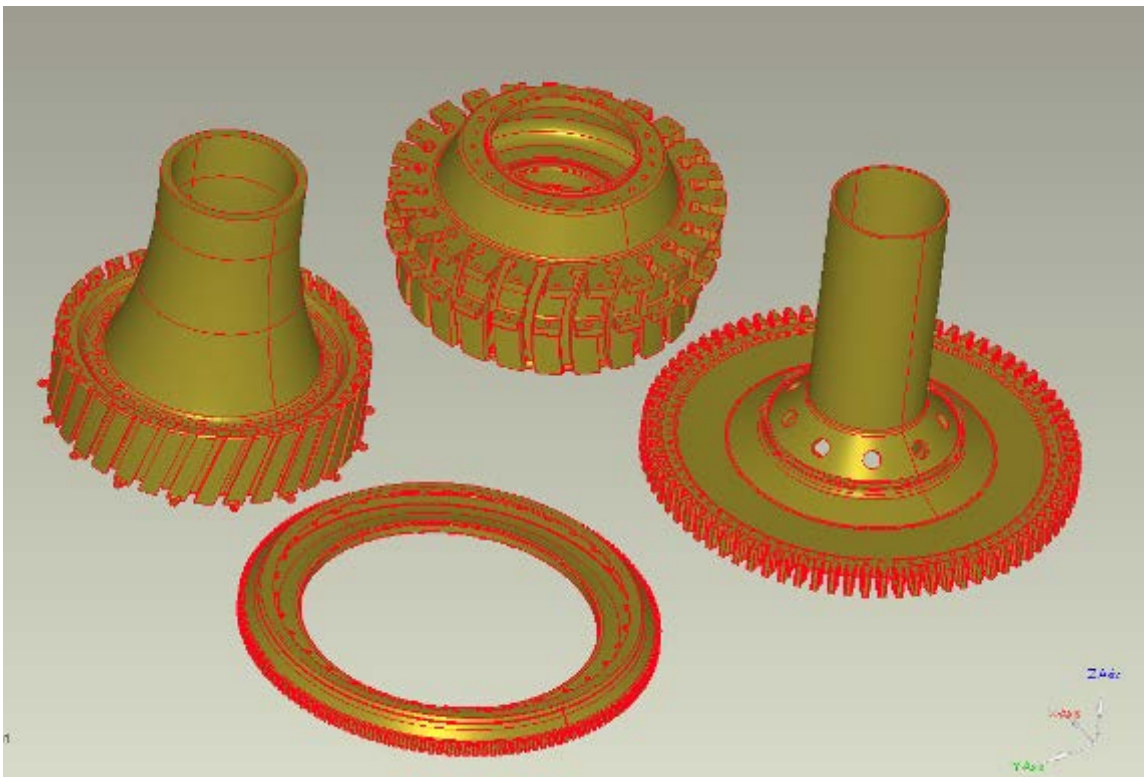

Figure 5. The CAD Models of Parts Created From Measurements Made at the Delta Repair Facility in Atlanta

Table 1. General Information and Dimensions Collected From Parts at the Delta Repair Facility

OEM	Engine Type	Disk Type	Disk #	OD (in.)	ID (in.)	Height (in.)	No. of Serrations	Material	Weight (lb)
Pratt & Whitney	JT8D	LPC	3	19	10	18	34	Ti	246
General Electric	CFM 56	Fan	1	20	6	11	24		
Pratt & Whitney	PW2037	HPT	19	21	7	8	64		
General Electric	CFM 56	LPC	4	25	17	3	148	IN-718	37
General Electric	CF 6	HPT	20	26	7	21	80	IN-718	

OEM = original equipment manufacturer, OD = outer diameter, ID = inner diameter

A large variation in disk size and shape was observed during a visit to the Delta Inspection and Repair Facility. This large variation in weight, size, and shape makes it unclear that the technology could be easily applied to all disks. It is imperative that each new disk part number be evaluated individually and approved for acoustic thermography inspection.

The current penetrant inspection process at the Delta Air Lines facility uses overhead chain hoists on tracks for the transport of the disks throughout the facility (figure 6, left). These hoists have disk transport fixtures attached to them that are designed to make the disk easier to inspect while protecting the disk. The two main types of fixtures used are shown in the center and right images of figure 6. Both of these fixtures hold the disks by their inner diameters (IDs).

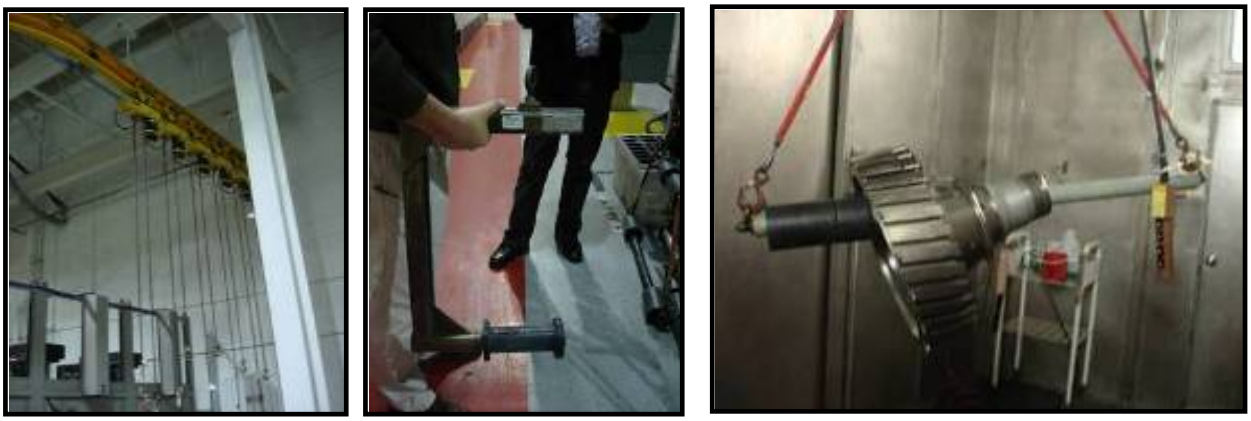

(a) (b) (c)

Figure 6. Overhead Chain Hoists Used to Transport Disks (a) and Disk Transport Fixtures (b and c)

When designing a fixture system for acoustic thermography, it is important to keep the number of part-specific fixtures to a minimum to reduce retooling time and to ensure that the method of holding the part does not restrict the vibratory motion needed for the acoustic thermography technique to work. Common features on all parts are looked for to keep the number of part-specific features to a minimum. For the disks observed at the Delta Air Lines repair facility, common features include an ID ranging in size from 6 in. to 17 in. and an outer diameter (OD) ranging in size from 19 in. to 26 in. From a vibratory standpoint, a fixture at the ID will allow the part to move more easily at the OD, where the inspection is more critical.

4. ARTIFICIAL CRACK DEFECT DEVELOPMENT.

4.1 INTRODUCTION.

Acoustic thermography is a developing NDT technique that exploits the thermal response of cracklike discontinuities when subjected to an ultrasonic stimulus. To date, there has been no cost-effective calibration defect that can be used to assess the proper acoustic thermography testing parameters for the inspection of various parts.

Currently, part-testing parameters are determined using either adhesive strips applied onto parts or service cracks in parts. Adhesive strips serve as poor calibration defects because they do not reproduce cracklike signals. Defects (service cracks) on service parts are challenging to obtain because safety standards require parts to be rejected long before cracks develop in many critical components. Furthermore, it is known that the sensitivity of acoustic thermography varies across the part. Locations that are thinner are more easily excited by the method. The ability to detect

defects is higher in these locations on the part than in more rigid ones. This makes it important to find parts with defects in the specific regions of interest set forth by engineering.

This chapter outlines the steps taken during this program toward the development of a cost-effective and versatile calibration defect for use in the acoustic thermography parameter selection process. The ideal calibration defect should display cracklike thermal signatures superior to those of adhesive strips. The ideal calibration defects should be applied to any location on any part, eliminating the need to find appropriate in-service parts with indications in regions of interest for the determination of detection capability. These defects are expected to provide a reliable assessment of the parameters under which acoustic thermography can detect a given crack in the region of the calibration defect.

The goal of this investigation was to develop samples with defects that could be attached to the part and would reproduce the signal observed by an actual indication in the part. Before this method of using defective samples can be accepted as an adequate one for determining the capability of acoustic thermography on a part, several questions need to be addressed, including: (1) What is the best attachment method? (2) Is the thermal (temperature vs. time) signature of the generated artificial defects similar to those of service-produced defects? and (3) Does the amplitude of the IR signal from the artificial defect represent that of an actual crack for a given excitation?

4.2 DEFECT FABRICATION METHODS.

It is hypothesized that an ideal artificial defect sample could be created out of a 0.006-inch-thick piece of steel shim stock. During this program, two approaches were used to create defects in the shim stock. In both cases, the shim stock was cut to half-inch square samples.

The first method used diagonal pliers to tear the side of the shim stock square, creating a pre-flaw from which a defect could be propagated by tearing the shim stock as one would a piece of paper. The shim stock was then flattened so that the facets of the tear would be contacting each other. This method is referred to as the diagonal pliers-initiated tear method. An example defect created by this method is shown in figure 7.

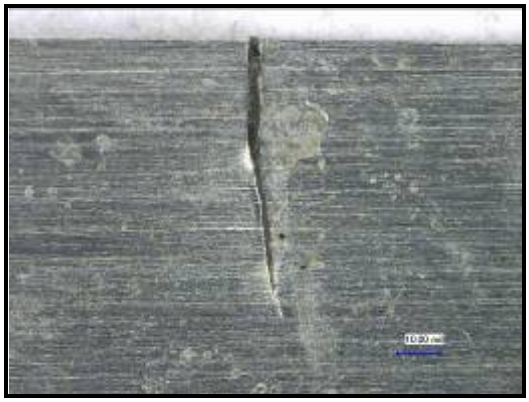

Figure 7. Resulting Defect Created by the Diagonal Pliers-Initiated Tear Method

The second method investigated was the electrical discharge machining (EDM) notch-fatiguing method. During this method, a 0.003-inch-deep by 0.005-inch-wide by 0.010-inch-long notch is machined into a tensile test specimen of 0.006-inch-thick steel shim stock. This sample is then fatigue-tested in a tensile test machine to propagate cracks from the EDM notch pre-flaws. The resulting defect is shown in figure 8. By varying the applied load and number of cycles in the fatigue-testing machine, different sizes of defects can be created. The fatigue specimens are cut into half-inch-square defect specimens to produce the final artificial defect samples.

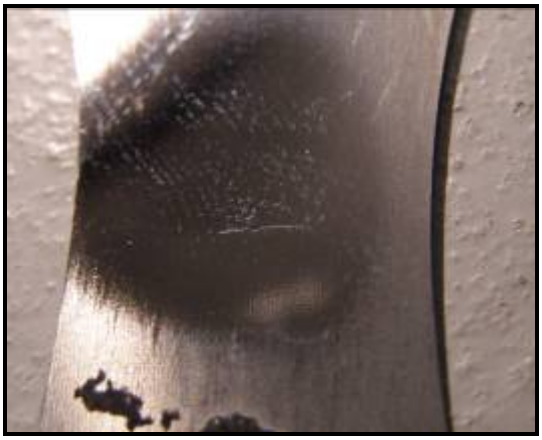

Figure 8. Resulting Defect in 0.006" Fatigue Specimen

4.3 DEFECT ATTACHMENT METHODS.

Once defects had been created, several adhesives were investigated for the attachment of the defect to parts. The ideal attachment method would not emit very much thermal radiation in response to acoustic excitation. During this investigation, six different adhesives were used to attach half-inch-square, 0.006-inch-thick shim stock to bar samples representing the actual part to be evaluated. These samples were provided by the NDI Testing and Validation Center at Sandia National Laboratories. Each 6-inch by 1-inch by 0.25-inch titanium bar sample had a small crack in it created by fatiguing the bar in 3-point bending. Table 2 shows the adhesives used to attach the shim stock samples to each bar sample and the size of the indication in the bar stock samples. The adhesives were then evaluated during an acoustic thermography test on how much thermal energy they emitted relative to the indication in the bar sample.

Table 2. Adhesive That Was Used to Attach Shim Stock Sample to Each Bar Sample

Adhesive	Bar Sample ID	Crack Length
Polyurethane construction adhesive (P)	00-069	0.154
Silicone adhesive (Si)		
Spray adhesive (SA)	01-013	0.082
Catalyzed cyanoacrylate (CCA)		
Moisture-cured polyurethane (MCP)	01-016	0.052
Epoxy (E)		

The bond locations on the bar samples and shim stock samples were cleaned with acetone before application of the adhesive. Each adhesive was applied according to the manufacturer's instructions. The samples were clamped to the bar samples during the cure period. Wax paper was used between the clamp and the shim stock samples to keep excess adhesive from attaching to the clamp. A completed bar sample with attached shim stock is shown in Figure 9.

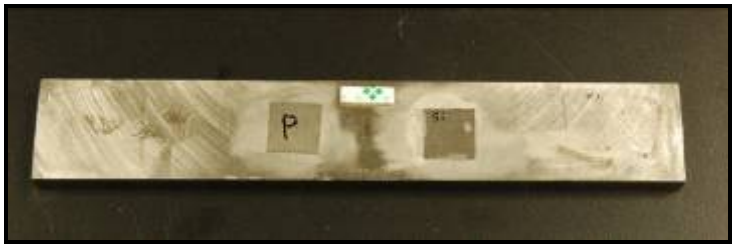

Figure 9. Completed Bar Sample With Attached Shim Stock Samples

The acoustic thermography inspection system was set up as shown in figure 10. In this setup, the bar sample is toe-clamped to a table that has a hole in it below the sample. During the test, the ultrasonic horn comes up through the hole in the table and contacts the bar sample to couple the ultrasonic energy into it. An isolation material between the bar sample and the toe clamps keeps the ultrasonic energy contained within the bar sample. The IR camera is positioned above the bar sample so that the samples on the bar sample are within its field of view, but the horn contact location and clamping locations are not.

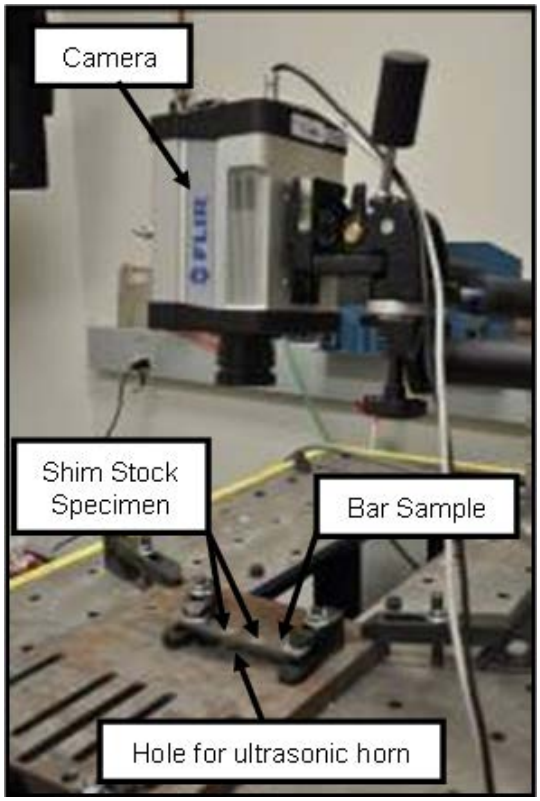

Figure 10. Acoustic Thermography Inspection Setup for the Evaluation of Adhesives

The system was set up using the parameters specified in table 3. These parameters were used based on previous experience exciting similar parts in similar configurations at Siemens.

Table 3. Acoustic Thermography Parameters for the Adhesive Study

Parameter	Setting
Excitation Time	1 second
Excitation Method	Standard Acoustic Thermography
Excitation Amplitude	90%
Excitation Frequency	Auto adjust around 20,000 Hz
Horn Pressure	30 psi
IR Camera	SC6000 InSb
Frame Rate	80 fps
Recording Time	2 seconds

4.4 TEST RESULTS.

All attachment methods were tested using acoustic thermography under similar conditions. Samples attached using moisture-cured polyurethane (MCP) broke free after three excitations while samples attached with epoxy (E) and catalyzed cyanoacrylate (CCA) all broke free on the first test. Therefore, there are no temperature vs. time data for E and CCA. It is hypothesized that, because these adhesives are stronger and more brittle, they transfer more energy to the shim stock sample, causing it to move more and to more easily break the adhesive bond. Figure 11 shows the pulse-phase result of the acoustic thermography test for each adhesive.

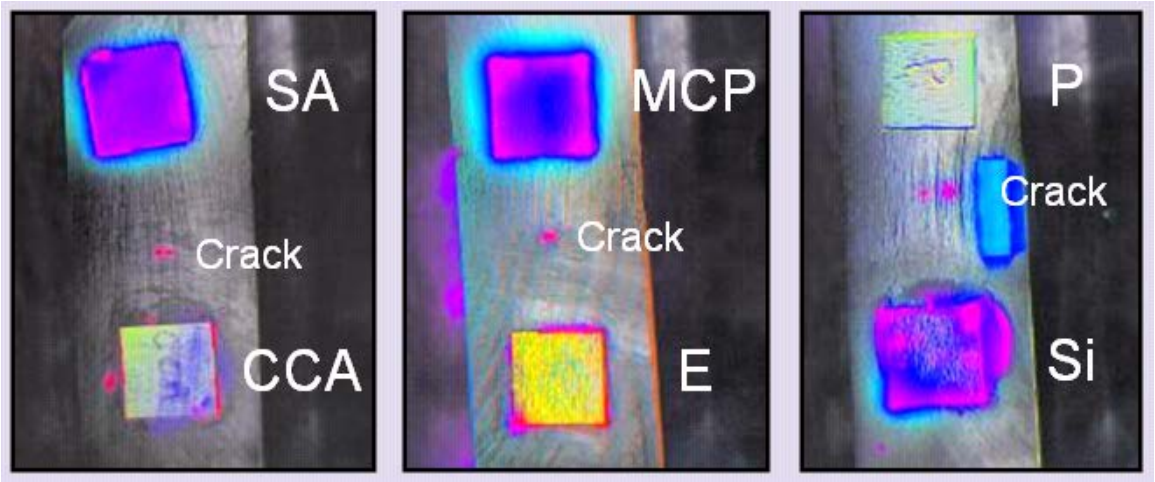

Figure 11. Pulse-Phase Results From Acoustic Thermography Test of Different Adhesives

From the pulse-phase resulting images in figure 11, it can be observed that the MCP and the spray adhesive generated the most thermal energy and would not be a good choice for an artificial defect adhesive. Silicone adhesive generated a moderate amount of thermal energy,

which was more than the amount of thermal energy generated by the crack in the bar sample substrate. The adhesive that generated the least amount of thermal energy during the test without breaking free was polyurethane construction adhesive. Polyurethane construction adhesive showed the least response after attaching multiple samples to different bars and testing multiple times.

Temperatures versus time plots for each thermal feature during the acoustic thermography test are shown in figure 12. It is clear from these plots that the only adhesive that generated less thermal energy than the cracks in the substrate bars was the polyurethane construction adhesive with a maximum thermal signal of 7 arbitrary units. The smallest crack signal observed was from the 0.082-inch-long crack and was 19 arbitrary units. This is almost three times the thermal emission of the polyurethane construction adhesive.

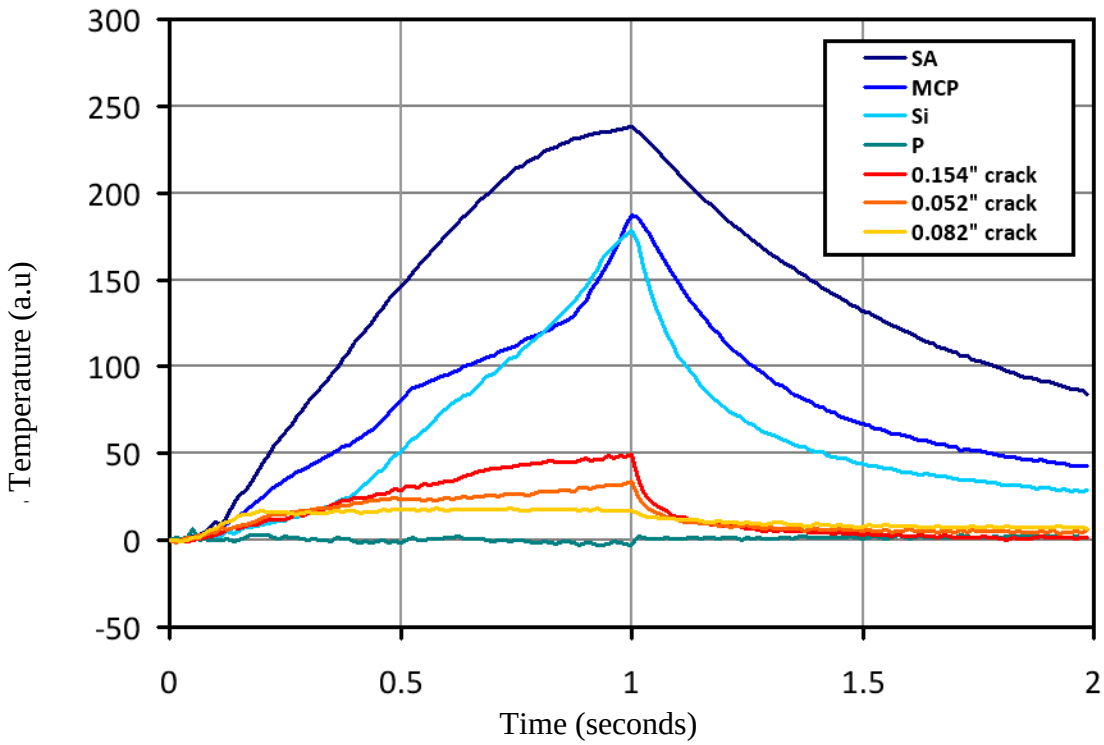

Figure 12. Temperature vs. Time Plot for Each Adhesive and Crack Emission

4.5 COMPARISON OF ARTIFICIAL DEFECT RESPONSE TO CONFIRMED CRACKS.

An artificial crack sample created by the diagonal pliers-initiated tear method was attached to the titanium bar sample 00-069, having a 0.154-inch-long indication in it. This sample was tested using the same acoustic thermography setup as in the previous testing of adhesive samples (figure 10). The excitation and recording parameters used to test this sample are shown in table 4.

Table 4. Test Parameters Used to Compare Artificial Defect to a Crack Created by Three-Point Bending in a Titanium Bar

Parameter	Setting
Excitation Time	1 second
Excitation Method	Standard Acoustic Thermography
Excitation Amplitude	90%
Excitation Frequency	Auto adjust around 20,000Hz
Horn Pressure	30psi
IR Camera	SC6000 InSb
Frame Rate	80 fps
Recording Time	4 seconds

During this test, a 1-second excitation time is combined with a 4-second recording time to better map the thermal decay of the power strip during and after the test.

The qualitative results of this test can be seen in figure 13. The fatigue crack produced in three-point bending is indicated in red. The artificial defect is indicated in orange and the power strip in green. It can be observed that, while the artificial defect looks more like a crack than the power strip does, it is much larger and brighter. It is difficult to cause a small defect using the diagonal pliers-initiated tear method. The ability to make reproducible defects with this method is questionable.

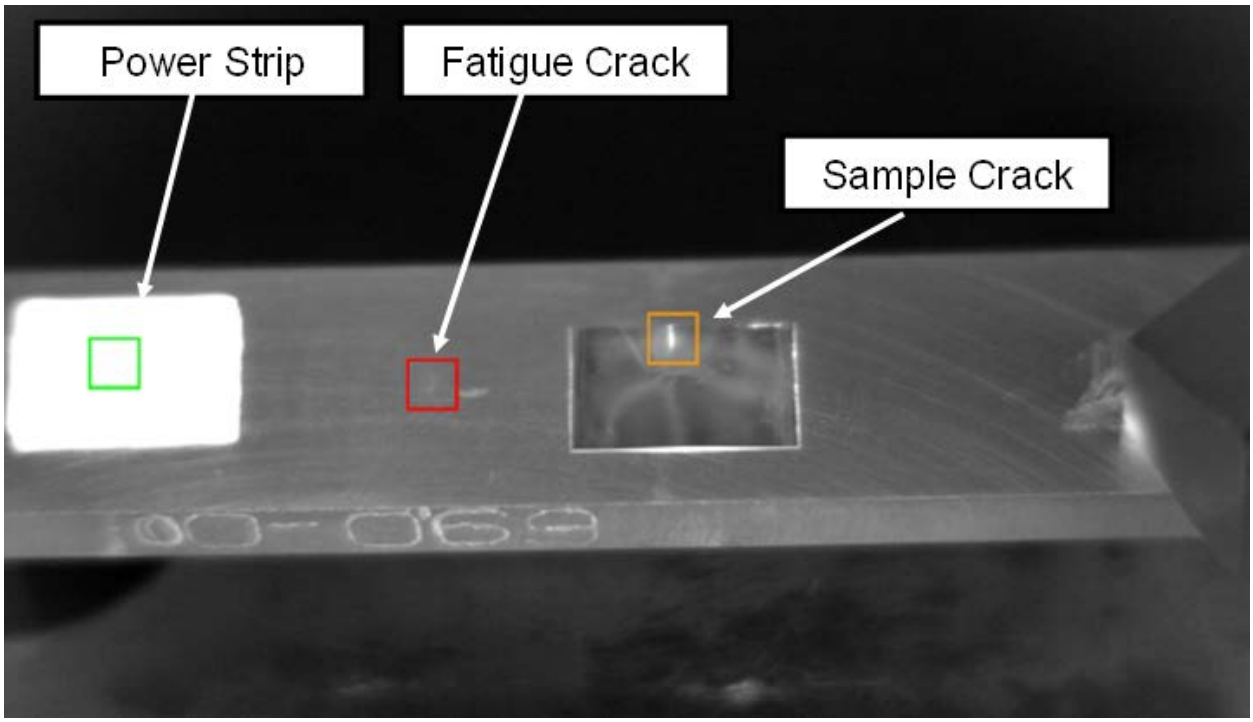

Figure 13. Thermal Signal From All Defects Just After the One-Second Excitation

These observations are confirmed when looking at the temperature-versus-time plots for the regions enclosed in the red, green, and orange squares of figure 13. The corresponding temperature-versus-time plots is shown in figure 14. Here, the difference in amplitude for the three calibration defects can be easily observed. Also, the difference in thermal profile between the power strip and the sample artificial defect is apparent. The power strip heats up more quickly and continues to heat after the end of the 1-second excitation. The power strip also dissipates the thermal energy more slowly than the sample artificial defect.

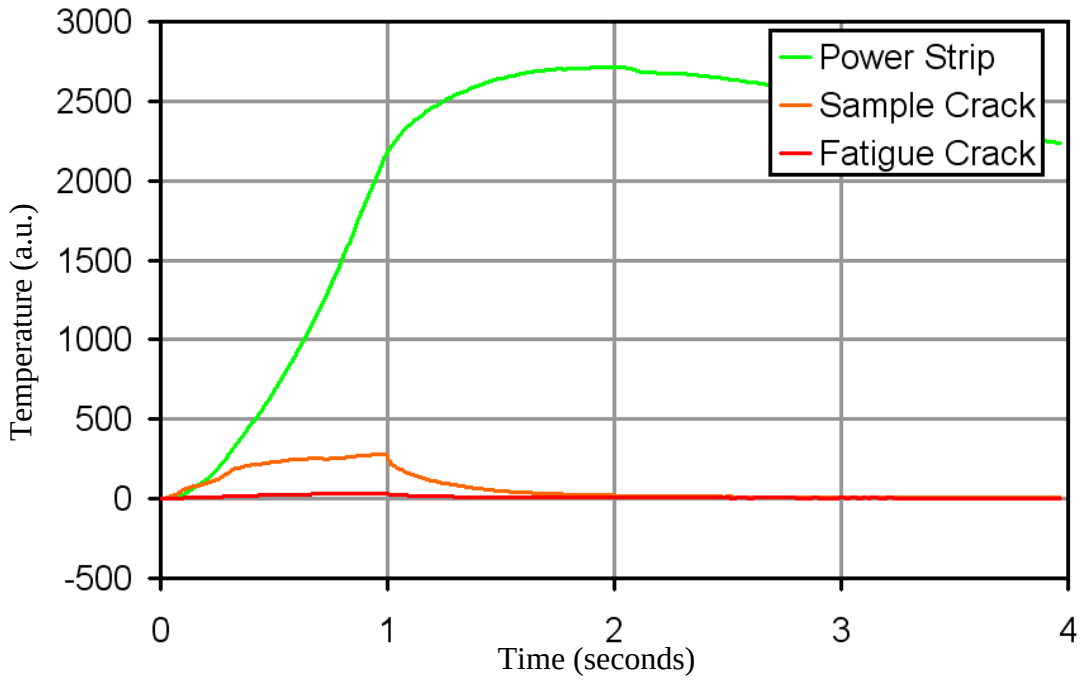

Figure 14. Temperature vs. Time Plot for the Power Strip, Sample Crack, and Fatigue Crack During the Test

To better compare the shapes of the temperature profiles for the three defects, the temperature-versus-time plot is normalized so that each curve's maximum signal is one (figure 15). From the normalized graph presented in figure 15, it can be observed how much better the sample artificial defect represents the thermal profile of the fatigue crack than the power strip.

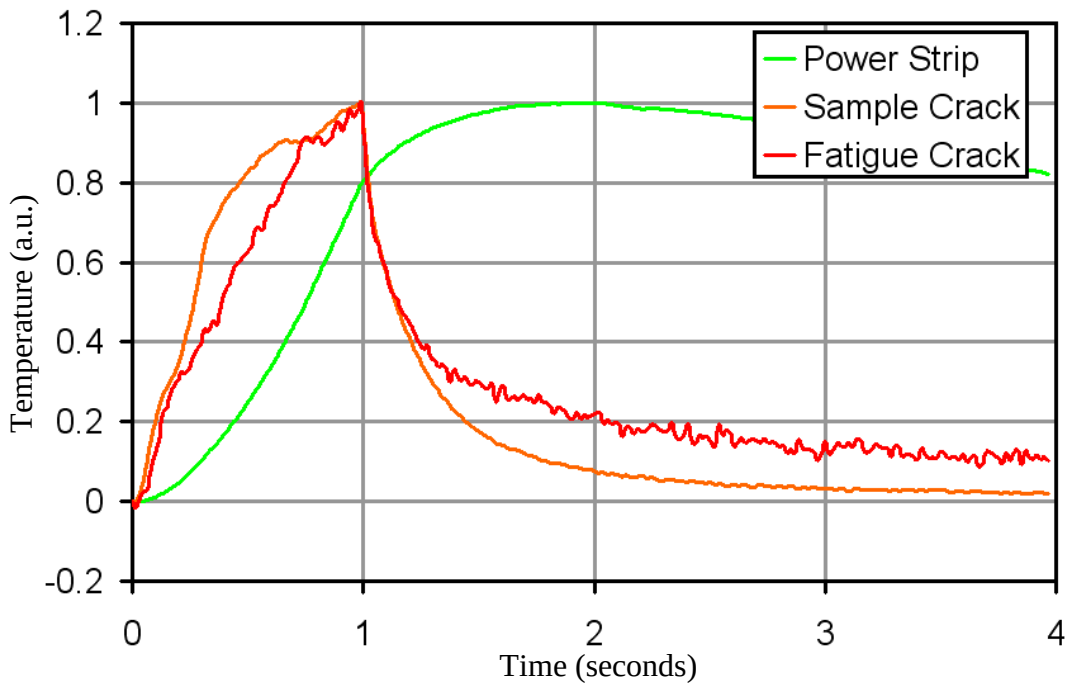

Figure 15. Normalized Temperature vs. Time Plot for the Three Defects Tested

While the sample artificial defect does not accurately represent the peak crack response of the fatigue crack, it is closer and much better represents the thermal profile of the fatigue crack than does the power strip. The artificial defects created by the diagonal pliers-initiated tear are not very reproducible and a better method needs to be developed to make smaller defects. Given these shortcomings, the artificial defects represent an improvement over the traditional use of power strips for parameter optimization.

Similar analysis was conducted with artificial defects created by the EDM notch-fatigue method. This method has the advantage of being much more reproducible than the diagonal-pliers-initiated tear method. Unfortunately, no indication signal was observed from these samples. It is hypothesized that the tensile testing used to produce cracks in the specimens from the EDM notch pre-flaws produces small cracks with little or no compressive forces holding the crack facets together. Therefore, vibrational energy coupled into the samples does not cause the crack facets to interact and, as a result, no thermal energy is produced for observation by the IR camera.

4.6 NEXT STEPS.

During this investigation, two methods of creating artificial defects were evaluated. The diagonal pliers-initiated tear method produced large defects in a somewhat uncontrolled manner that better reproduced the temperature-versus-time profile of fatigue cracks, but not the maximum amplitude. The EDM notch-fatigue method produced defects that were much smaller and more reproducible, but did not produce a thermal signal. Future research should concentrate on the evaluation of other methods for the production of artificial defects that are reproducible and accurately imitate fatigue cracks. The experimental process that can be used for the evaluation of artificial defects produced by various methods follows. Once methods are

developed, the following experiments can be used to evaluate them and our acoustic thermography systems.

Five artificial crack samples with defects approximately 150 mills long and five artificial crack samples with defects approximately 50 mills long were used. A 150-mill and a 50-mill artificial crack sample were attached to each of the five cracked bar specimens provided by Sandia Laboratories. For each cracked bar, the signal amplitude of the two artificial crack specimens to the signal from the crack in the bar was then compared (figure 16).

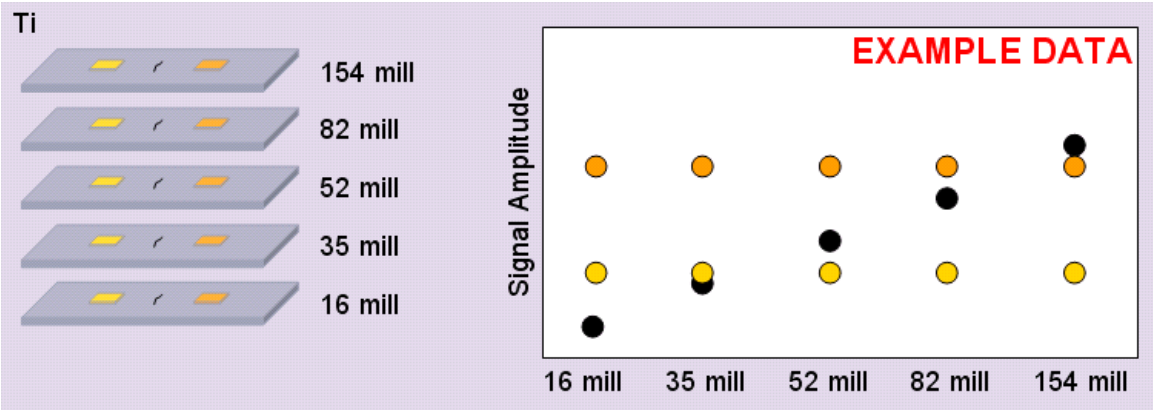

Figure 16. Experiment 1: Do the Artificial Defects Represent Real Crack Amplitude?

Five artificial crack samples with defects approximately 150 mills long and five artificial crack samples with defects approximately 50 mills long were used. A 150-mill and a 50-mill artificial crack sample were attached to each of the five cracked bar specimens provided by Sandia Laboratories. For each cracked bar, the time-versus-temperature curves of the two artificial crack specimens to the signal from the crack in the bar were compared (figure 17).

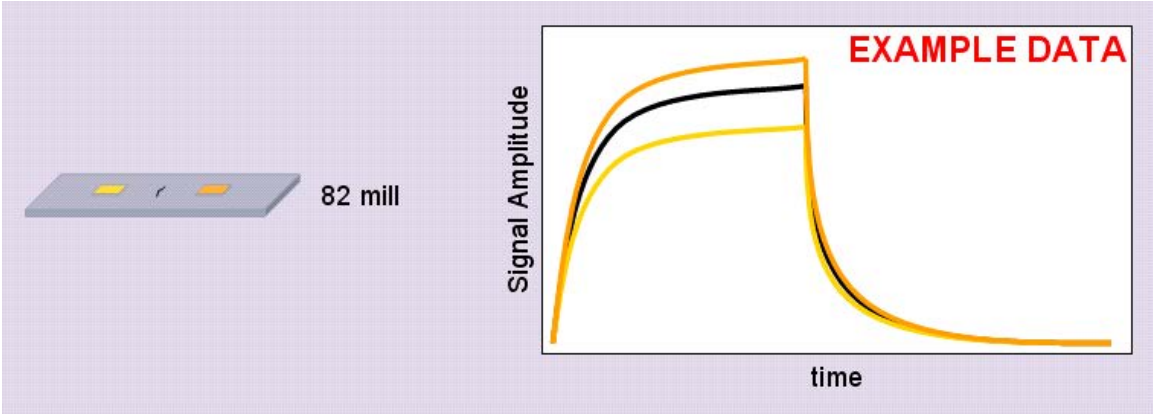

Figure 17. Experiment 2: Do the Artificial Defects Represent Real Crack Temp vs. Time?

Artificial defects of different sizes were attached to a plate. After the plate was excited, it was determined which size indications could be observed by graphing the signal amplitude as a function of artificial crack size. This experiment could be conducted on a part rather than a plate.

The three described experiments reveal the capabilities and the best practices for the use of the developed artificial defects. Those experiments require 20 samples without cracks and 20 samples with cracks. The following is a sample quote for 20 samples from MarTest®. It is recommended that a second set of samples, as shown in figure 18, be created for a more accurate capability assessment. The distribution of crack sizes recommended for use with a set of experiments is:

- Eleven 150-mill cracks
- One 100-mill crack
- One 70-mill crack
- Six 50-mill cracks
- One 30-mill crack

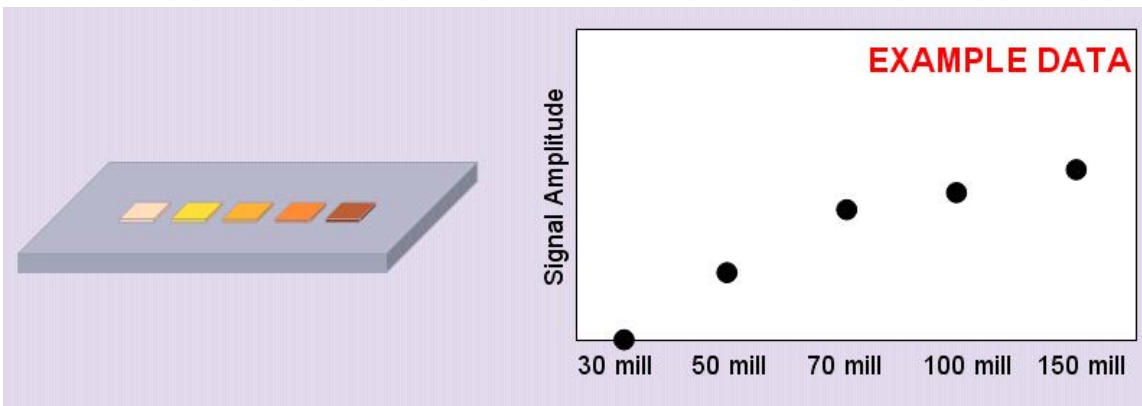

Figure 18. Experiment 3: First Approximation of How Small of An Indication We Can See

5. ACOUSTIC ANALYSIS OF PARTS.

The acoustic thermography inspection method relies on the motion of the surface of the part to cause crack facets to interact, creating the thermal energy that is detected by the IR camera. The location of excitation and the position of the fixture contact points affect the amplitude and resonances of the part. When designing a new acoustic thermography setup for the testing of parts that have never been inspected with this technique, the question of how to hold and where to excite the part must be answered. In this section, the questions of how to hold aircraft engine disks and where to excite the part are investigated by simulation and empirical studies.

5.1 PROPOSED TESTING SETUP.

Several methods of holding and exciting the disk are possible, although it is helpful to understand some general concepts about fixture design. First, the location where the ultrasonic converter is coupled to the part is the excitation location, which is where the ultrasonic energy enters the part. Second, the locations where the fixture holds the part serve to keep the part from being pushed away as the actuator loads the ultrasonic horn against the part. Therefore, it is helpful to design the fixture in a way that provides force equal and opposite to the actuator to keep the part from moving. Third, the fixture-to-part contact locations can transmit the

ultrasonic energy from the part to the fixture and the table to which the fixture is mounted. When this happens, less energy remains in the part to illuminate indications. It is generally understood that the amount of energy transferred through contacting surfaces is proportional to the area of contact and the transmittance of the interface. Therefore, the loss of acoustic energy can be reduced by minimizing the area of contact between the fixture and the part and by using materials that do not transmit sound well at these contact locations.

The symmetry of aircraft engine disks allows them to be excited in two general ways: from the edge (radial excitation) or from the top or bottom (axial excitation). Figure 19 shows a top view of a cylindrical disk in a radial excitation fixture (left) and an axial excitation fixture (right). In radial excitation, the horn approaches and contacts the OD of the part from the radial direction inwards (red triangle in figure 19, left). The fixture holds the disk in place by expanding on the inner bore of the disk (green circles in figure 19, left). During axial excitation, the disk is contacted on a flat surface with the horn parallel to the axis of rotation at some location between the ID and OD of the part (red triangle, figure 19, right). The part is constrained by clamping it between contact points on the top (green circles in figure 19, right) and bottom (blue circles in figure 19, right) surface of the part.

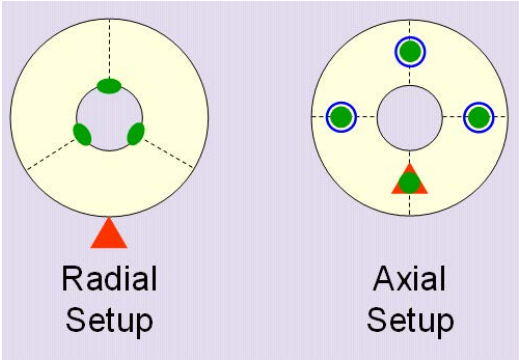

Figure 19. General Excitation Methods for Cylindrical Aircraft Engine Disks: Radial Excitation (left) and Axial Excitation (right)

There are some variations on the radial and axial excitation that may improve or reduce the vibration response of the disk to the horn excitation. For radial excitation, the number of evenly spaced fixture contact locations can be varied to determine if this significantly affects the response from the disk. Figure 20 shows radial excitation using three (left) and four (right) constraints.

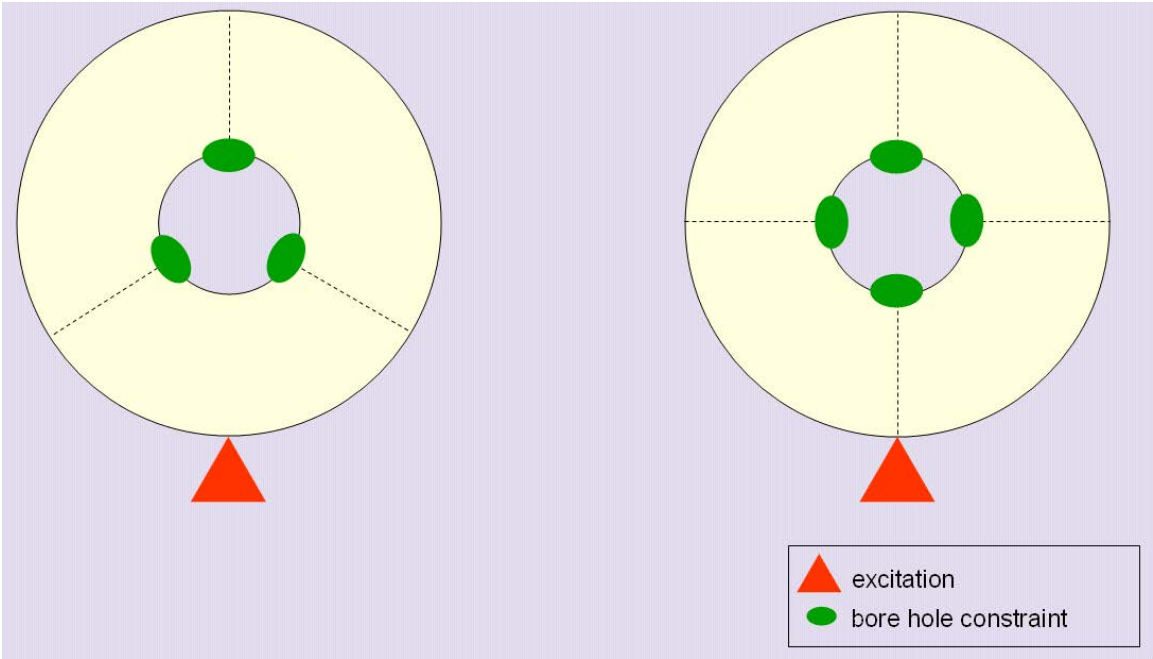

Figure 20. Demonstration of the Variation in the Number of Contact Locations for Radial Excitation

For axial excitation, the number and orientation of the constraints can be changed. Figure 21 shows the orientations proposed for fixtures using five (left, top, and bottom) and seven constraints (right, top, and bottom).

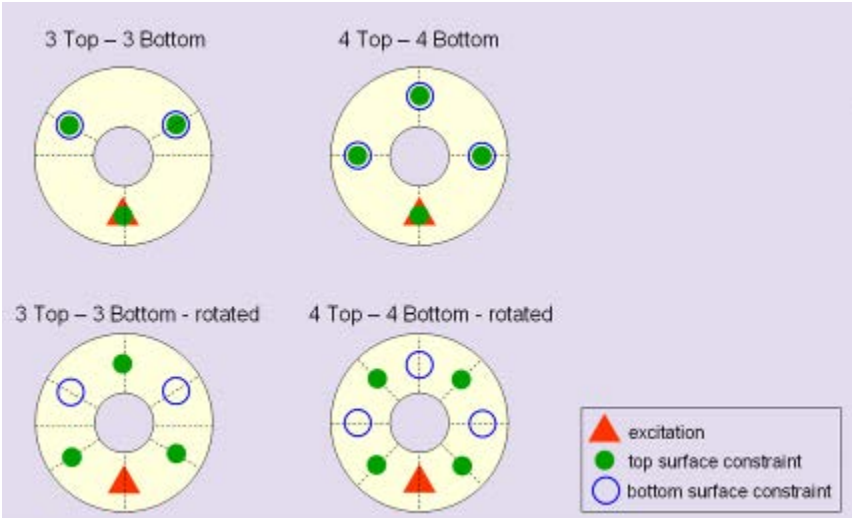

Figure 21. Demonstration of the Number and Orientation of Constraints That Can Be Used in Axial Excitation

5.2 THE FEM ANALYSIS.

It can be quite time-consuming and costly to investigate all of the ways to excite a disk empirically. Therefore, it was decided that simulation could be used to determine which of the above proposed methods were most likely going to give the best results. To conduct the FEM analysis simulation, a model of a disk was needed. Once obtained, it was observed that the model of the real disk (figure 22, left) contained many different features that required many millions of nodes to model. The more nodes in a model, the longer it takes to conduct the FEM analysis of the part.

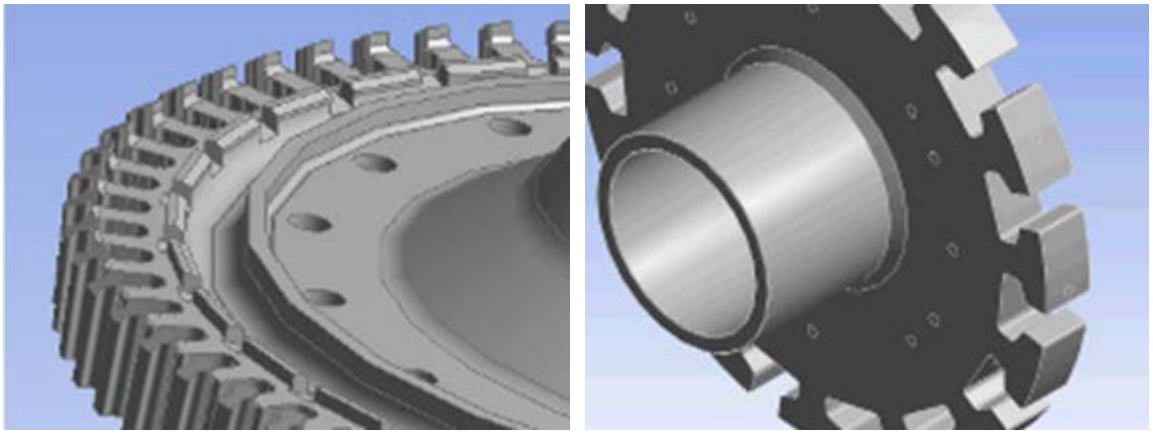

Figure 22. Real Disk Model (left) and Simplified Disk Model (right)

In order to complete the analysis in a timely manner, a simplified model of the disk (figure 22, left) was constructed that had only 60,000 nodes. This simplified model disk was run in the ANSYS FEM software with the constraints placed as described in figures 20 and 21. The location and orientation of the constraints on the simplified disk model for the axial and radial excitation techniques is shown in figure 23.

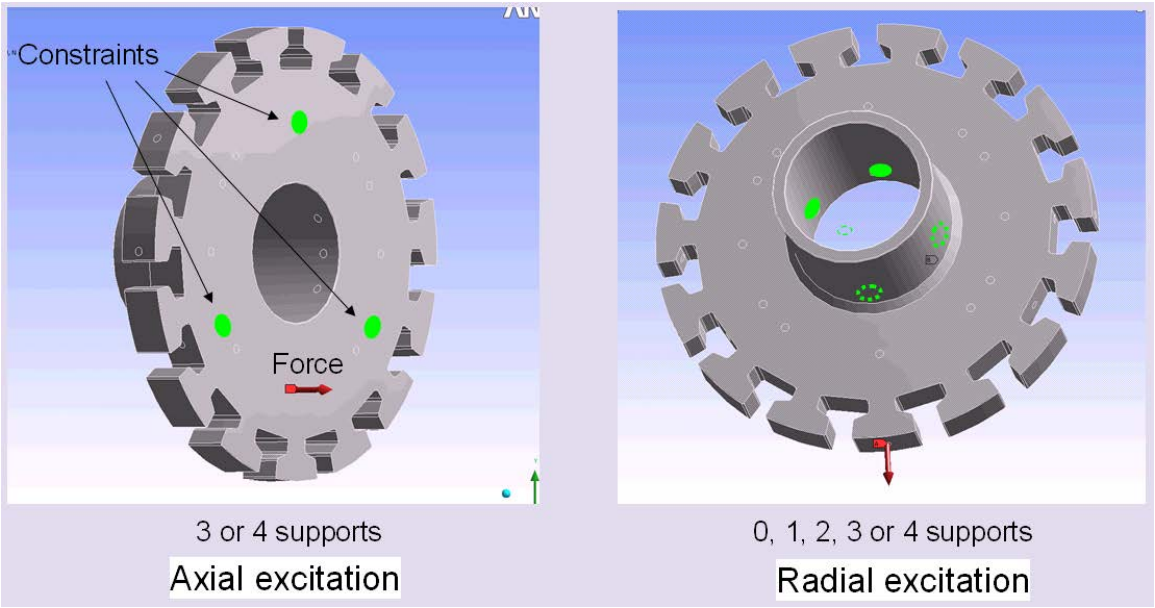

Figure 23. Excitation and Support Positions for FEM Analysis

The part was excited with 20,000 Hz at the location of the red arrow marked "Force" in figure 23. The average deformation amplitude at the hub and attachment locations on the disk between 19,500 Hz and 21,500 Hz was recorded for each excitation configuration.

For axial excitation, the average deformation amplitude at the disk hub and attachment points were observed to be similar (~0.04 µm). The number and orientation of the fixture contact points did not significantly affect the average deformation amplitude of the disk, but did slightly redistribute the amount of energy between the hub and attachment locations of the disk. The graph in figure 24 shows the average vibration response of the hub and attachment points of the model disks in the axial excitation configuration.

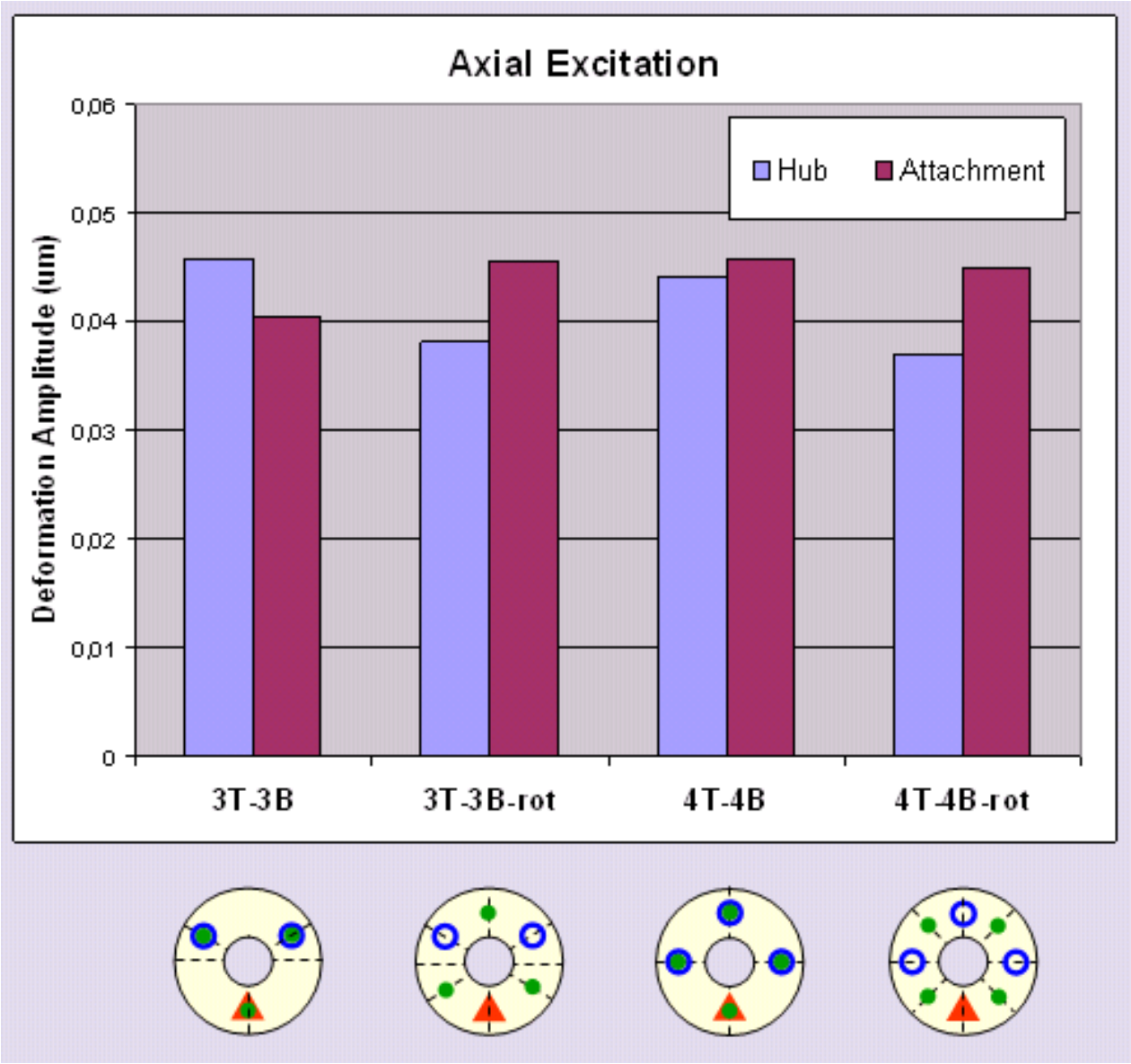

Figure 24. Average Deformation Amplitude as a Function of Axial Excitation Configuration

For radial excitation, it was observed that the average deformation amplitude at the disk hub and attachment points were similar (~0.005 µm). The number and orientation of the fixture contact points did not affect the average deformation amplitude of the disk. A graph showing the average vibration response of the hub and attachment points of the model disks in the axial excitation configuration is shown in figure 25.

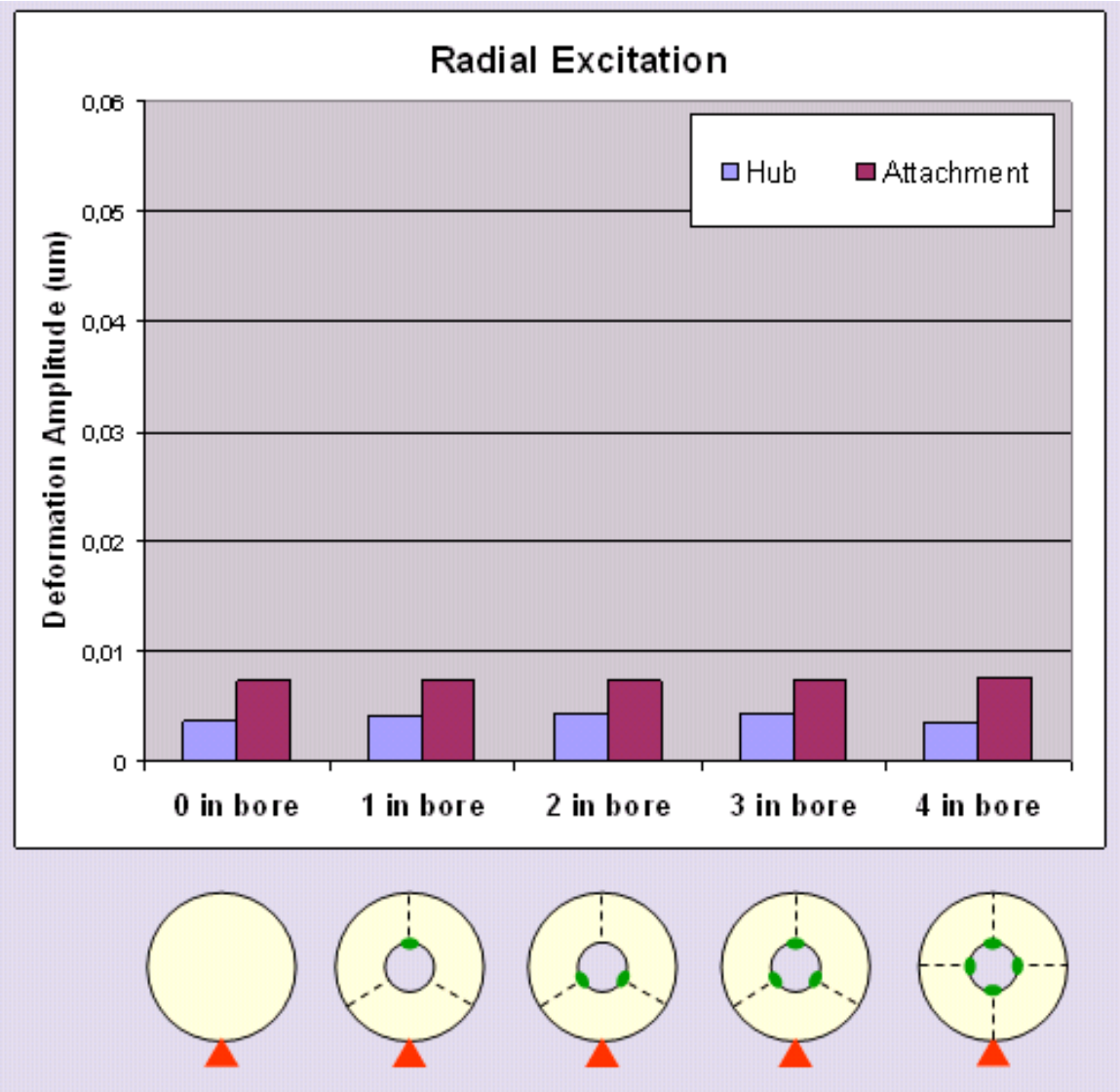

Figure 25. Average Deformation Amplitude as a Function of Radial Excitation Configuration

The results of the FEM analysis indicate that the number and location of the constraints do not affect the average deformation amplitude of the disk in either the axial- or radial-excitation method. The results do indicate that the axial-excitation method provides more average deformation amplitude (~0.04 µm) than the radial-excitation (~0.005 µm) method.

5.3 EXPERIMENTAL INVESTIGATION.

Experimental investigation of the best excitation test setups and excitation methods were also conducted. From the results of the FEM analysis of the test setup described in section 5.2, it was determined that radial excitation with three fixtures-to-part contact locations on the inner bore of the disk and axial excitation with seven constraining locations should be experimentally verified.

The ultrasonic energy can be coupled into the part using three methods: auto-adjust-frequency

excitation (ff_{adj}), modulated-frequency excitation (ff_{mod}), and fixed-frequency excitation (ff_{ix}).

During auto-adjust frequency excitation, the Branson ultrasonic power supply adjusts its output frequency to approximately 20 kHz, to minimize the power reflected back to it by the piezoelectric converter. During modulated frequency excitation, the excitation frequency is changed during the test. Typically, the excitation frequency is adjusted between an upper and lower bound within a range of 200 Hz from the system base frequency of 20 kHz. This is done to provide more overlap between the excitation frequency and the part resonances. During fixed excitation, the frequency of excitation is set and does not change during the test. It is set manually to a resonant frequency of the system. With this method, a microphone is used while sweeping the excitation frequency from 19.8 kHz to 20.2 kHz. The response of the part recoded by the microphone is analyzed by a Fourier transform and the resonance frequency is picked for fixed-frequency excitation.

For this investigation, the JTS (JTS Corporation) disk was used for all tests. The disk was instrumented with 3M foam poster strips arranged in a radial array and taking up a fourth of the disk surface area (figure 26). The 3M foam poster strips emitted thermal energy proportional to the amount of vibration in their immediate vicinity. The more the part vibrated, the higher the detectability of the technique. Therefore, the poster strips offered a method for accessing the relative detectability at different locations of a part and under different excitation conditions.

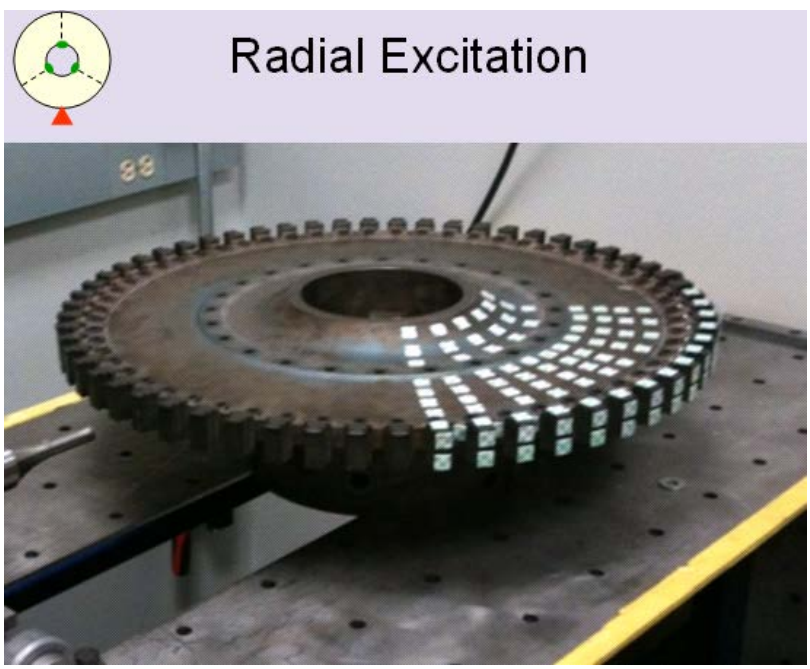

Figure 26. Inspection Setup for the Radial Inspection Methods

For testing of the radial excitation, the JTS disk was held in place with a three-jaw lathe chuck attached to the inspection table. The Branson ultrasonic actuator was attached to the table so that it would press the ultrasonic horn against the OD of the disk. Figure 26 shows a picture of this setup.

For testing of the axial excitation, the JTS disk was supported from the table at three locations, 90 degrees apart, with the horn contact location making the fourth support. Then the disk was held down by a steel plate that contacted the part in four locations and was bolted to the table. This plate kept the part from lifting off the table when the ultrasonic horn, mounted under the table, came up through a hole in the table to contact the part (red arrow in figure 27, bottom).

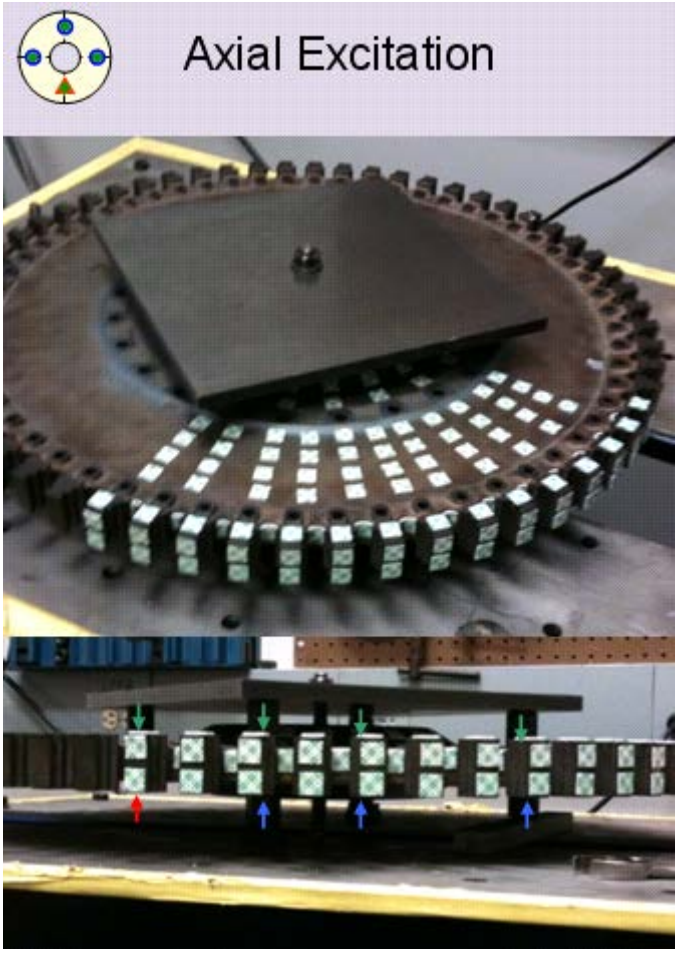

Figure 27. Inspection Setup for the Axial Inspection Methods

The excitation of the JTS disk was accomplished with a Branson 2000 ultrasonic welding system. The test parameters were set as shown in table 5. Longer excitation and recording times were used to obtain a better response from the indicator strips and to capture the slower thermal dissipation of the power strips.

Table 5. Test Parameters for Testing of the Different Excitation Methods

Parameter		Setting		
Excitation Time		2 seconds		
Excitation Method		ff_{adj}	f_{mod}	ff_{ix}
Excitation Amplitude		90%		
Excitation Frequency	Axial Excitation	Auto	19.8 – 20.2 kHz	22,297 Hz
	Radial Excitation	Auto	19.8 – 20.2 kHz	22,996 Hz
Horn Pressure		30 psi		
IR Camera		SC6000 InSb		
Frame Rate		80 fps		
Recording Time		8 seconds		

The results of testing the three methods and two excitation setups are shown in figure 28. The orange rectangle in each image is the region of interest (ROI), where pixel values were made more visible and averaged on the brightest frame of the video sequence to get an overall relative signal representing how much the poster strips heated during the test.

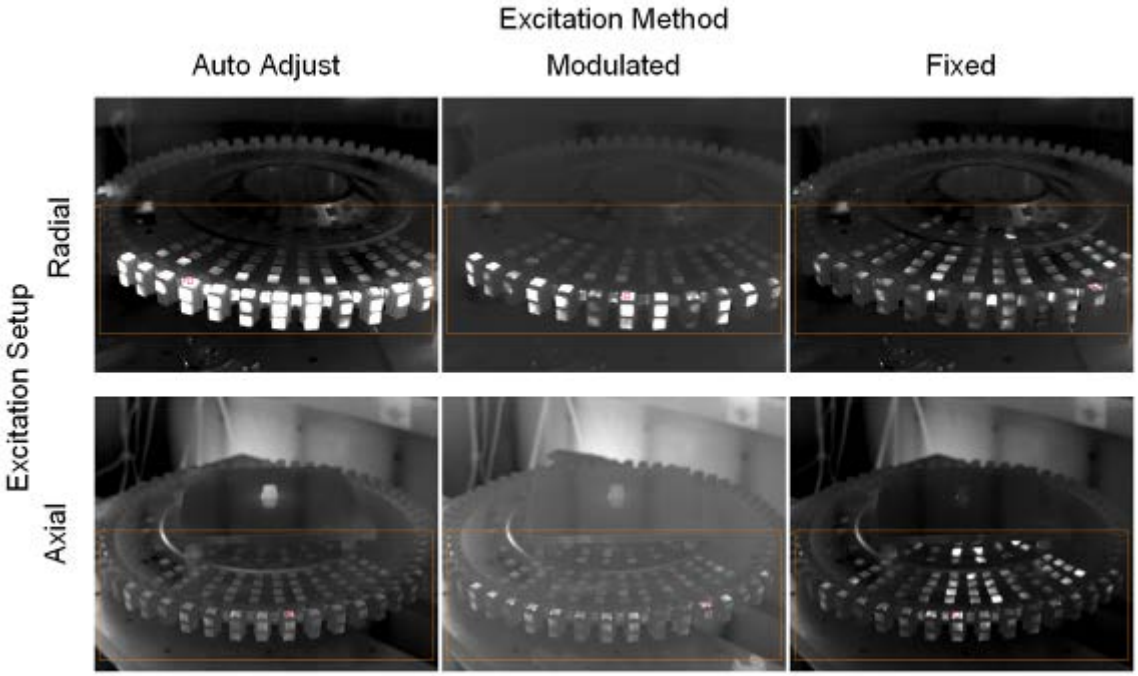

Figure 28. Results of the Excitation Method and Setup Experiments

These values were recorded and are presented in figure 29 as a function of the excitation setup and excitation method. The combination of setup and method across the *x*-axis is arranged in order of decreasing average poster-strip signal. The largest signal observed from all of the poster strips was seen when using the radial excitation setup and the auto frequency adjusts method.

For all methods of excitation, the radial inspection setup performed better than the axial setup. Based on these results, it is recommended that axial excitation and automatic frequency adjustment be used for the inspection of disks.

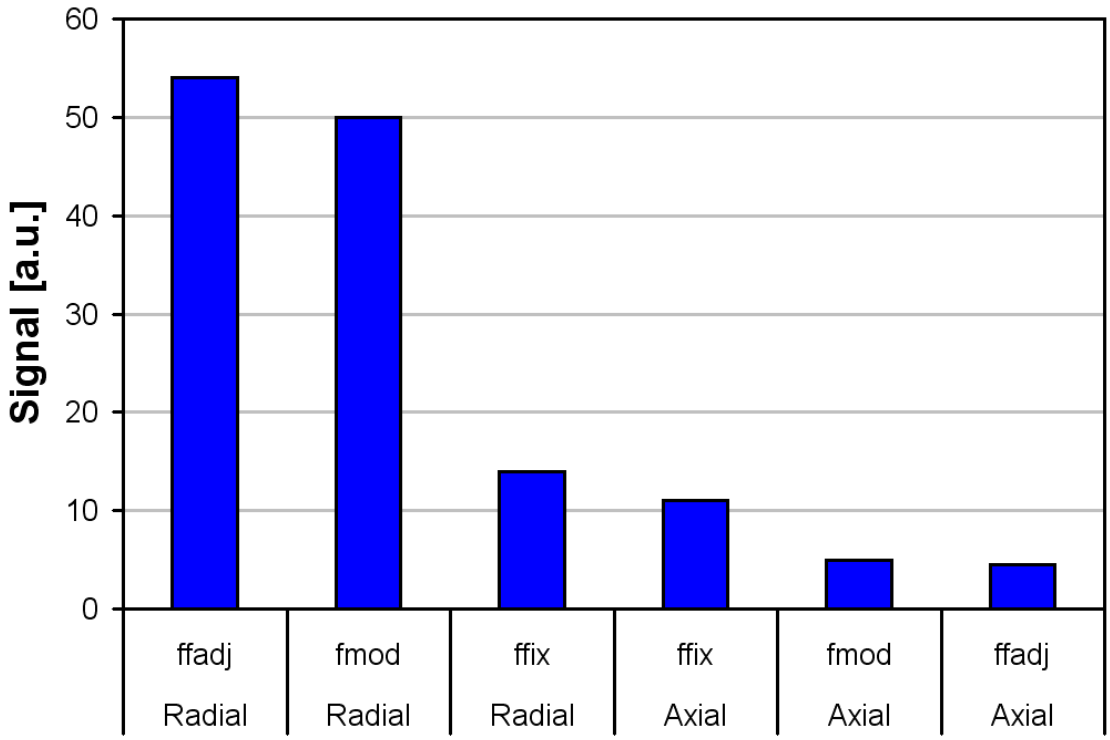

Figure 29. Average Pixel Values From the Brightest Frame in the Video Sequence That Fall Within the Orange ROI

It was also observed that the poster strips did not illuminate uniformly across the surface of the disk. The overall observed trend using any excitation method and setup combination was decreasing poster strip signal (vibration) as poster strips were placed closer to the center of the disk (figure 30). No consistent trend was observed in the circumferential direction.

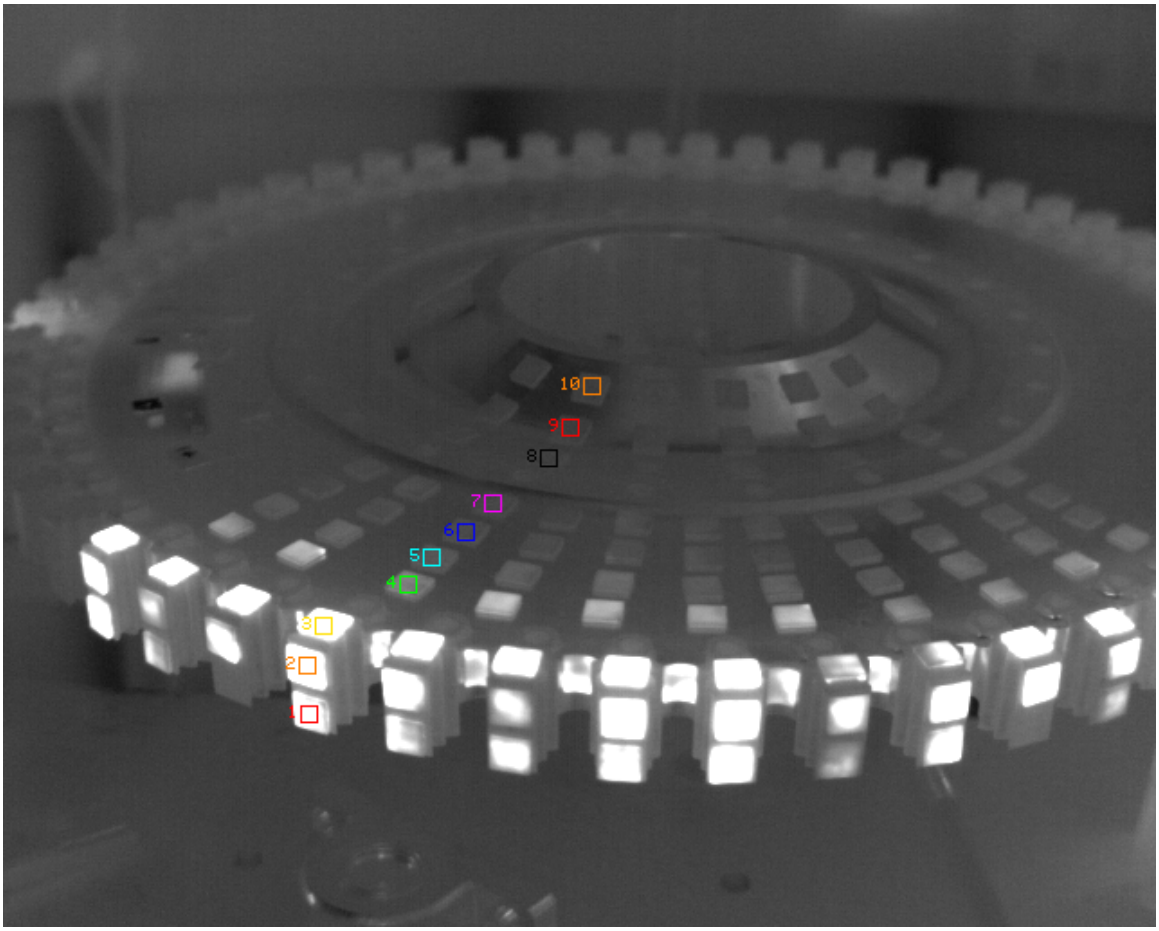

Figure 30. Nonuniformity of the Surface Excitation of the JTS Disk Excited by the Automatic Adjustment Frequency Method Using the Radial Excitation Setup

This trend was quantitatively investigated by measuring the signal produced by poster strips at various radial distances from the center of the JTS disk. Poster-strip signal was measured by averaging the pixels contained within the numbered ROI in figure 30 on the brightest frame of the background-subtracted video sequence. The signal acquired for each ROI is plotted from the OD to the ID of the disk (figure 31). This plot clearly shows the radial dependence of poster strip signal, indicating that the OD of the disk moves more than the ID.

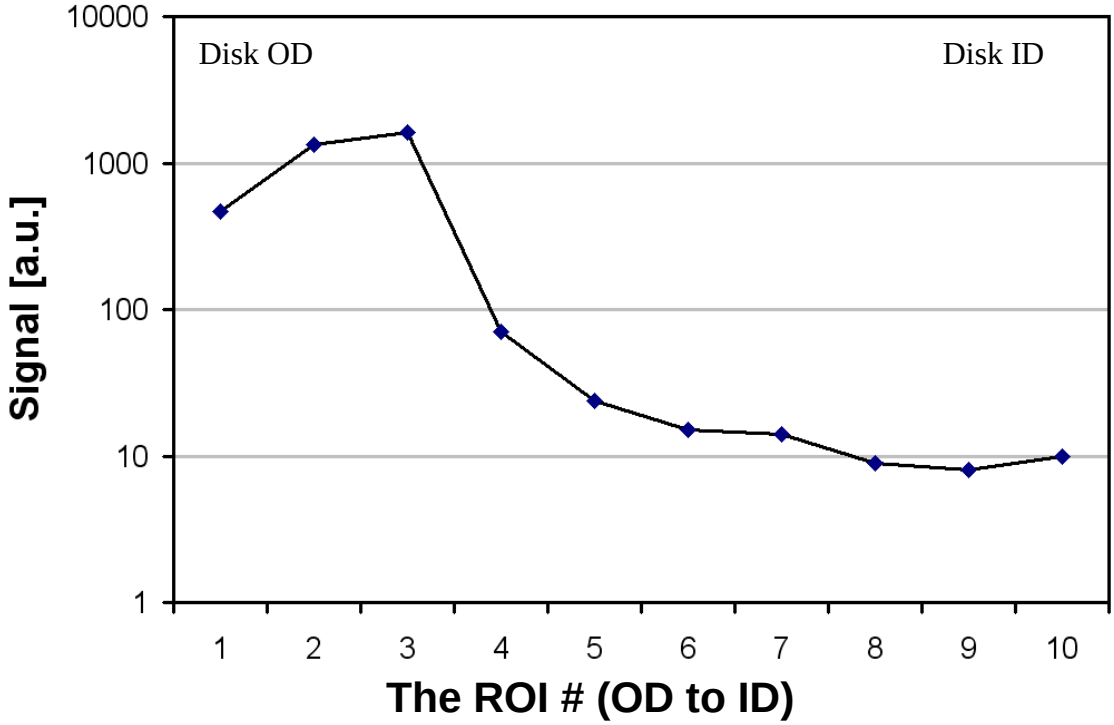

Figure 31. Radial Signal as a Function of ROI Arranged From Disk OD to ID

The fact that this trend is similar for each setup and method (as can be qualitatively verified in figure 28) indicates that this trend is more a function of the part than of the inspection. It is hypothesized that the part will have higher amplitude vibrations in locations where the part is less rigid. Parts of uniform material tend to be less rigid where they are thinner or the part geometry is not well reinforced. On the JTS disk, the part gets thinner toward the OD. Furthermore, the blade attachment steeples on the OD are not as reinforced when no blades are present, as when being inspected. Therefore, it is expected that the acoustic thermography technique will be more effective at detecting defects in locations on the part that are less rigid.

5.4 SUMMARY.

Two methods were used to determine the best excitation setup to be used for the inspection of aircraft engine disks. The first method was a theoretical FEM analysis of a theoretical representative disk excited using the axial and radial setup with different numbers of fixture points. This analysis indicated that axial excitation setup provides up to eight times more deformation amplitude than the radial excitation setup. The analysis also showed that the number and position of the fixture contact locations did not significantly affect the deformation amplitude in either radial or axial setups.

The empirical investigation using the JTS disk was conducted to determine which combination of setup (axial or radial) and excitation method (auto-adjust frequency, modulated frequency, fixed frequency) would generate the largest vibration response on the disk. It was observed using this method that the radial excitation setup with the automatic frequency adjustment generated ~5

times more signal than the best test achieved with the axial excitation setup. It was also observed that the part does not become excited uniformly; rather it is more active in regions that are less rigid. It is expected that the technique will perform better in regions of a part that are less rigid and, thus, move more easily in response to the acoustic stimuli.

The results of the FEM do not correlate with the results from experiments performed. The FEM analysis indicates that the axial excitation setup should be eight times better than the radial setup, while the experimental investigation indicates that the radial excitation setup should be five times better than the axial excitation setup. There are several possible reasons for this discrepancy. First, the interaction between the horn and the disk has not been well characterized for simulation. In the FEM, the horn contact is simulated by a full-contact sinusoidal push-pull force on the disk, while in reality the horn only pushes on the part. Also, the FEM represents the input frequency at a perfect 20 kHz, but in reality, the interaction of the horn and the part may generate higher harmonic input frequencies. It should also be noted that the output parameters of both investigations, while related, are not the same. Therefore, exact agreement is not expected. However, general trends, such as which excitation setup generates more activity in the part, should agree. The disk used in the FEM was not the same as the one used in the experiment. This is because the complexity of the real disk model would require more resources than were available for this investigation. It is possible that some disks will respond better to the axial excitation setup and others will respond better to the radial excitation setup. Possible reasons for discrepancy between the FEM results and the experimental results are summarized in table 6.

Table 6. Reasons for Discrepancy Between FEM Results and Experimental Results

	Simulation	Experiment
Horn/disk contact	Sinusoidal excitation with 100% perfect contact (Perfect push pull force)	Delta peak excitation due to horn hammering Only push force
Higher harmonics	Vibration close to 20 kHz	Higher harmonics not simulated may contribute to vibration amplitude
Output parameter	Displacement	IR radiation
Disk geometry	Simplified disk	Real disk

6. MODIFICATION OF THE SIEMAT SYSTEM.

6.1 FIXTURE DEVELOPMENT.

The SIEMAT system is designed for the inspection of gas turbine blades and veins. During this program, the SIEMAT system was modified to inspect a variety of aircraft engine disks. This required the development of new fixtures. The SIEMAT software was also modified to incorporate the digital documentation of parts so that future automatic defect-recognition algorithms could be trained and evaluated.

While developing fixtures for the inspection of aircraft engine disks, it was important to make

fixtures as flexible as possible. To accomplish this, the fixture needed to maintain a feature that is on most all aircraft engine disks and allows the disk to vibrate as freely as possible. The central bore was selected as a universal fixture location. Most disks have an ID bore, which may vary in size from disk to disk. A good universal method of holding on to the ID of a disk is with the use of a lathe chuck (figure 32). The chuck teeth can be expanded to securely hold the ID of the disk. The 10-inch lathe chuck used for this application was bolted to a 0.5-inch-thick plate of aluminum that bolted to the Siemens flex table system. The chuck teeth were replaced by custom aluminum chuck teeth with Nylatron contact surfaces.

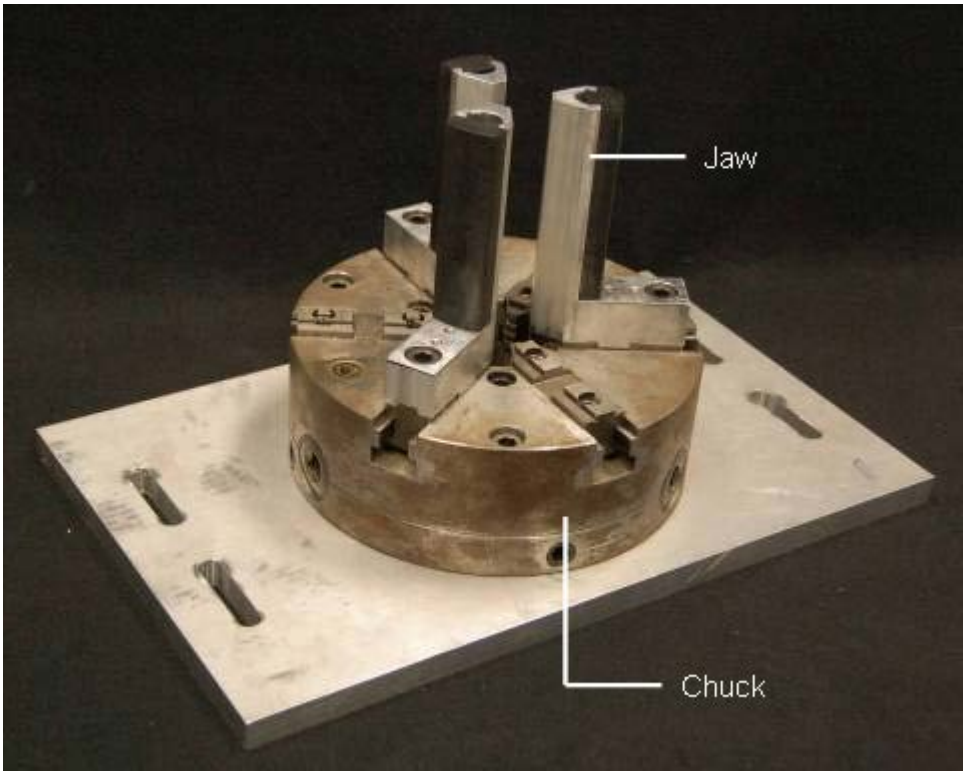

Figure 32. Lathe Chuck Fixture for Horizontal Excitation Setup Used to Inspect Aero Turbine Disks

A second fixture was developed for the inspection of disks that respond well to axial excitation. Aircraft auxiliary power unit (APU) disks were tested with success using this fixture (figure 33), which is designed to hold the plane of the disk parallel to the table by clamping the fore and aft surfaces of the ID using the bolt and nylon spacers. The excitation source comes up from under the table to contact the disk in the axial direction for excitation.

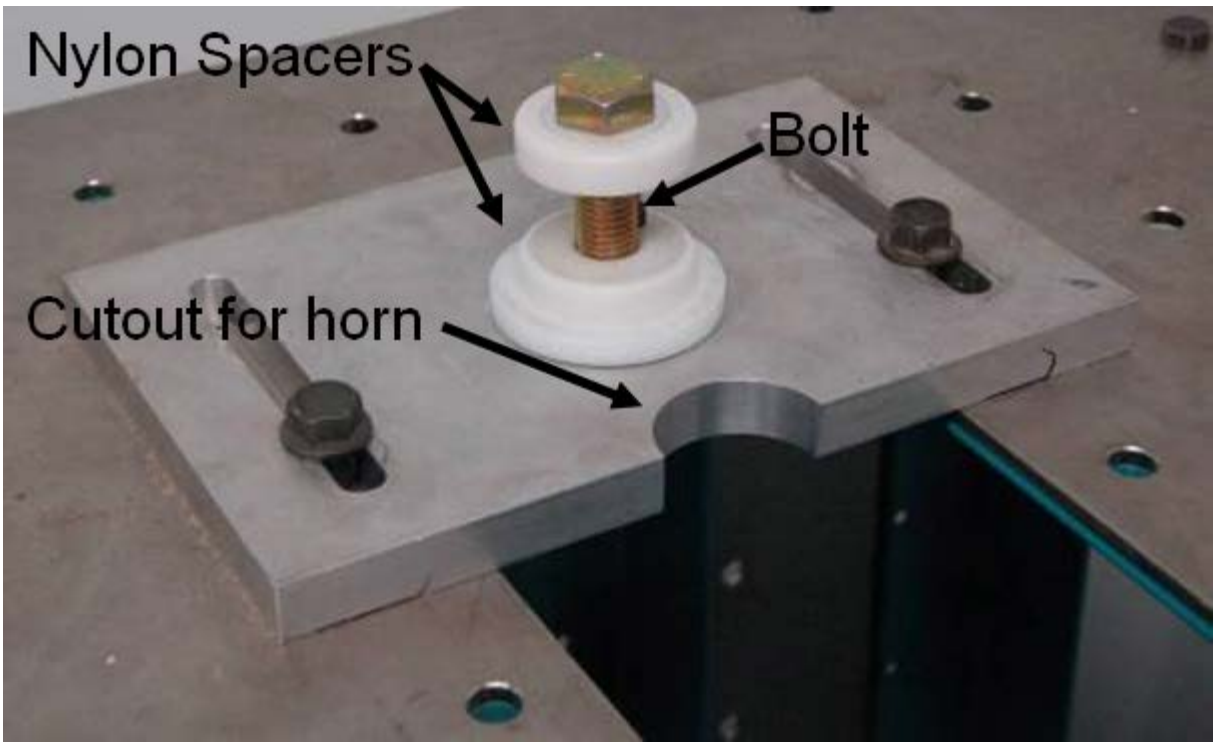

Figure 33. Fixture for Axial Disk Excitation Setup Used to Inspect Aero Turbine Disks

6.2 EVALUATION OF INTERFACE MATERIALS.

6.2.1 Introduction.

When inspecting parts using the acoustic thermography system, the most efficient way to transfer energy to the part being inspected is by direct contact of the titanium horn onto the surface of the part. However, this may cause surface scuffing or fretting at the excitation location due to metal-to-metal contact. To prevent scuffing, non-metallic materials are placed between the part and the horn. These interface materials are softer than either the part or the horn and deteriorate to protect the part. A drawback of these materials is that they reduce the amount of acoustic energy delivered to the part. The amount of energy reflected or absorbed by the interface material is a function of the interface material being used. The purpose of this study is to access a variety of interface materials for their ability to protect the part and transmit the ultrasonic energy.

6.2.2 Test Setup and Procedure.

To test the interface materials, the acoustic thermography system was set up in the horizontal desk-mount configuration as shown in figure 34. A steel block in an aluminum fixture represents the part. The interface material to be tested is placed between the titanium horn and the steel block. The ultrasonic horn is pressed against the interface material on the part by the actuator and the acoustic energy is transmitted through the horn and interface material, and into the part. The interface material will reflect some incident energy, absorb some, and transmit the rest. The absorbed energy will degrade the interface material during excitation. The part is said to have failed when the amount of damage on the interface material results in a hole, allowing the horn to

contact the part directly. The remaining energy transmitted to the part will cause its surface to move and will excite the power strip placed in the camera's field of view on the part. The more energy present in the part, the hotter the power strips will become. The Branson power supply, which is used to drive the piezoelectric transducer that excites the part through the horn, reports the amount of energy absorbed by the interface material and part.

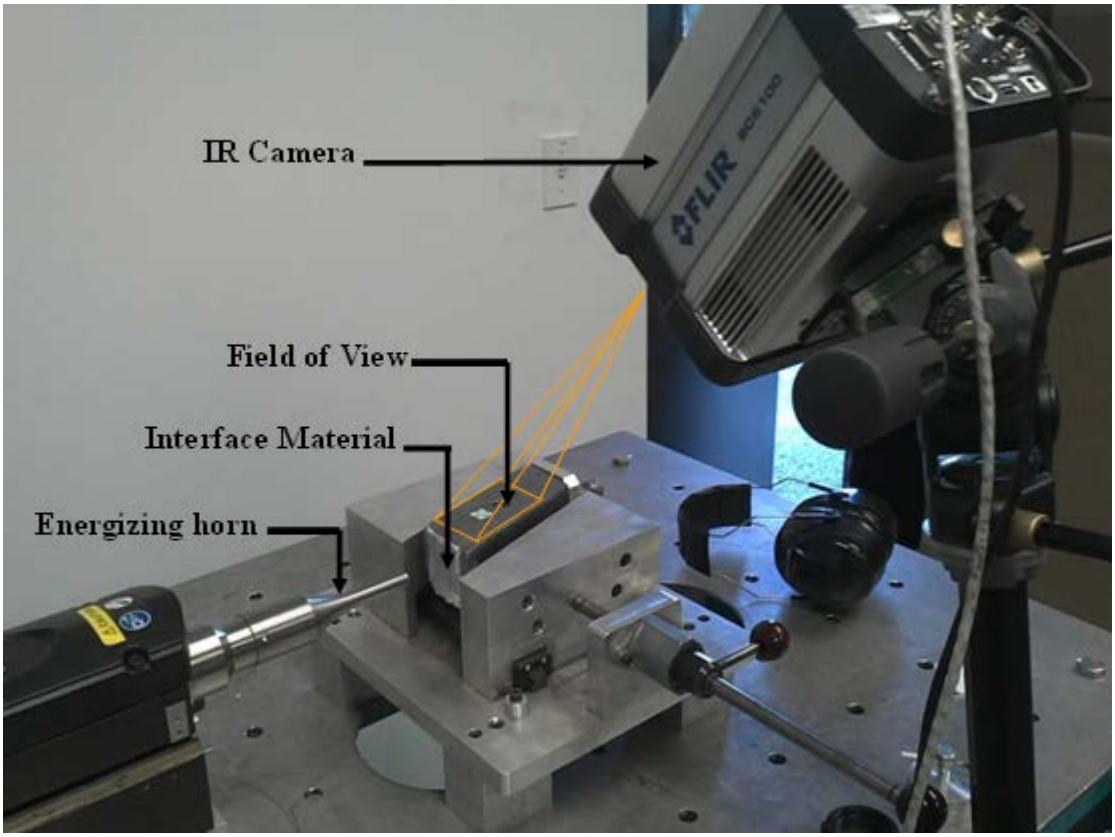

Figure 34. Test Setup Used for Interface Material Testing

Each interface material type was tested at increasing amplitude from 40 to 100% in 10% increments at 40 psi of horn pressure or until interface material failure, depending on which came first. If an interface material did not fail after being excited at 100% amplitude, the excitation pressure would be increased from 40 psi in increments of 10 psi until it did fail or the excitation system could not deliver any more energy. At the end of each excitation, the material was removed from the block and inspected for signs of failure (e.g., light passing through the points of failure, or obvious signs of the horn passing through the material). At the beginning and end of each excitation, pictures were taken to document the interface material before and after excitation, as shown in figure 35.

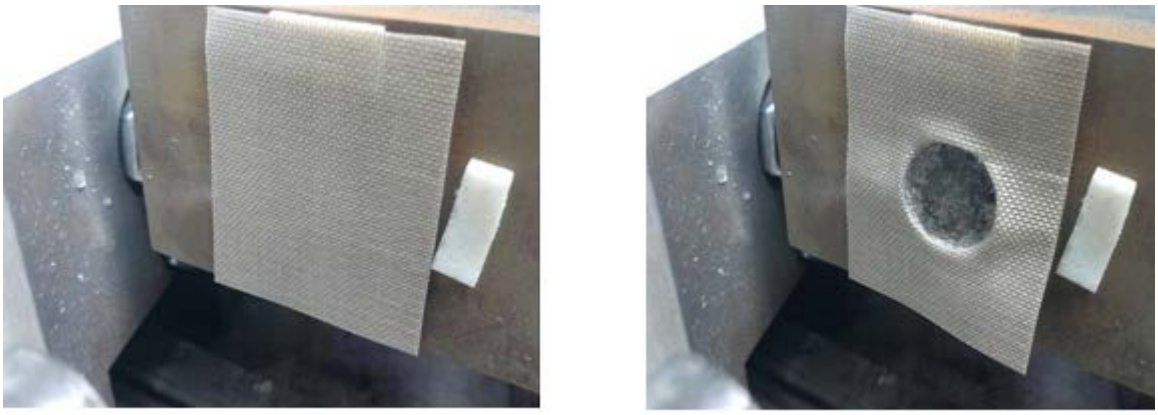

Before Excitation After Excitation

Figure 35. Example of Photo Documentation of Interface Material (Two-Ply PTFE Glass Fabric Tape by 3M™) Before and After Excitation

A new piece of interface material was used for each test. The following parameters were recorded for each test point:

- Material name
- Thickness
- Excitation amplitude
- Excitation pressure
- Resulting excitation energy
- Power strip temperature rise signal
- Whether or not the material failed

The data gathered by varying the type of material, amplitude, and pressure values were then analyzed to narrow down on the amplitude and pressure range for a material that would result in maximum power-strip signal.

6.2.3 Data Analysis.

The results of the interface material experiments were analyzed to sort the tested interface materials from best to worst, taking into account the two material characteristics. The first material characteristic of interest is its ability to protect the part. This is quantitatively recorded as the excitation energy at which the interface material failed. The more energy an interface material can receive without allowing the horn to touch the part, the better it protects the part. For each interface material, the lowest excitation energy recorded by the Branson power supply that caused the interface material to fail was plotted in figure 36.

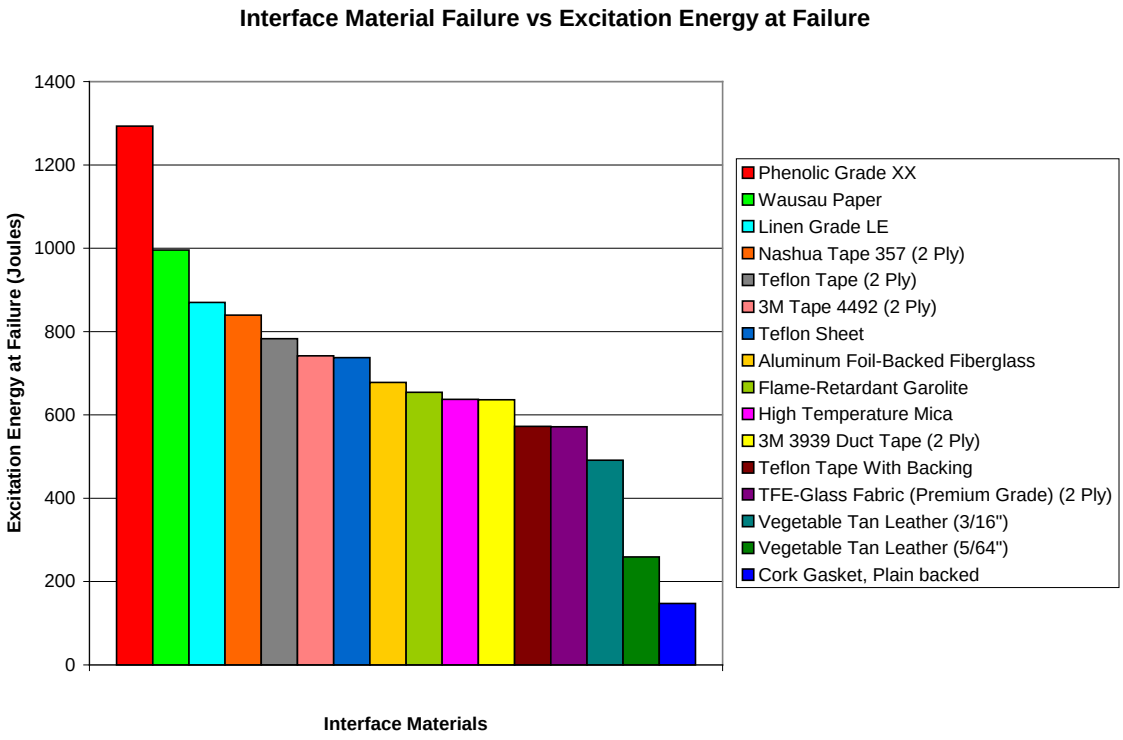

Figure 36. Excitation Energy at Failure for Various Interface Materials

Figure 36 shows that the top three interface materials for protecting the part are Phenolic Grade XX, Wausau Paper, and Linen Grade LE. It is common for a material that protects the part well to also insulate the part from acoustic energy. This would reduce the signal from indications and, thus, inspection capability.

The increase in thermal signal of the power strip during the test was used as a measure of the amount of acoustic energy that made it into the part. The more the power strip signal increased during the test, the more energy was in the part and the better the inspection detectability. The maximum increase in thermal signal that was recoded at material failure was plotted as a function of material in figure 37.

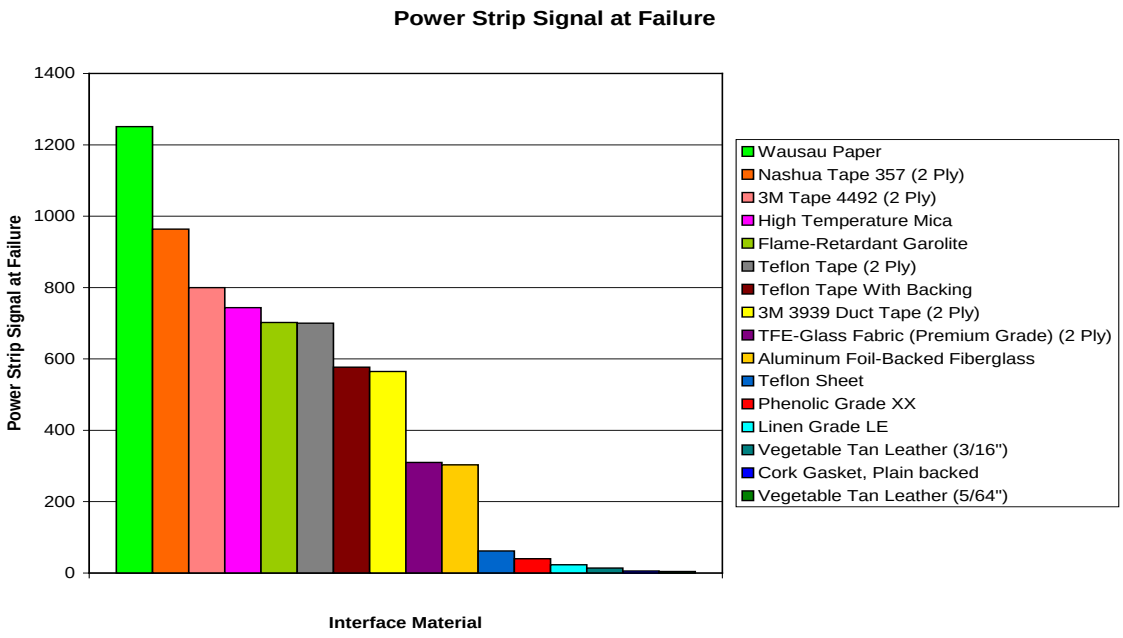

Figure 37. Energy Levels for Which Failure Occurs for Each Material

These results show that, while Phenolic Grade XX was very good at protecting the part, it transmitted little vibration energy to the part. This vibration energy did not cause the power strip temperature to increase very much. The Wausau Paper did transmit a lot of vibration energy to the part as shown by the >1200 counts increase in power strip signal.

To determine which material had the best combination of both properties, each material was assigned a place number specifying how well that material performed relative to the other materials for each test. The material that performed the best is assigned first place and the material that performed the worst is assigned 16th place. This was done for both the excitation energy test and the power strip signal test. For each material, the place values were added up to get an overall score related to the performance of the material on both tests. The lower the overall score, the better the material as an interface material. When materials are sorted smallest to largest by their overall score, the best interface materials appear at the top of the list. This analysis is shown in table 7.

Table 7. Place Number Assigned to Each Material in the Excitation Energy and Power Strip Signal Analysis and the Overall Score and Preference Place of Each Material

Material	Excitation Energy Place	Power Strip Signal Place	Overall Score	Preference Place
Wausau Paper	2	1	3	1
Nashua Tape 357 (2-Ply)	4	2	6	2
3M Tape 4492 (2-Ply)	6	3	9	3
High-Temperature Mica	10	4	14	4
Flame-Retardant Garolite	9	5	14	5
Teflon Tape (2-Ply)	5	6	11	6
Teflon Tape With Backing	12	7	19	7
3M 3939 Duct Tape (2-Ply)	11	8	19	8
TFE-Glass Fabric (2-Ply)	13	9	22	9
Aluminum Foil-Backed Fiberglass	8	10	18	10
Teflon Sheet	7	11	18	11
Phenolic Grade XX	1	12	13	12
Linen Grade LE	3	13	16	13
Vegetable Tan Leather (3/16")	14	14	28	14
Cork Gasket, Plain Backed	16	15	31	15
Vegetable Tan Leather (5/64")	15	16	31	16

6.2.4 Summary and Conclusions.

This experiment has tested 16 potential interface materials. These interface materials were evaluated by how well they protect the part and by the amount of acoustic energy they transmit. How well an interface material protected the part was evaluated by measuring the amount of ultrasonic energy required to cause the material to degrade to the point that they allow the horn to contact the part directly. The amount of acoustic energy the material transmitted to the part was evaluated by measuring the increase in thermal signal from a power strip on the part during the test. Analysis was conducted to determine which materials had the best combination of the two evaluated characteristics. This analysis resulted in the conclusion that the Wausau Paper, Nashua Tape 357 (Two-Ply), and 3M Tape 4492 (Two-Ply) were the best candidates for interface materials.

6.3 AUTOMATIC DEFECT DETECTION.

One of the great advantages of the acoustic thermography method is its ability to be automated. Currently, the inspection operates in a semiautomated mode. In this mode, the inspector is

presented with not just the video from the camera, but also the postprocessed pulse-phase result (figure 38). These results highlight the indications and make their identification easier for the inspector. The current semiautomated acoustic thermography techniques still require the inspector to understand how to interpret the pulse-phase result and conduct final interpretation.

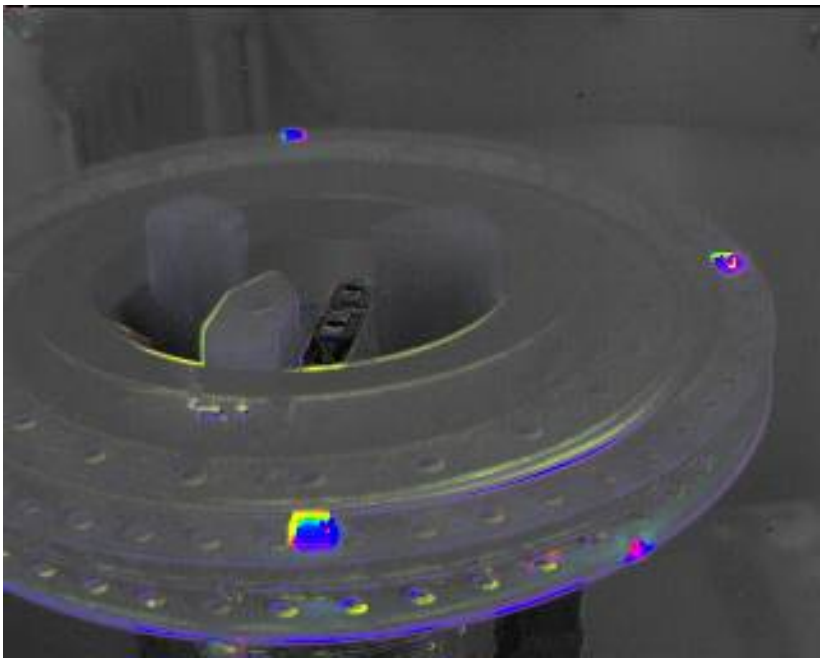

Figure 38. Pulse-Phase Result From Which Inspectors Make Interpretations of the Indication Types and Relevancy

Fully automated defect detection would consistently identify and categorize the indications without inspector intervention. This type of system will need to be developed over time and with proper software evaluation and training. Presented in this section is the outline for the development of an automatic defect-recognition system. Also presented are the results from the first steps taken toward an automatic defect-recognition system.

The proposed automatic defect-recognition system will use the temperature-versus-time evolution, 2D geometry, and the location of IR emission on the part to evaluate the relevancy of an indication. It is known that different indications will have different temperature-versus-time curves. Poster strips cool down very slowly and show peak emission at some time after the end of excitation. Cracks heat and cool fairly quickly because of the thermal diffusivity of the part. These differences can be used to determine the type of indication. The 2D geometry can help discern between linear cracklike indications and area delaminations. It is also known that, as inspectors become more proficient, they learn how to evaluate the accuracy of the result.

The system will use a set of trainable classifiers for these characteristics, which will be used to decide the probability that an indication is of a certain type. The steps necessary for training the classifiers are shown in figure 39. The classifiers will be trained using a set of marked-up acoustic thermography results that indicate the regions of known indications. This set is known as a training set and has the locations of linear indications, poster strips, delaminations, and other

indications marked by inspectors. The training set is used as an input to the training routine to generate a set of coefficients used by the classifier algorithms for deciding the type and relevancy of the indications observed in raw resulting data. The classifiers are then tested using the training set and a set of blades that have not been used to train the system (test set), but have known indications on them. If the classifiers correctly identify the indications in the training and test sets they are certified for use on inspection parts.

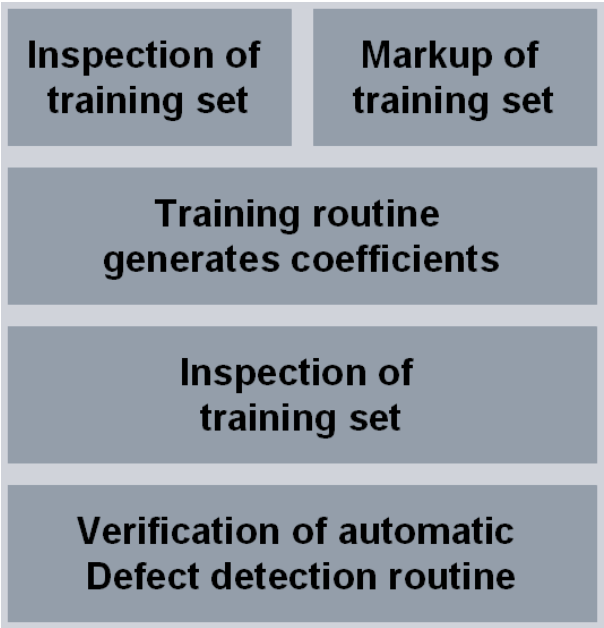

Figure 39. Steps Necessary for Training of the Classifiers

During this program, initial steps were taken toward the development of an automated defect recognition system. This included the integration of several features into the SIEMAT software ($SInE^2$). These features were chiefly aimed at enabling the inspector to document the indications observed in a digital form that can be used to train classifiers for automatic defect recognition. A screen shot of the updated $SInE^2$ software is shown in figure 40. The first feature added to $SInE^2$ was the tool bar displayed on the left side of the screen. This tool bar enables the inspector to identify and annotate indications on the acquired pulse phase resulting image. Rectangles and ovals can be drawn around observed indications on the screen. These objects are listed in a table at the bottom of the screen where the inspector can note the type of indication observed within each object. The color of the outline and fill is unique to the type of indication selected. For example, square 2 in figure 40 has a red outline and red fill defined as having a crack inside it. This data is documented with the *.sec file saved for each inspection image and can be used by the training routine to generate a set of coefficients for the classifiers. This software also enables the user to add text and arrow annotations to the image. While this is not currently planned for use in the automatic defect recognition program, it does provide useful information to other users of the data about what the inspector observed. The software was also updated to include the ability to define a scale for the image and measure the object in the image field of view. A scale definition is defined using the bottom icon in the markup toolbar on the right of the screen. A popup window asks for the real-world dimension to be defined in the image, then the user draws

a black and white checkered line across that dimension to define the pixel scale factor. This information may be used by the automatic defect recognition system to provide approximate indication lengths. The third-from-the-bottom tool in the markup toolbar on the right of the screen allows the user to measure other objects on the screen using the defined scale bar. One should keep in mind that this is a simple spatial calibration and, thus, error in measurements can increase when measuring objects that are not parallel to the focal plane array of the camera.

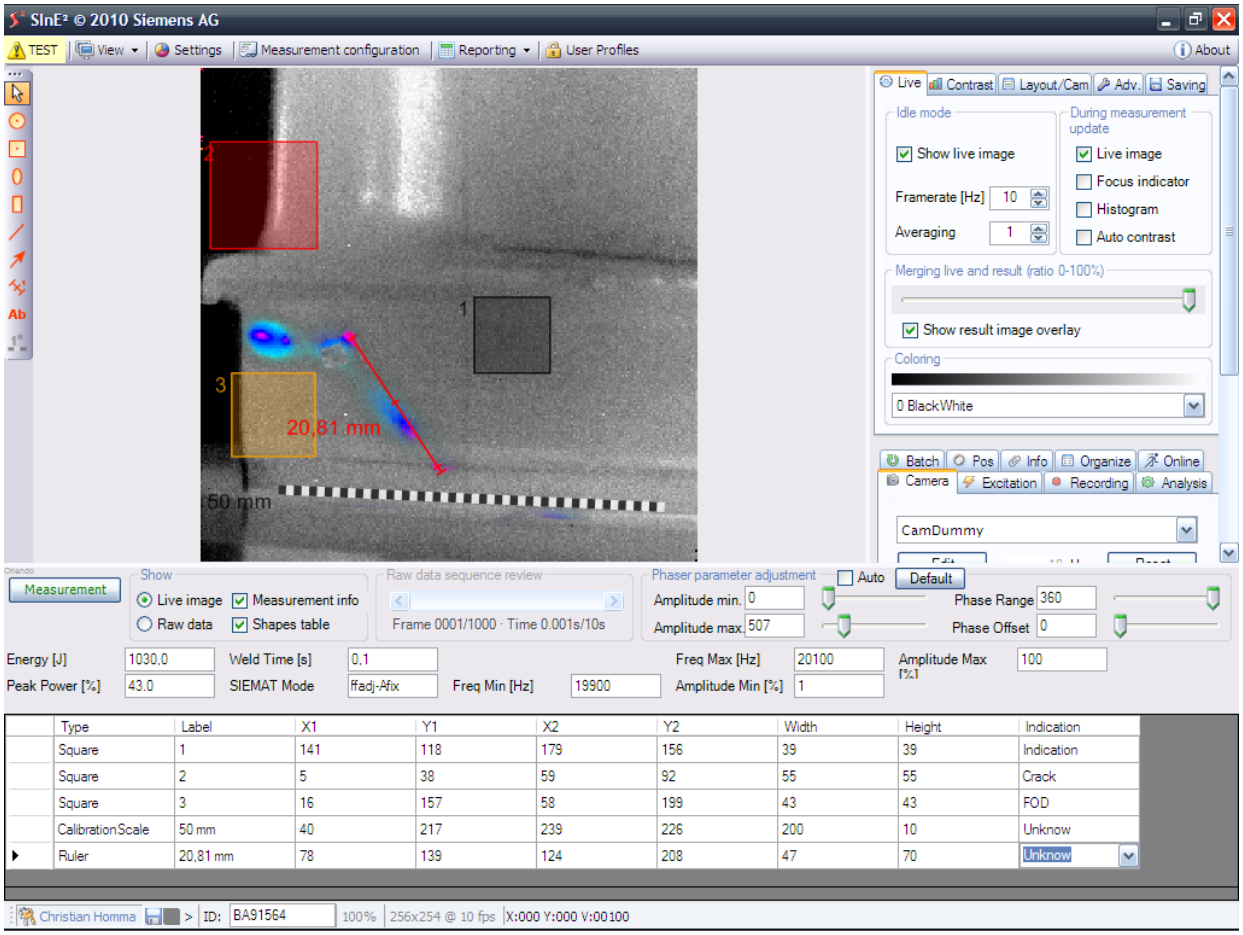

Figure 40. Updated Version of SInE^2 Showing the Ability to Digitally Document Indications

7. INSPECTION OF SELECTED DISKS.

7.1 INSPECTION PROCEDURE.

An inspection procedure was developed for inspecting both sides of each disk. The inspection process was broken down into the following four subprocesses.

7.1.1 Start-up Process.

This process involves starting up all the systems required to perform the inspection. This system includes the following components:

- Branson Power Supply—This system generates the high voltage 20 kHz ultrasonic signal and controls the actuator.

- Compressed Air System—This system moves the horn so that it comes into contact with the disk and excites it with acoustic energy.

- Computer—This orchestrates the triggering and recording of the disk-excitation process and stores data that can be reviewed to search for possible anomalies.

- Connector Box—This system plays a key role in enabling the computer and the Branson to communicate.

- Thermal Camera—This enables viewing of the thermal signature of the disk during excitation in order to detect any possible anomalies.

After the above systems are turned on, the $SInE^2$ software is started and the appropriate measurement configuration file for the part is loaded. The IR camera then undergoes a non-uniformity correction and is set up to view the inspection ROI. Finally, the saving directory and parameters are set.

7.1.2 Inspection Process.

The inspection process involves the actual inspection of the disks and can be divided into the following six steps:

1. Software Setup—This involves recording the disk serial number, setting an amplitude value, and customizing options in the "Saving Level" tab in the software.

2. Angle–Pressure Adjustment—This involves adjusting the Branson air pressure from 20 psi (for the horn-down process) to 30 psi (for the disk-inspection process) and setting an angle so that the horn-disk contact area is maximized.

3. Disk Mounting—This step involves the selection of proper jaws as per the disk ID and moving the mounting assembly up to a proper height so the horn is centered at the disk. The disk is held in place by tightening the jaws that contact the ID of the disk.

4. Power Strip—A power strip is stuck on the disk so that it is visible in the "Live Image" of the software. The letter *A* or *B* is written on the power strip, depending on the side of the disk, and an arrow is drawn on the power strip indicating the direction in which the disk would be rotated on the mounting assembly.

5. Measure and Evaluate—During this step, the "Measurement" button on the software screen is pushed and the live image is studied for any indications that show up during the excitation process. Once the horn retracts after excitation, the indications observed are marked on the disk.

6. Disk Rotation—The disk is rotated on the mounting assembly in the direction of the arrow after each excitation, until the disk comes back to its original position.

The disk is now flipped over and the six steps are repeated for this side of the disk until the disk comes back to its original position. Then the jaws are loosened and the mounting assembly is lowered to remove the disk from the assembly.

7.1.3 Shutdown Process.

After all the disks have been inspected, the $SInE^2$ software is closed and the air supply, Branson, computer, connector box, and thermal camera are turned off.

7.1.4 Horn–Down Process.

This process is performed to make sure that the horn contacts the disk at the correct position. It is important to perform this process prior to beginning the inspection process because contacting the disk at an improper surface and angle could damage the horn and the disk surface. The horn–down process involves adjusting the Branson air pressure to 20 psi. The pressure should be increased from less than 20 psi to 20 psi rather than being decreased from a higher pressure to 20 psi. This is done to ensure that there is no backlash in the pressure system during inspection.

After adjusting the pressure and locking the pressure knob in position, the "Horn–Down" button on the Branson is pushed and the instructions on the Branson screen are followed.

A detailed flow chart for the process can be found in appendix A.

The horn–disk contact angle is adjusted in such a way that the area of contact is maximized (see appendix B for the horn–disk contact angle optimization pictures).

The process is completed once the angle of contact is optimized and the "Horn–Down" mode is changed to "Run" mode.

7.2 OPTIMIZATION OF TEST SYSTEM FOR DISKS.

Optimization of the inspection procedure was done by using design of experiments. A range of three to four levels for each independent variable was considered. Signal strength data were collected for a power strip, which was used as a crack analogue. Power strips produce a thermal signal that is proportional to the vibration amplitude at their location. This process is similar to how cracks produce thermal emission from local vibration. The power strips often generate more thermal signal and cool off more slowly than cracks, but can be used to determine the relative peak crack signal that could be observed under different conditions. For example, if it is observed that a power strip produces a peak signal of 400 counts with an excitation amplitude of

70% and 600 counts with an excitation amplitude of 100%, it can be concluded that a crack in the location of the power strip would show a larger signal if excited at 100% amplitude rather than at 70% amplitude. The following picture shows a power strip (circled in figure 41) stuck on a disk, which serves as an excitation reference.

Figure 41. Power Strip (circled) Used to Optimize the Acoustic Thermography System

For each independent variable, a correlation coefficient was calculated to determine how much of the signal coming from the power strip was affected by each of the independent variables. The coefficient is on a scale from -1 to 1, where values close to 0 indicate no correlation and values close to -1 or 1 indicate a very strong inverse or direct correlation, respectively. The following independent variables were selected to determine how they affect the signal observed from a power strip.

7.2.1 Amplitude.

The range of 70 to 100% was selected to study the effect of amplitude on power-strip signal. A scatter plot of the recorded measurements can be seen in the graph (figure 42).

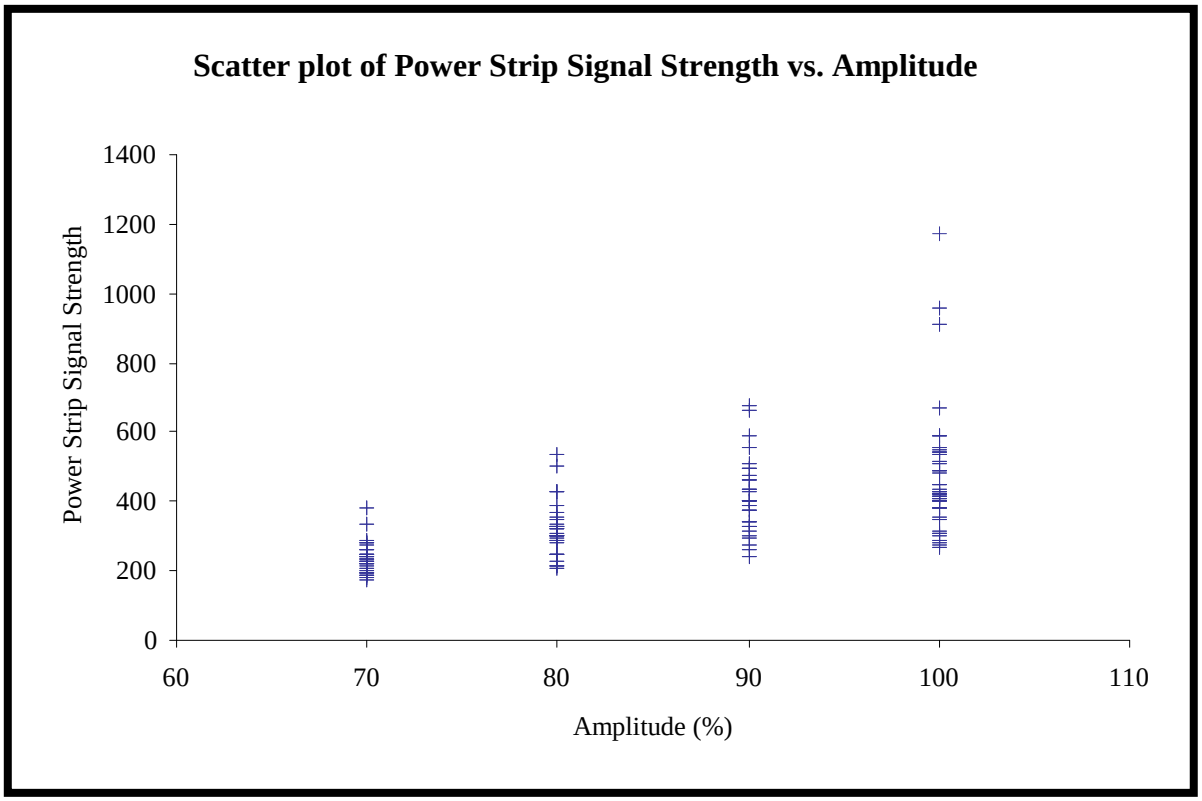

Figure 42. Scatter Plot of Power Strip Signal Strength vs. Amplitude

The correlation coefficient between the amplitude and the power-strip signal strength was calculated to be 0.604. The correlation coefficient indicates that the horn contact pressure has a moderate effect on power-strip signal. This positive value of correlation indicated that, to achieve higher signal strength, the amplitude needs to be maximized. It should also be noted that the higher the amplitude setting, the greater the scatter in signal from the power strip. This would indicate that the same crack excited several times at high amplitude would give a large range of thermal signals compared to the same crack excited at low amplitude. It should also be noted that the lower bound of the power strip signal rises with increased amplitude, even though the variation in signal also increases with amplitude. Therefore, it is concluded that the amplitude should be maximized to achieve the best signal.

7.2.2 Horn Contact Force.

The Branson system uses a pneumatic cylinder to load the horn against the part, as shown in figure 43.

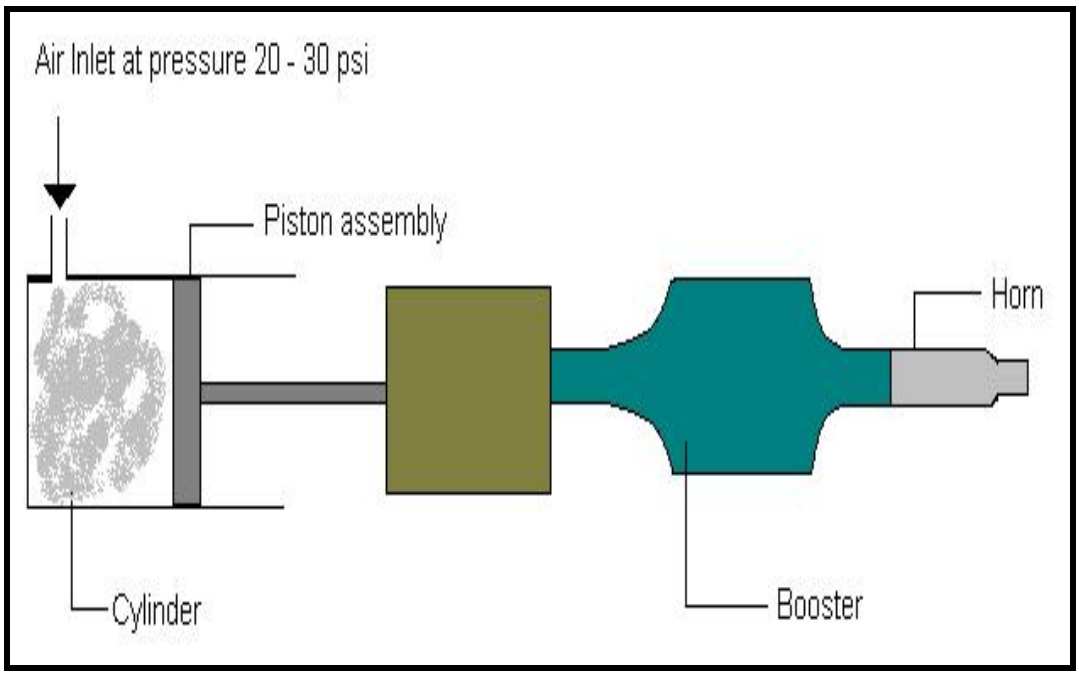

Figure 43. Schematic of the Horn Assembly

The force with which the horn is pressed onto the part is defined by:

Force = Pressure x Area

Pressure = pneumatic cylinder inlet air pressure

Area = cross-sectional area of the pneumatic cylinder

The diameter of the cylinder used in the Branson 2000ea actuator is 76.2 mm (as specified by the manufacturer). Optimization of the horn contact force was conducted at three air inlet pressures (20 psi, 30 psi, and 40 psi). This corresponds to 628N, 943N, and 1257N, respectively. A scatter plot of the recorded measurements can be seen in figure 44.

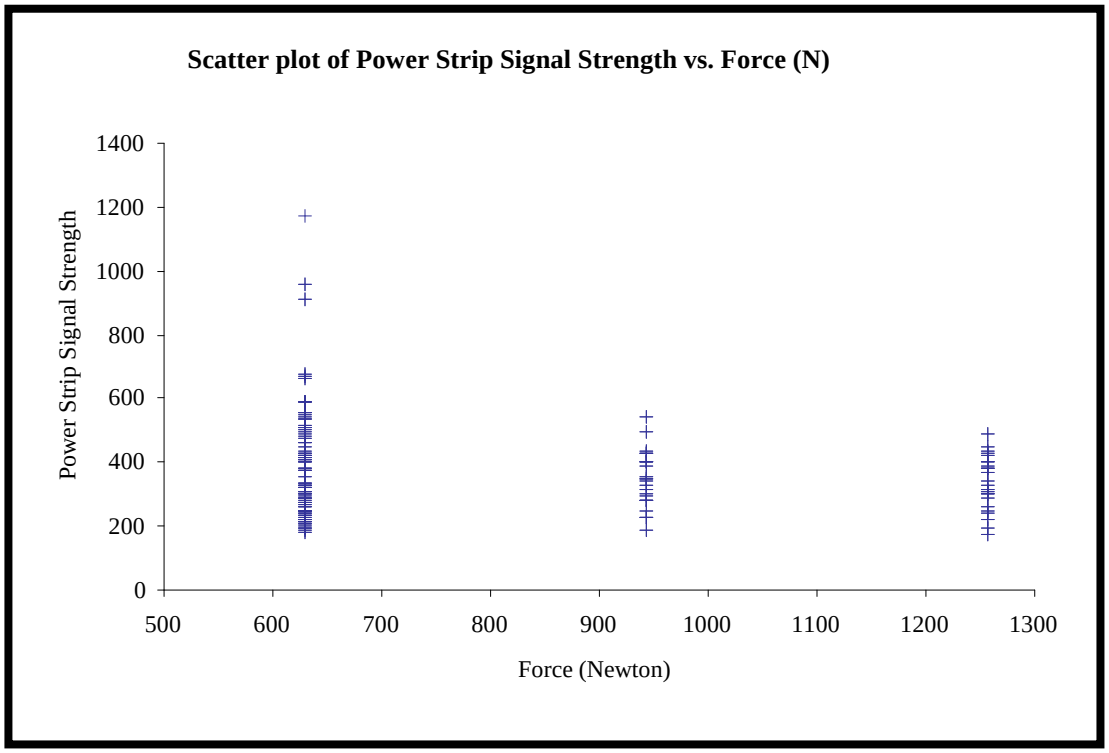

Figure 44. Scatter Plot of Power Strip Signal vs. Horn Contact Force

The correlation coefficient between power-strip signal strength and pressure was calculated to be -0.143. The coloration coefficient indicates that the horn contact force has a moderate effect on power strip signal. The negative correlation meant that, to obtain higher signal strength, the contact force needs to be minimized. It was observed that the signal from the power strip shows more variability at lower pressures than at higher pressures. In this study, it was also observed that the increase in the variation in signal with lower contact force is compensated for by an increase in the average signal with the decrease in contact force. Therefore, it is expected that decreasing the force will not decrease the lower bound of the indication signal, even though the variability increases. At lower contact pressure, there is a better probability of getting a larger indication from the same location. Thus, it is recommended that the contact pressure be minimized.

7.2.3 Horn/Disk Contact Area.

The contact area is determined by coating the horn tip with a dry erase marker and placing a paper on the surface of the disk where the horn would contact the disk. A horn-down procedure is then followed and, when the horn is made to retract, it leaves a mark on the paper covering the area where it contacted the disk with ink. A picture of the setup used is shown in figure 45.

Figure 45. Setup Used to Determine the Horn Contact Area

The angle of the horn assembly is changed and the horn-disk contact area test is performed at every new angle position. Appendix B shows the result of the horn-disk contact area test on side A and side B of the disk used for optimization purposes. The angle with the maximum area impression is then used for inspecting one side of the disk. As soon as the disk is flipped over, the horn-disk contact area test is repeated. The correlation coefficient between the power-strip signal and the horn-disk contact area is 0.044. This indicates that variation in contact area from 20 to 30 mm^2 might not play a very large part in determining the signal from the power strip.

7.2.4 Clamping Torque.

The clamping torque is the torque used on the chuck key to open the disc grips on the ID of the disk holding it in place (figure 46). A torque of 20 ft-lb was selected to determine the optimum clamping torque to hold the disk in position so that the signal strength increased and the edge effect was at the minimum.

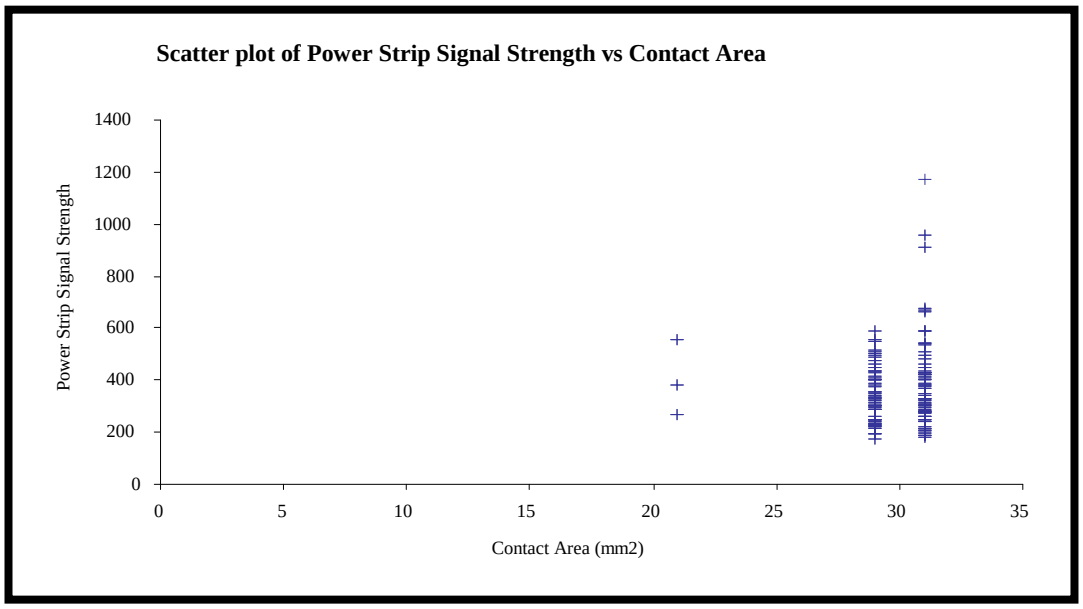

Figure 46. Scatter Plot of Power-Strip Signal vs. Contact Area

A torque of 15 ft-lb was not chosen because, when it was excited with the horn, it was not strong enough to hold onto the disk. The power strip signal measurements recorded for the experiments presented the following scatter plot as seen in figure 47.

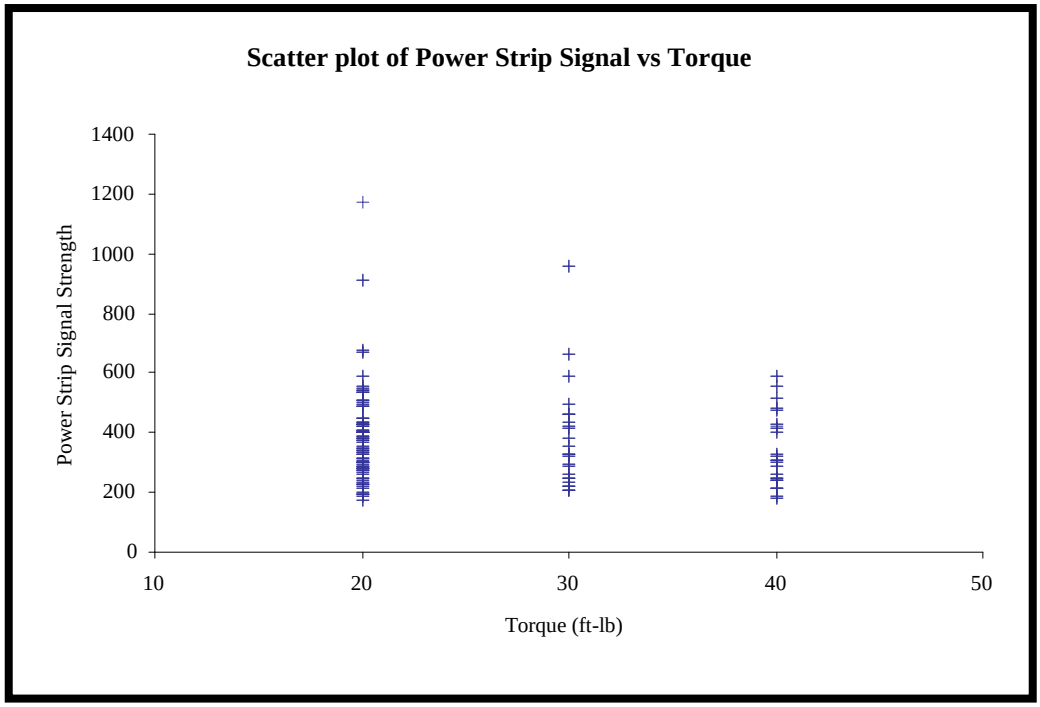

Figure 47. Scatter Plot of Power Strip Signal vs. Clamping Torque

The correlation coefficient for the relationship between power-strip signal strength and torque was calculated to be -0.080. This low value for the correlation coefficient indicates that the clamping torque does not affect the power strip signal.

The clamping torque should be large enough to hold the disk steady, but increasing it does not affect the thermal signal from the power strip. A disk that is held too loosely will show edge effect in the resulting acoustic thermography images. The edge effect is the result of the disk shifting during the measurement cycle. It is identified by an outline of the edges of the part in the background-subtracted and pulse-phase results.

7.2.5 Ambient Temperature.

Since the experiments were being performed in a temperature-controlled environment, variations were possible. Thus, the ambient temperature varied in a range from 67°F-75°F. The correlation coefficient calculated was -0.007. Although this coefficient is negative, it is extremely close to zero, meaning that temperature has hardly any effect on the signal strength. A scatter plot of signal strength versus temperature shows that this conclusion is valid (figure 48).

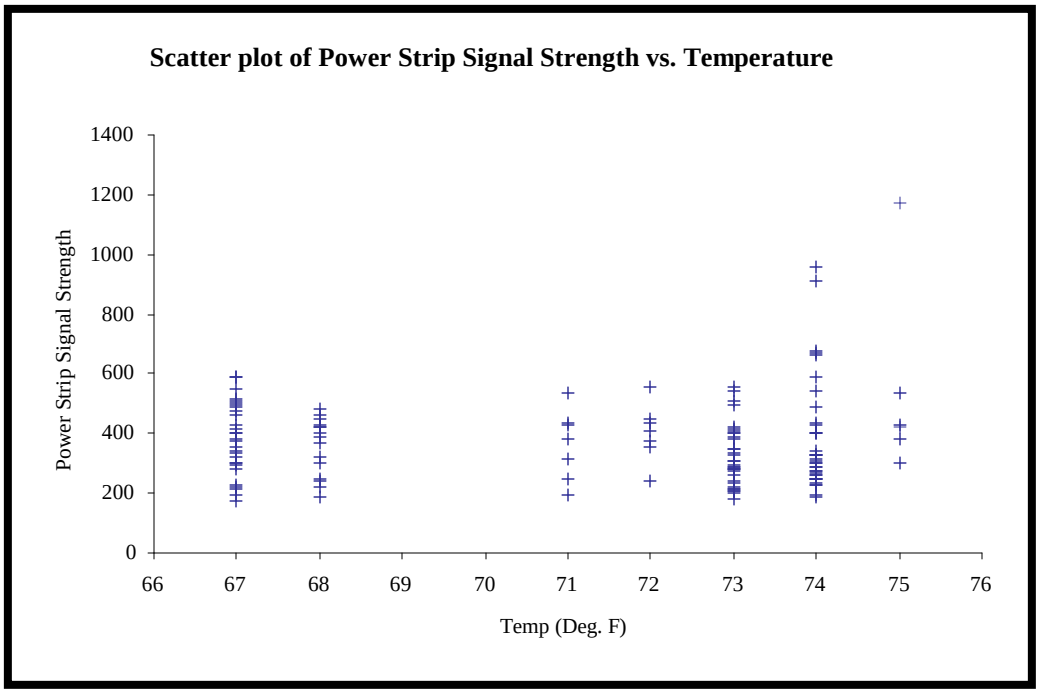

Figure 48. Scatter Plot of Power Strip Signal vs. Ambient Temperature

Data was collected for experiments that were carried out using design of experiments and the values of each of the independent variables were changed in the following range:

- Amplitude: 70% - 100%
- Contact Force: 628N-1257N
- Contact Area: 21 mm^2 + 31 mm^2
- Clamping Torque: 20 ft-lb to 40 ft-lb
- Ambient Temperature: 67°F to 75°F

7.2.6 Multiple Linear Regression.

After collecting the data, a multiple linear regression was made to correlate each independent input variable with the max signal observed from the power strip. This regression accounted only for independent linear coefficients (ignoring cross terms) and takes the form shown in the following equation of regression:

$$ThermalSignal_{\text{Max}} = C_{Amp} * Amplitude + C_{Force} * Force + C_{ContactArea} * ContactArea + C_{Torque} * Torque$$

Table 8 summarizes the results of multiple linear regressions.

Table 8. Multiple Linear Regression Results

Summary	*R*-Square	Standard Error of Estimate	*p*-Value
	0.3820	113.4048591	< 0.0001
Regression Table	Coefficient	*t*-Value	*p*-Value
Constant	-439.921	-2.5777	0.0105
Amplitude (%)	7.331257	11.8547	< 0.0001
Force (N)	-0.07583	-2.3061	0.0219
Contact Area (m^2)	9624472	2.2824	0.0233
Torque (Nm)	-1.10757	-1.4436	0.1501
Temperature (°C)	-0.70997	-0.1643	0.8696

R-square—This is also called the coefficient of determination and is a measure of the closeness of fit. It shows how much of the dependent variable (in this case, the crack signal strength) is explained by the independent variable (in this case, the amplitude, pressure, horn-disk contact angle, tightening torque, ambient temperature, and the total number of prior excitations). The greater the value of *R*-square, the closer the fit, thus implying that the dependent variables (in this case, amplitude, torque, force, contact area, and ambient temperature) play a crucial role in determining the outcome of the independent variable (in this case, the power strip signal).

This multiple linear regression has an *R*-square value of 0.38. This is typically considered a fairly poor fit. Low *R*-square values indicate that either there is a lot of noise in the system, causing it not to behave deterministically, or that a significant independent variable is missing from the analysis. It is likely that there is a significant amount of noise in the system that is introduced at the horn–part contact location.

Standard error of estimate—This gives the error of the fit. For any values substituted in the regression equation, the result will have an error indicated by the standard error of estimate. For this regression, the result will have an error of 113 counts.

P-value—For *p*-value less than 0.0001, there is a strong relation between independent and dependant variables.

Coefficient—This value is the multiplying factor for each variable in the equation of regression.

t-value—If t-value<|1|, then the variable is not useful for the regression model and has no effect on the dependent variable. As seen from the regression results, ambient temperature as a variable is not useful for the regression model.

If |1|<t-value<|2|, then the variable's effect on the dependent variable is indeterminate. As seen in the regression results, the effect of torque on power strip signal is indeterminate. It could take many experiments to ultimately conclude whether the effect of torque is useful or not useful on

the power strip signal.

If t-value>|2|, then the variable is a good predictor of the regression model and has a significant effect on the dependent variable. As seen from the regression results, amplitude, force, and contact area are all good predictors of the regression model. However, the positive t-values indicate that an increase in values of amplitude and contact area will lead to an increased power strip signal, while the negative t-value of force implies that the lower the force, the higher the power strip signal will be.

The following conclusions were drawn regarding the crack signal strength:

- Amplitude is the most important factor affecting signal. Signal strength increases with increase in amplitude.
- Crack signal strength increases with decrease in force.
- Horn–Disk contact area does affect the signal strength. A larger contact area yields higher signal strength.
- Effect of torque on crack signal strength is still judgmental.
- Ambient temperature has no effect on the power-strip signal strength

7.3 TESTING RESULTS OF SELECTED DISKS.

7.3.1 United States Air Force Disk Inspection.

The inspection of four compressor United States Air Force (USAF) disks was completed during this program. This inspection included acoustic thermography and digital microscope inspection techniques. For each disk, an acoustic thermography test was conducted viewing the forward side and aft sides of the disk. For each marked location on the disk, a macro view acoustic thermography test and digital microscopy was conducted. The setup for the inspection of the USAF disks is shown in figures 49 and 50.

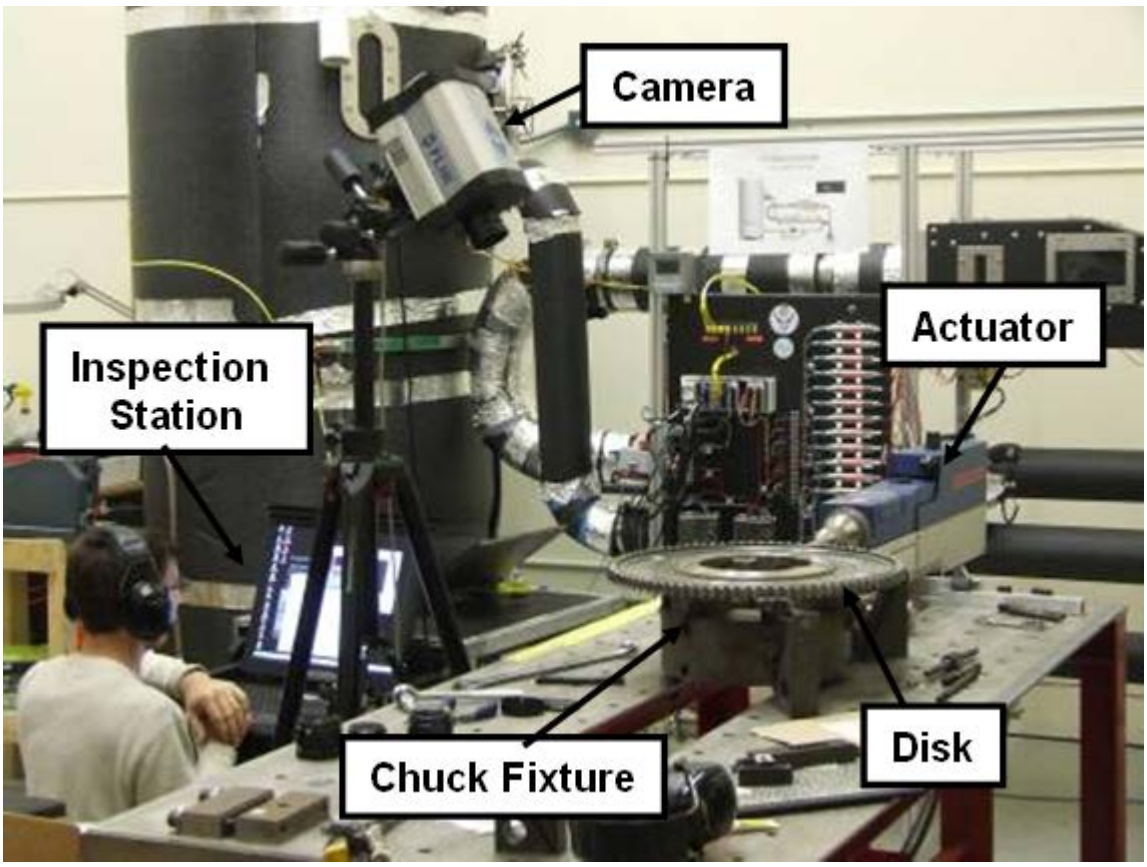

Figure 49. Overview of Acoustic Thermography Testing Setup for the Inspection of the USAF Disks

In this setup, the actuator is oriented so that the horn contacts the OD of the disk at the steeples to couple the 20 kHz ultrasonic energy into the part. The part is held in place with a lathe chuck where the three jaws of the chuck are in contact with the ID of the disk. The camera is oriented at an oblique angle above the disk to image the full upper face and the edge of the disk closest to the camera. The inspection station is placed out of the field of view of the camera and where the reflection of the inspector cannot be observed by the camera.

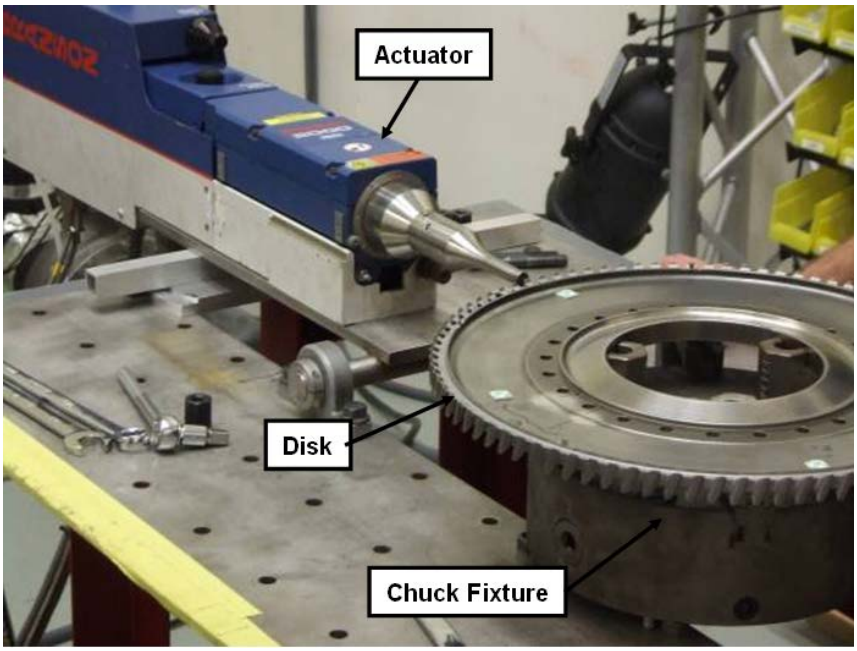

Figure 50. Detailed View of the Acoustic Thermography Test Setup Showing How the Fixture, Part, and Actuator Are Oriented

Observed indications and marked regions were inspected with the use of a digital microscope to determine if indications marked or detected by acoustic thermography could be visually verified. The setup for the digital microscope inspection is shown in figure 51.

Figure 51. Setup for the Digital Microscope Verification of Marked Indications

Figures 52 through 61 show the indications observed by either acoustic thermography or digital microscopy. Indications are organized by disk and marked according to the designation observed on the disk at the marked location.

7.3.1.1 Disk AF 1.

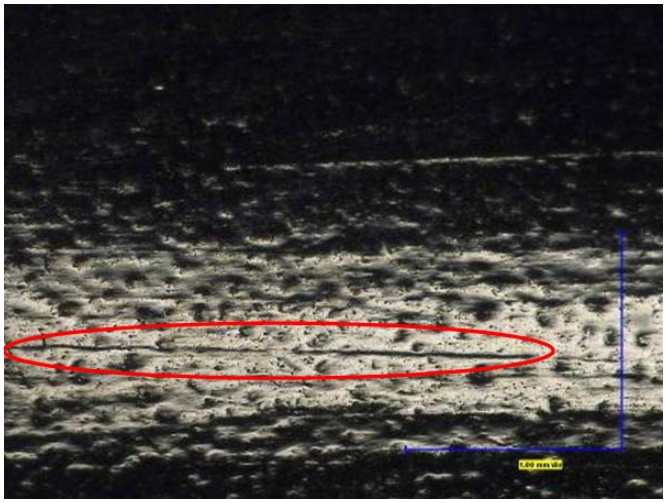

Figure 52. Indication 1b on Disk AF1 Observed by Digital Microscopy

This indication was observed by digital microscopy on disk AF1 and in marked location 1b. The indication was not observed by acoustic thermography. It is not clear that this indication should give a thermal signal when excited by acoustic thermography.

7.3.1.2 Disk AF 2.

Figure 53. Indication 1b on Disk AF2 Observed by Digital Microscopy

The indication shown in figure 53 was observed by digital microscopy on disk AF2 and in marked location 1b. The indication was not observed by acoustic thermography and it is not

clear whether this indication should give a thermal signal when excited by acoustic thermography.

7.3.1.3 Disk AF 3.

The indication shown in figure 54 was observed by acoustic thermography on disk AF3 and in marked location #2. The indication was not conclusively observed by digital microscopy.

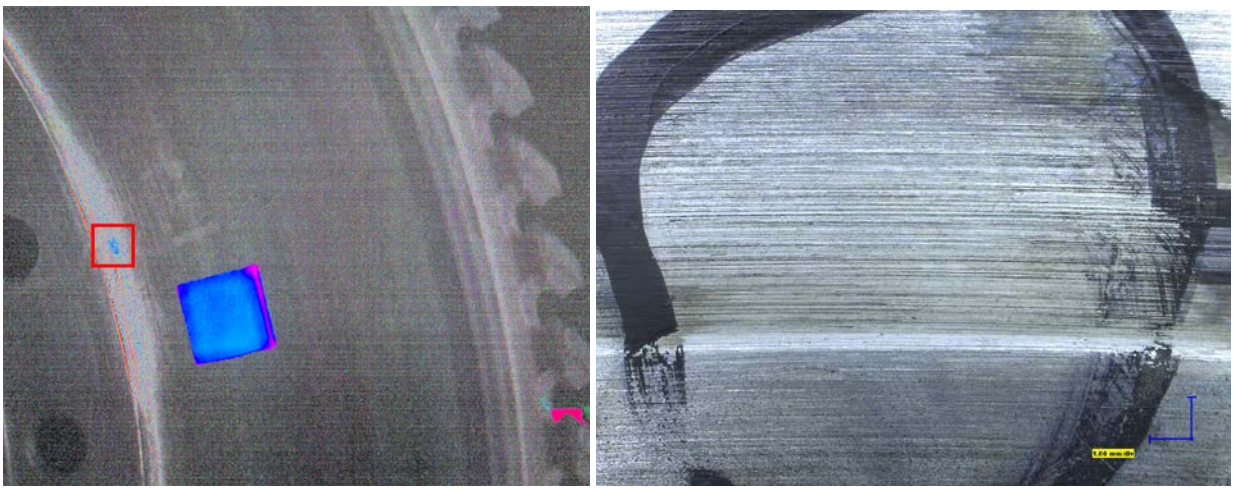

Figure 54. Indication #2 on Disk AF3 Observed by Acoustic Thermography (left) and Digital Microscopy (right)

While several indications were observed in the region marked #4 on disk AF3, no indication was conclusively observed in the digital microscopy image shown in figure 55.

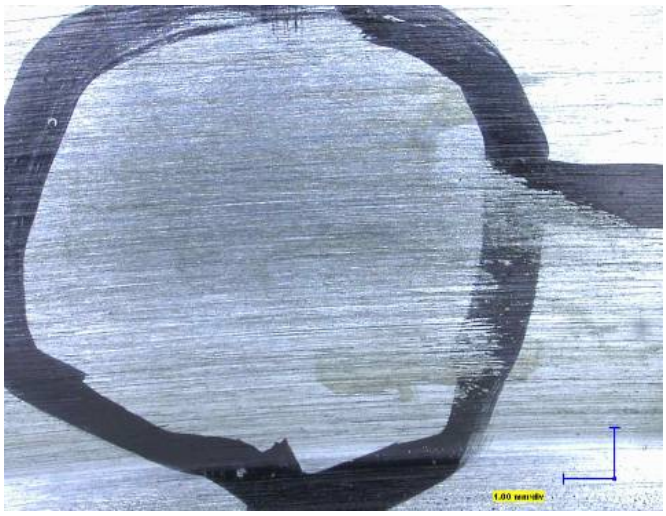

Figure 55. Indication #4 on Disk AF3 Observed by Digital Microscopy

While several indications were observed in the region marked #5 on disk AF3, no indication was conclusively observed in the digital microscopy image shown in figure 56.

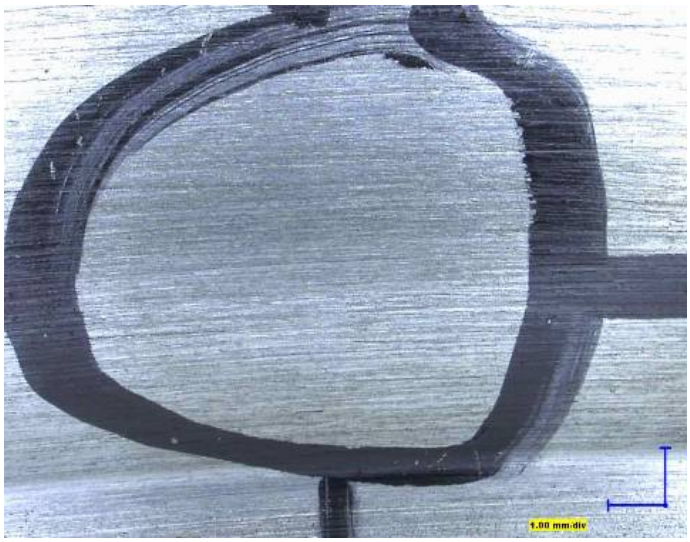

Figure 56. Indication #5 on Disk AF3 Observed by Digital Microscopy

7.3.1.4 Disk AF 4.

Acoustic thermography did observe thermal emission from an anti-rotation tab on disk AF4 (figure 57). This indication was not originally identified by a USAF mark and was not subsequently identified in digital microscopy images. The large amount of thermal energy released in this area suggests that there are many microcracks in this region. This has not been verified by destructive testing.

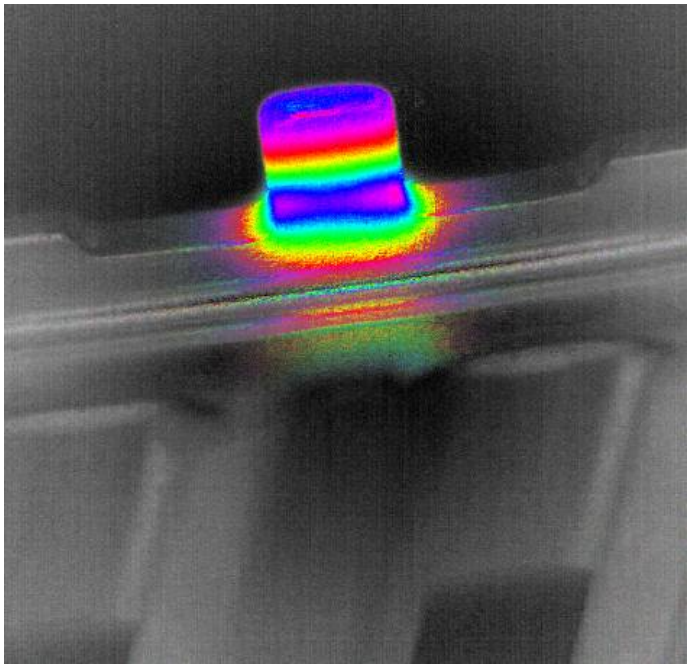

Figure 57. Disk AF4 Anti-Rotation Indication

The indication shown in figure 58 was observed by acoustic thermography on disk AF4 and in marked location #1. It is not clear that this indication should give a thermal signal when excited by acoustic thermography.

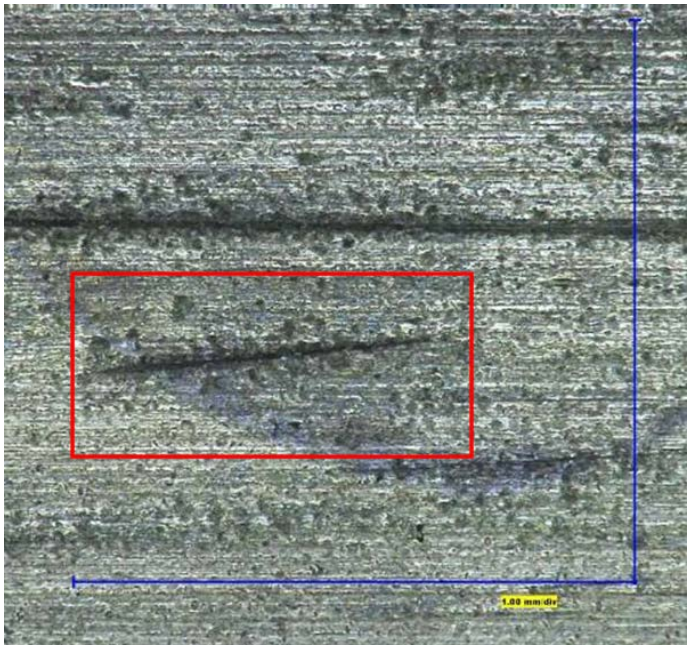

Figure 58. Indication #1 on Disk AF4 Observed by Digital Microscopy

The indication shown in figure 59 was observed by acoustic thermography on disk AF4 and in marked location #4. It is not clear that this indication should give a thermal signal when excited by acoustic thermography.

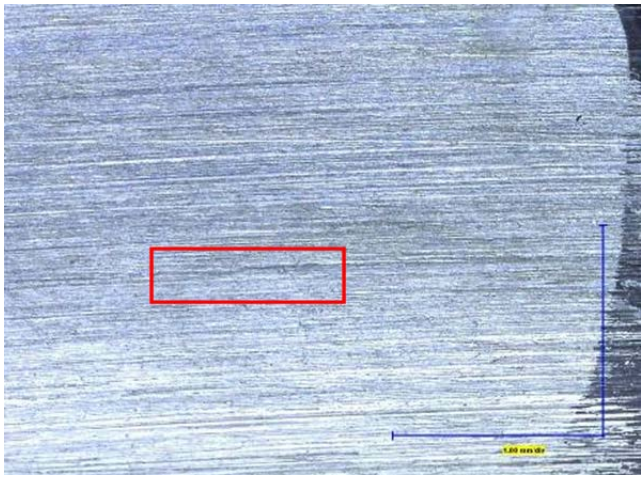

Figure 59. Indication #4 on Disk AF4 Observed by Digital Microscopy

The indication shown in figure 60 was observed by acoustic thermography on disk AF4 and in marked location #13. This indication was proven to be a scratch on the surface and is not expected to be detected by acoustic thermography, but may be detected by other inspection techniques.

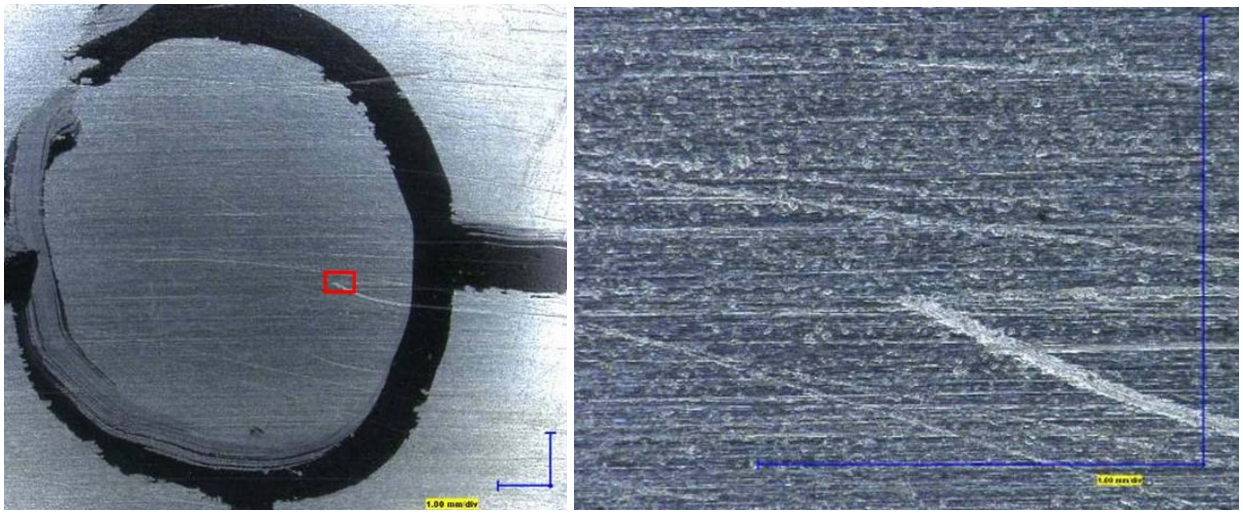

Figure 60. Indication #13 on Disk AF4 Observed by Digital Microscopy

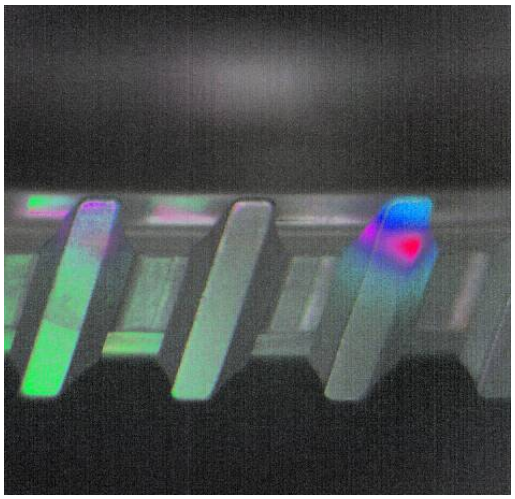

Figure 61. The USAF Disk AF4 Indication on Blade Attachment Point

Thermal emission was also observed from one of the serrations that hold the blades to the disk on disk AF4 (figure 61). This indication was not marked prior to inspection and no corresponding indication was observed using digital microscopy. It is hypothesized that this indication could be a collection of microcracks in the region. This has not been verified by destructive testing.

7.3.1.5 Summary of USAF Disk Inspection.

It was observed that only one of the marked indications on the four disks showed a very small indication signal (AF3–#2), as shown in table 9. Subsequent verification with the use of the digital microscope provided information on surface features that may have caused an eddy current indication, but no obvious signs of actual cracking were present. It is recommended that this indication be further investigated for relevancy.

Table 9. Summary of Acoustic Thermography Results for USAF Disks

Indication ID	USAF Marked	Siemat Indication	Microscope Indication
AF1 - #1a	Yes	No	No
AF1 - #1b	Yes	No	Yes
AF2 - #1a	Yes	No	No
AF2 - #1b	Yes	No	Inconclusive
AF2 - #1c	Yes	No	No
AF3 - #1	Yes	No	No
AF3 - #2	Yes	Low Signal	Inconclusive
AF3 - #3	Yes	No	No
AF3 - #4	Yes	No	Inconclusive
AF3 - #5	Yes	No	Inconclusive
AF4 – AR	No	Yes	No
AF4 - #1	Yes	No	Yes
AF4 - #4	Yes	No	Yes
AF4 - #13	Yes	No	Yes
AF4 - #Ind	No	Yes	No

Another two indications were observed by acoustic thermography that were not originally marked by the USAF (AF4 – AR and AF4 – Ind). These indications are marked on the part and indicated with the AT label. These indications also showed no visible signs of cracking during digital microscope verification. It is hypothesized that these indications could be the result of localized variations in metallurgical properties, microcracking, or subsurface heating sources. These two indications should be further investigated.

7.3.2 Results From Acquired Disk.

Disks were acquired for inspection from our program industry partners: Delta, Rolls-Royce, and the NDI Testing and Validation Center. Disks were also acquired from Miami NDT, an aircraft engine overhaul and inspection facility.

Disks were inspected using acoustic thermography, fluorescent penetrant inspection (FPI), and visual inspection techniques. Indications observed by any of the inspection techniques were further investigated with the use of a digital microscope. Acoustic thermography was conducted twice on each disk. First, the IR camera was placed so as to observe the disk from an oblique

angle, allowing for inspection of the edge of the disk as well as the top (figure 62). When the camera was placed above the disk, a mirror was placed so that the edge of the disk could also be observed at the bottom of the field of view, as indicated in the right-hand image of figure 62.

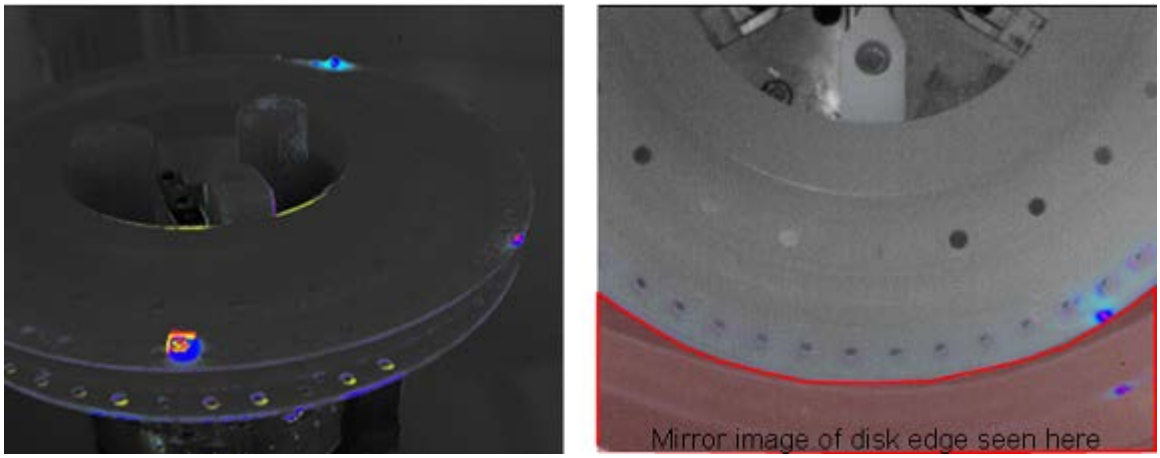

Figure 62. Acoustic Thermography Performed With the Camera Placed at an Oblique Angle to the Disk (left) and Placed Above the Disk Using a Mirror to See the Edge of the Disk (right)

Figure 63 shows the physical placement and geometry of the mirror when used with the horizontal mount setup and the lathe chuck fixture. The use of mirrors can increase the inspection area at the cost of spatial resolution as long as there is sufficient depth of field to keep both images in focus.

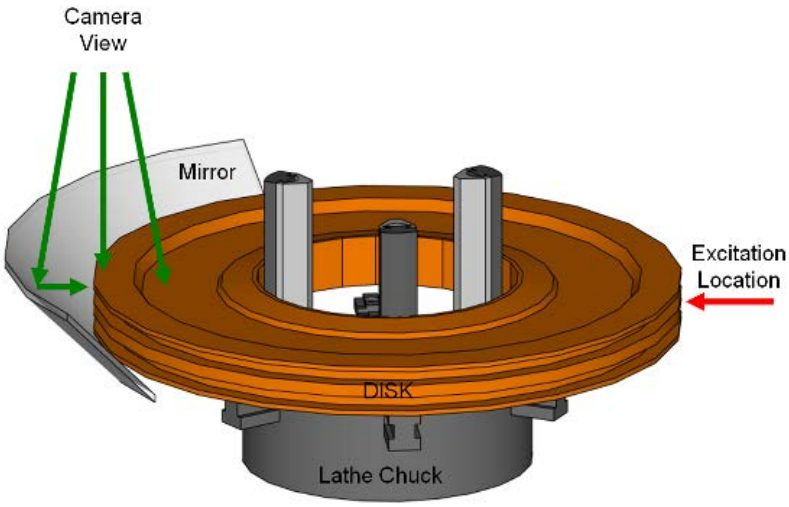

Figure 63. Use of the Mirror in the Horizontal Mount Setup for Viewing the Edge and Top of the Disk at the Same Time

7.3.2.1 Rolls-Royce Solid Head Disk.

Rolls-Royce provided a solid head disk that is used for quality control in their FPI process (figure 64). This disk is approximately 200 lbs and 30 in. in diameter.

Figure 64. Top (left) and Bottom (right) of the Solid Head Disk Provided by Rolls-Royce

This disk has several indications documented by Rolls-Royce by FPI in four specified zones located in the web close to the bolt circle.

Figure 65 (left) shows the marked inspection zones 23 and 24 on the solid head disk. Rolls-Royce provided photocopied images of the indications observed by an FPI conducted in those zones under white-light and black-light illumination (figure 65 (right)).

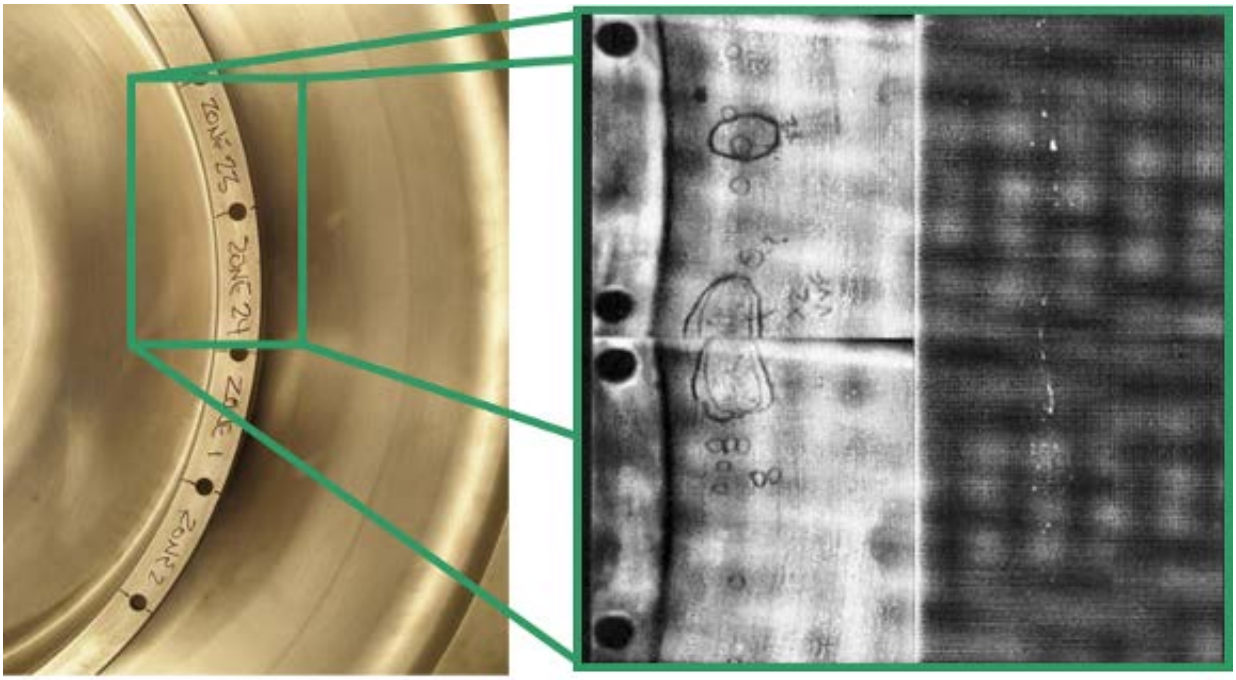

Inspection Zones | White-Light Illumination | Black-Light Illumination

Figure 65. Locations of Observed Indications in Zones 23 and 24 on the Rolls-Royce Solid Head Disk

Inspection zones 1 and 2 on the solid head disk are shown in figure 66. The left-hand side of this figure shows the zones marked on the part as received. Rolls-Royce also provided the documentation of FPI indications in zones 1 and 2 under white-light and black-light illumination (figure 66, right).

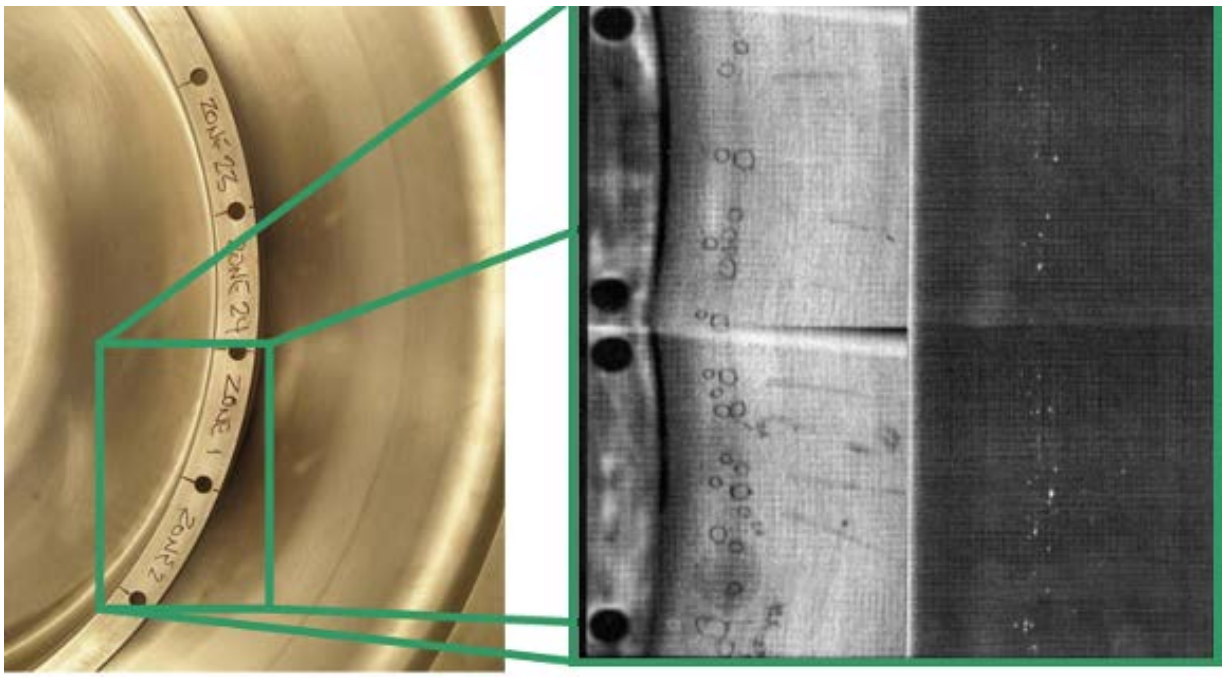

Inspection Zones | White-Light Illumination | Black-Light Illumination

Figure 66. Locations of Observed Indications in Zones 1 and 2 on the Rolls-Royce Solid Head Disk

In all four marked zones, several FPI indications were observed, providing several inspection opportunities.

The initial acoustic thermography inspections of the solid-head disk using a 20 kHz system in the horizontal-mount configuration did not result in any indications in any of the four inspection zones. The disk was sent for inspection with a 40 kHz acoustic thermography system to Wayne State University, where one indication with the 40 kHz excitation system was identified.

The FPI of the four zones on the solid-head disk revealed 13 indications shown in figure 67. Each of these indications was investigated with the digital microscope.

Figure 67. Thirteen Indications Observed by FPI at Siemens

Three types of features were observed in eight of the 13 indications detected by Siemens' FPI (figure 68). Several indications were identified as somewhat deep pits in the surface that could easily hold penetrant, but would not be expected to generate an acoustic thermography signal. One overlap indication was observed, which looked like some metal had been smeared over and pressed to the surface. The indication was about one-tenth of a millimeter long. Indications like this should be detected by acoustic thermography. The last type of indication observed is a fine crack that may or may not be accompanied by a pit. Acoustic thermography is expected to find these indications.

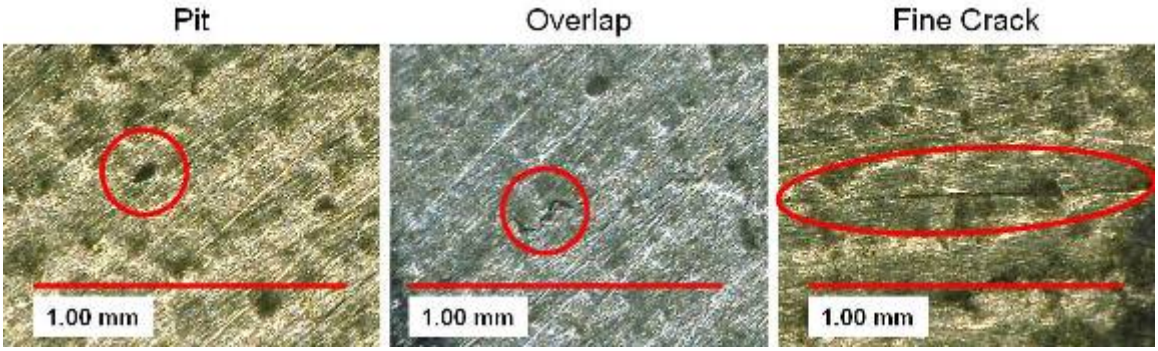

Figure 68. Types of Indications Observed on the Solid Head Disk

Table 10 shows the type of indication observed at each numbered indication in figure 67.

Table 10. Type of Indication Observed by Digital Microscopy for Each Observed Penetrant Indication

Indication Number	Observed Indication Type
1	Pit and fine crack
2	Overlap
3	Nothing
4	Pit
5	Pit
6	Nothing
7	Nothing
8	Nothing
9	Nothing
10	Pit
11	Pit
12	Pit
13	Pit and fine crack

There are three potential reasons why these indications were not observed by acoustic thermography. First, the indications are not very large and, thus, are not expected to propagate very deeply into the disk. The smaller the area of interacting surfaces within a cracklike indication, the less thermal energy is generated; thus, a smaller IR signal is observed. No destructive analysis was done to validate this. Second, the solid head disk is very rigid, so it may not move easily in response to the acoustic stimuli. This would cause less thermal energy to be generated. It was observed that indications closer to the hub of the disk will produce smaller signals than the same indications toward the rim of the disk (figure 28).

7.3.2.2 Disk-SN: BBDUAR7726.

Disk serial number BBDUAR7726 is a P&W second stage compressor disk. An orange adhesive rubber found painted on one of the inside flanges was very difficult to remove (figure 69). The rubber did produce some indications; thus, this region of the part could not be inspected.

Figure 69. The P&W Second-Stage Compressor Disk (SN: BBDUAR7726) (side A on left and side B on right)

The rest of the part was inspected by acoustic thermography using the horizontal mount setup and the mirror fixture so that both the side and edge of the disk could be inspected at the same time. A representative acoustic thermography image from each inspection setup is shown in figure 70. One can see in this image the indications related to the rubber coating (circled in red).

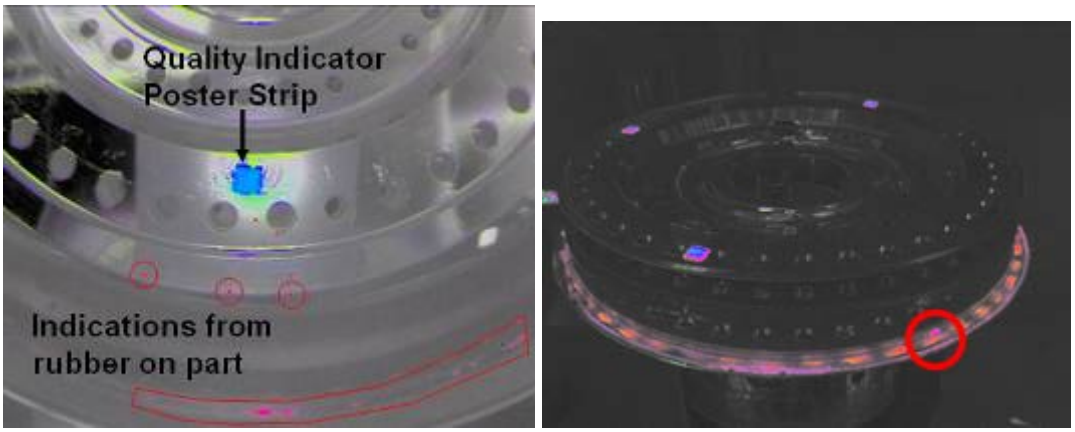

Figure 70. Representative Acoustic Thermography Results for the P&W Second-Stage Compressor Disk (SN: BBDUAR7726)

One indication observed in the region of the disk that had the rubber coating on it was further investigated by the removal of the rubber and further inspection with the digital microscope. The indication was not observed visually or by acoustic thermography after removal of the rubber. While other indications were observed, subsequent visual examination revealed that all of these indications were related to the rubber coating. No crack-like indications were observed on this disk by acoustic thermography, FPI, or visual testing.

7.3.2.3 Disk-SN: BENCAK4805.

Disk serial number BENCAK4805 (as shown in figure 71) is a P&W eighth-stage compressor disk. This disk was more challenging to hold onto using the lathe chuck fixture because of the small inner-bore diameter and chamfer on side B ID. It is suggested that a better fixture be developed for this style of disk if large quantities are expected to be inspected.

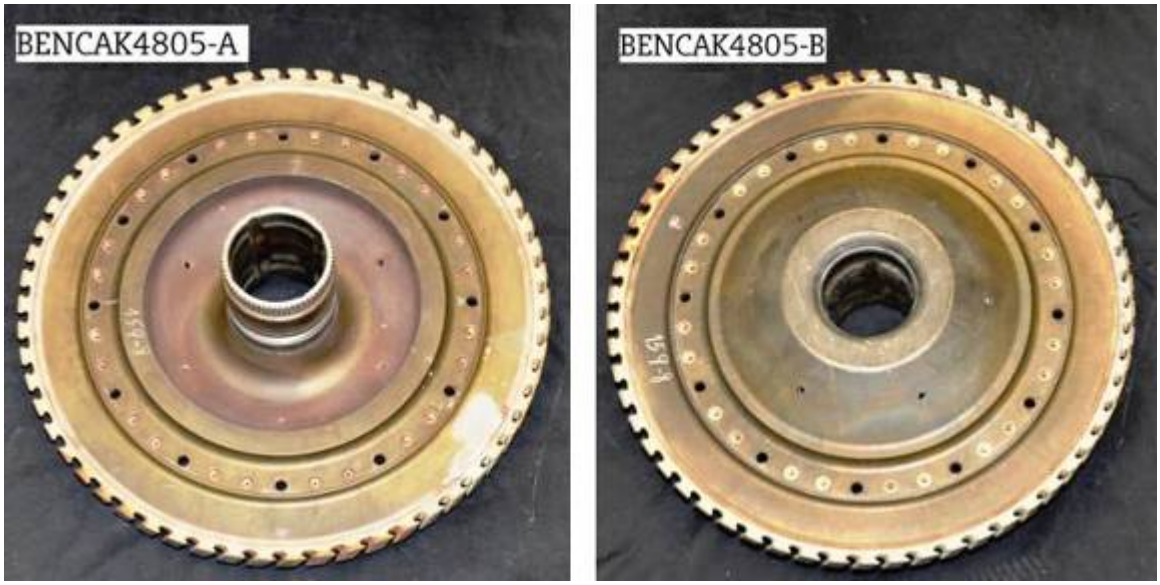

Figure 71. The P&W Eighth Stage Compressor Disk (side A on left and side B on right)

Every second and third bolt hole in the web of the disk contained a press fit bushing that emitted thermal energy when the disk was excited (figure 72). No other linear indications were observed on this disk by acoustic thermography.

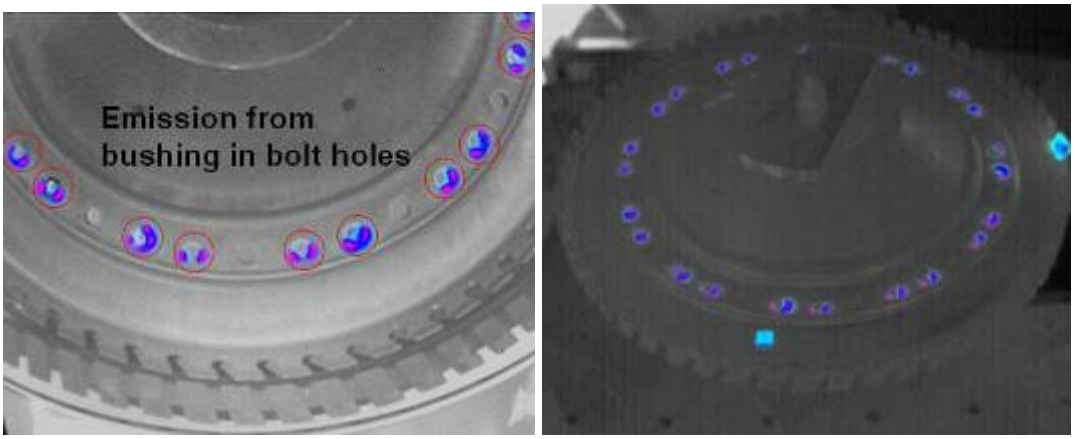

Figure 72. Representative Acoustic Thermography Results for the P&W Eighth Stage Compressor Disk (SN: BENCAK4805)

The FPI of this disk did result in one linear indication that was later observed to be a surface scratch by visual inspection (figure 73).

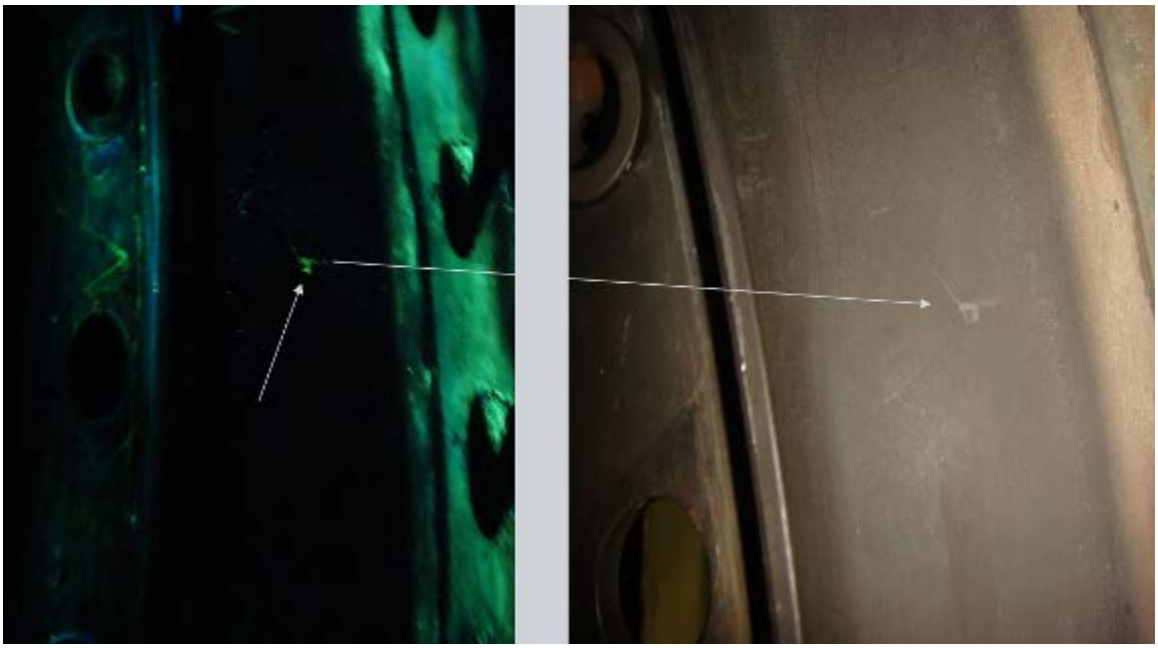

Figure 73. The FPI Observation of a Linear Indication (left) and an Indication Observed Under White Light Illumination (right)

7.3.2.4 Disk-SN: BENCAL3598.

Disk serial number BENCAL3598 is a P&W seventh-stage compressor disk (see figure 74). The disk displayed two visible indications on side A. The first, at the 2:00 position, is a clear crack going from the edge of the disk to the edge bolt hole. The indication is about 2-3 cm in length. The other indication, at the 10:30 position, appears to be an impact location where the thin edge of the disk has been bent up toward the camera. This indication was likely caused while the disk was being handled out of the engine.

Figure 74. The P&W Seventh-Stage Compressor Disk (side A on left and side B on right)

Acoustic thermography inspection of this disk revealed two linear indications. The first is related to the crack located at the 2:00 position on side A (figure 75). The indication is about 16-mm long and propagates from the edge of the disk to a bolt hole near the outer parameter.

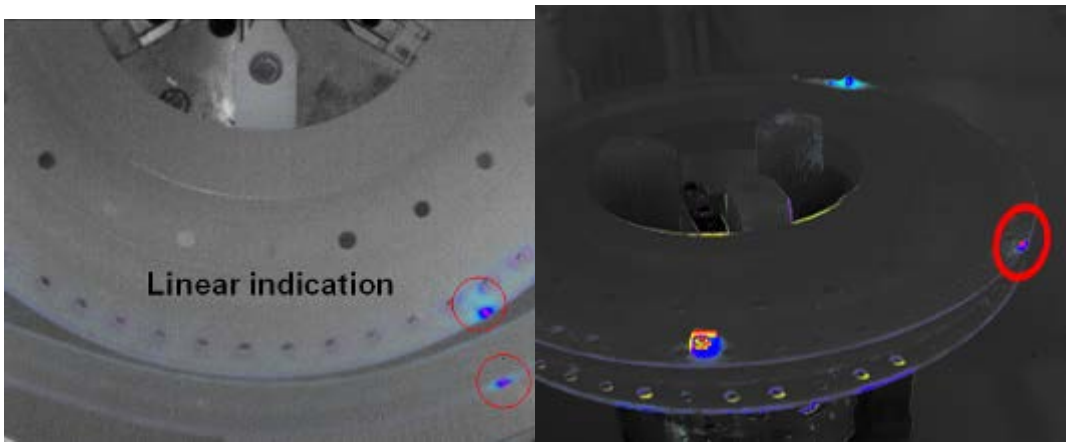

Figure 75. Linear Indication on BENCAL3598 at the 2:00 Position on Side A

The second indication is related to the impact location observed at 10:30 on side A. Each excitation caused the indication to grow. Figure 76 shows the indication after several excitations. In both images, the large amount of energy can be observed from the propagation of the indication during the test.

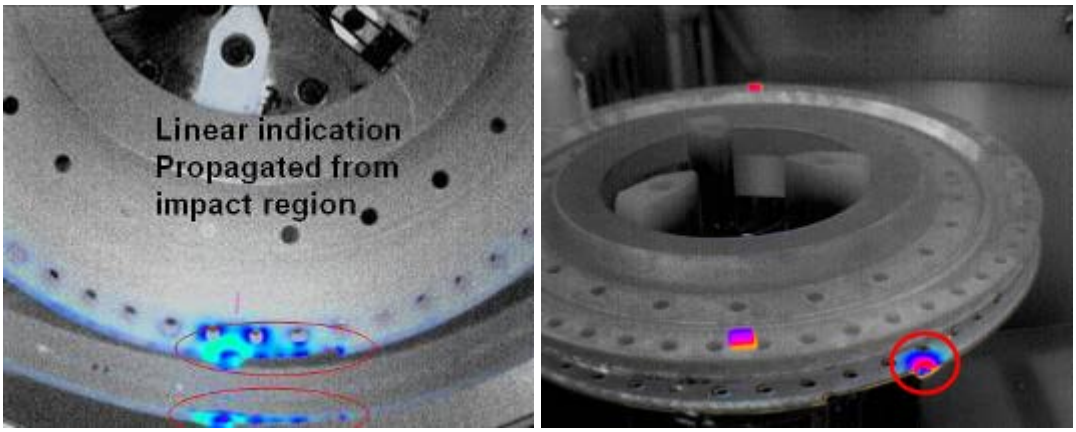

Figure 76. Linear Indication on BENCAL3598 at the 10:30 Position on Side A Propagated From Initial Indication in Impact Location

The pieces that came off from the propagation of the original indication were recovered and fit the location of missing material, shown in figure 77, top and the fracture surface can be seen at the bottom of that figure.

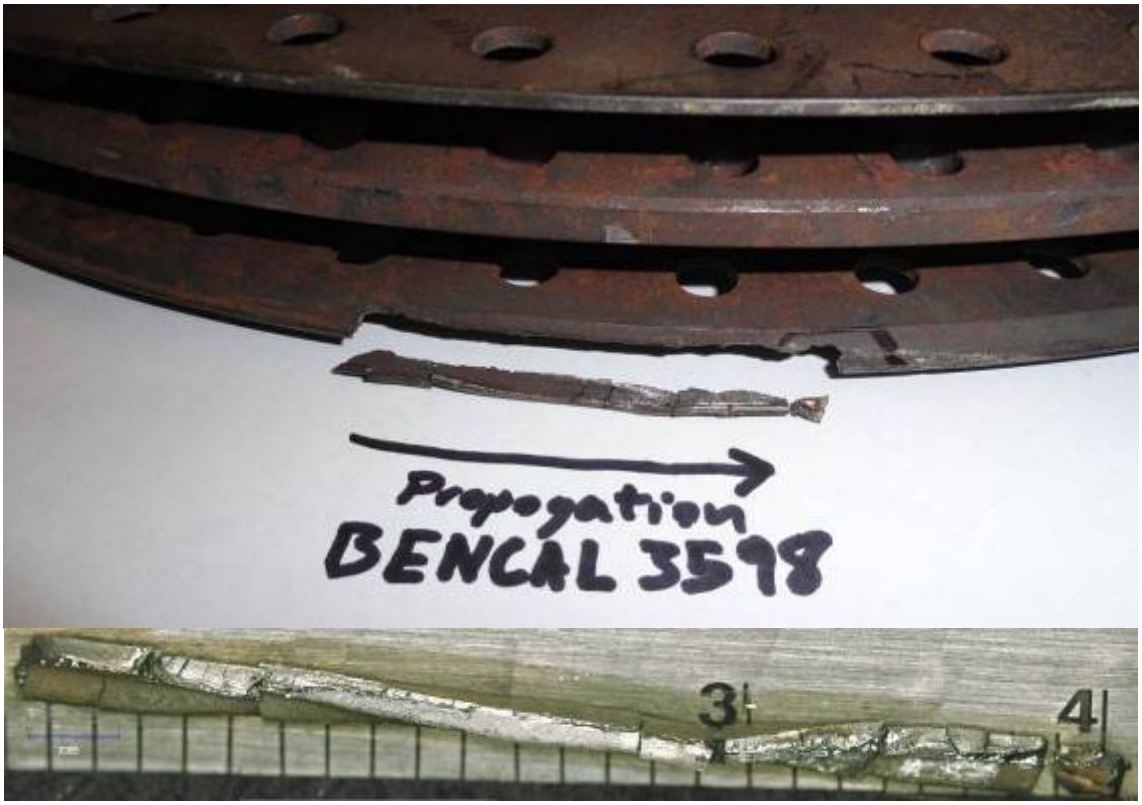

Figure 77. Pieces of the Disk SN: BENCAL3598 That Fell off Because of Crack Propagation: Fit (top); Fracture Surface (bottom)

An FPI revealed a chip in the rim of the disk that was verified by visual inspection. The results of the FPI and visual inspection are shown in figure 78. This indication was not detected by acoustic thermography and would not be expected to be.

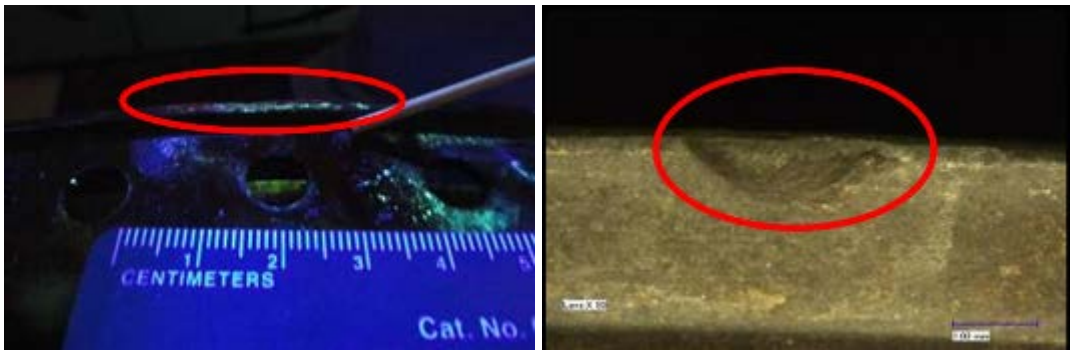

Figure 78. The FPI Indication (left) and Subsequent Visual Indication (right)

7.3.2.5 Disk-SN: BENCAN4671.

Disk serial number BENCAN4671 is a P&W eleventh-stage compressor disk (figure 79). No indications were observed on this disk by acoustic thermography (figure 80). One indication was observed on this disk by FPI. Visual verification showed that the FPI indication was caused by a surface scratch (figure 81).

Figure 79. The P&W Eleventh Stage Compressor Disk (side A on left and side B on right)

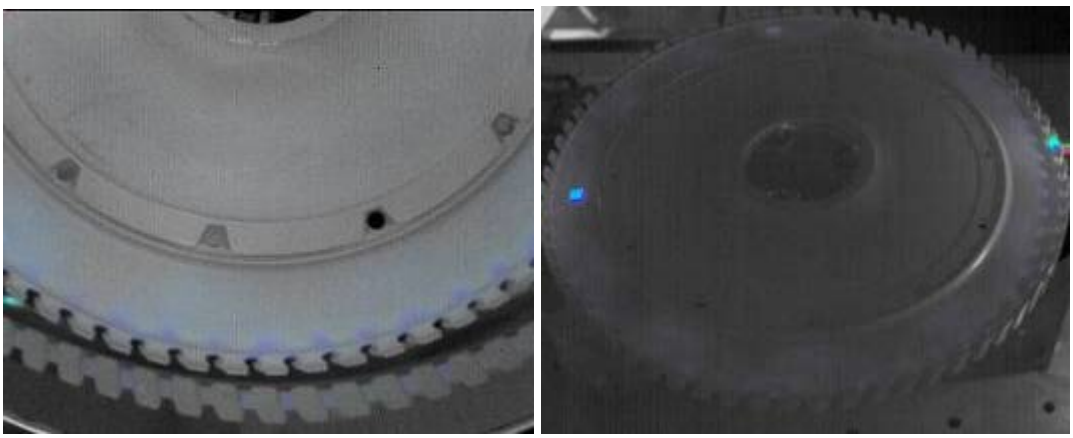

Figure 80. Representative Acoustic Thermography Results for Disk SN: BENCAN4671

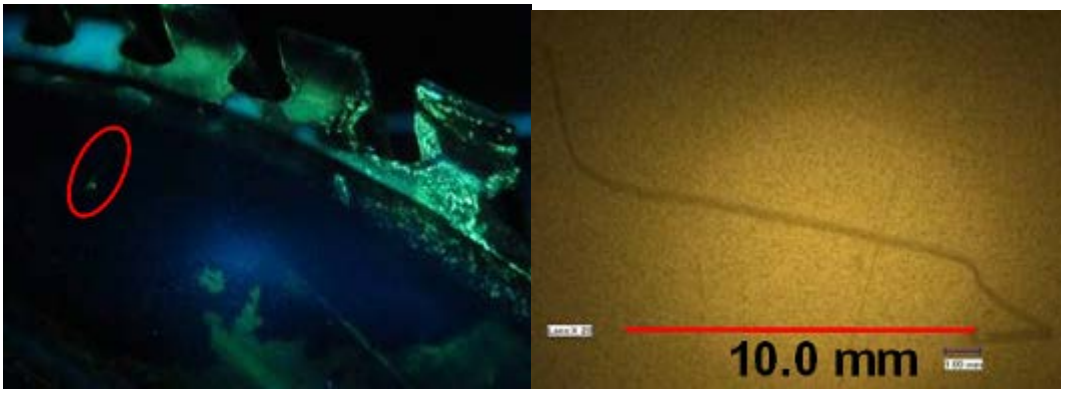

Figure 81. The FPI Indication (left) Related to a Surface Scratch (right)

7.3.2.6 Disk-SN: BENCAR6446.

Disk serial number BENCAR 6446 is a P&W tenth-stage turbine disk (figures 82 and 83). This disk showed no acoustic thermography or FPI indications.

Figure 82. The P&W Tenth-Stage Compressor Disk (side A on left and side B on right)

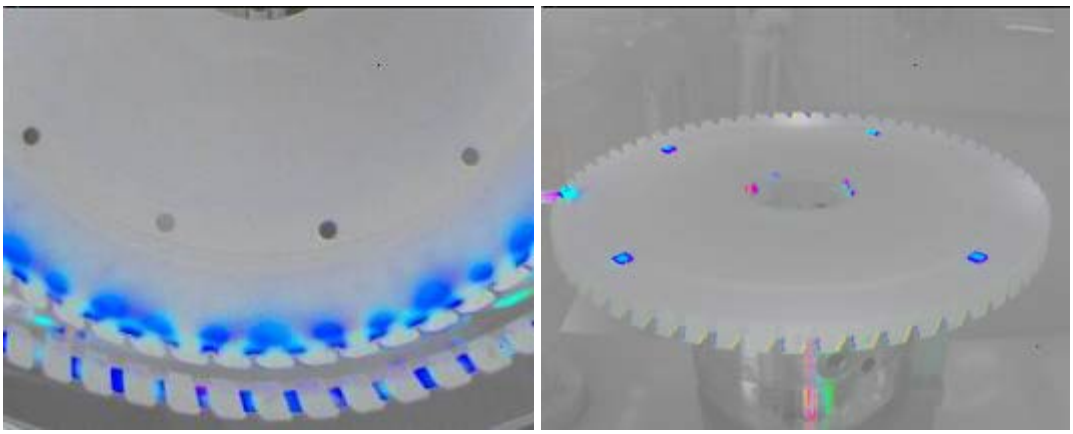

Figure 83. Representative Acoustic Thermography Results for Disk SN: BENCAR6446

7.3.2.7 Disk-SN: BENCAR9734.

Disk SN: BENCAR9734 is a P&W seventh stage compressor disk (figure 84). One indication was observed by acoustic thermography and two indications were observed by FPI on this disk.

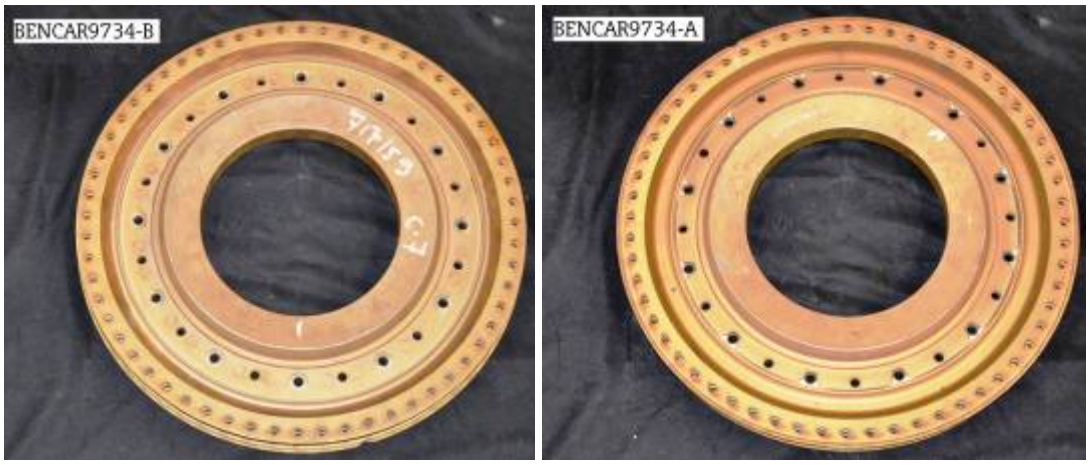

Figure 84. The P&W Seventh Stage Compressor Disk (side A on left and side B on right)

The first indication observed by acoustic thermography, FPI, and verified visually was located in an impact location (figures 85 and 86). The material was stressed to failure during the impact. No growth of the indication was observed during the acoustic thermography test.

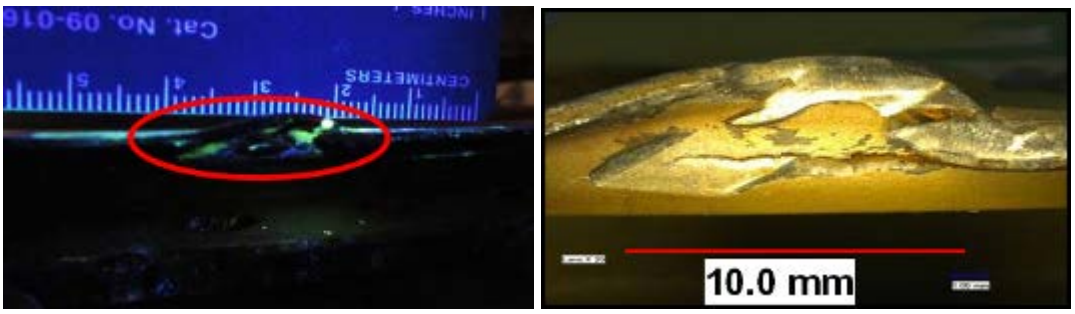

Figure 85. The FPI Indication (left) and Microscope Verification Image (right) for the First Indication Observed on Disk SN: BENCAR9734

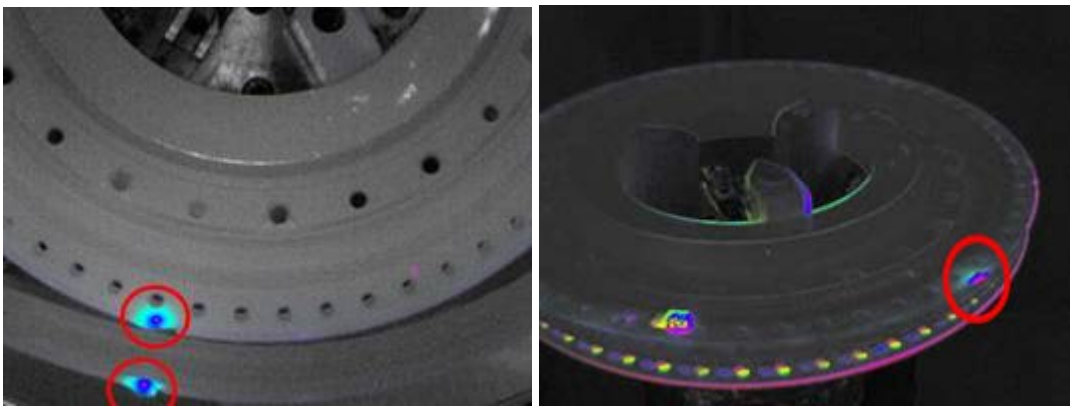

Figure 86. First Acoustic Thermography Indication Observed on Disk SN: BENCAR9734

The second indication was observed by FPI, but not acoustic thermography. The indication was further investigated with the use of a digital microscope and observed to be coming from chipped coating that was evidently holding penetrant (figure 87). Acoustic thermography would not be expected to find coating chips.

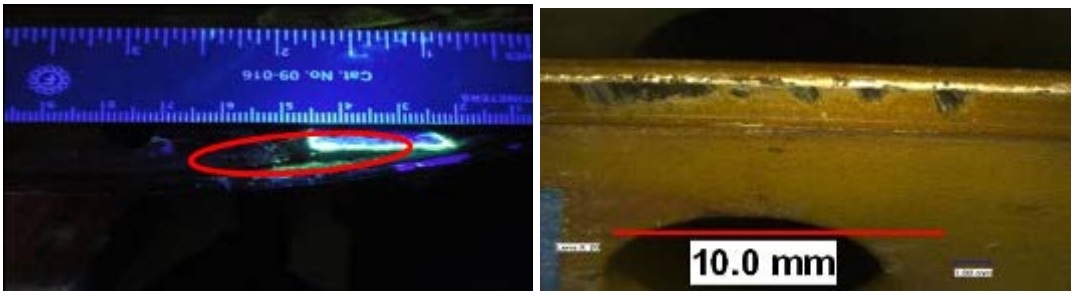

Figure 87. Second Indication Observed by FPI (left) and the Corresponding Microscope Observation (right)

7.3.2.8 Disk – SN: M8320.

Disk SN: M8320 is a P&W first stage compressor fan disk (figure 88). The disk had a long central bore, which made it difficult to inspect both sides with the lathe chuck fixture. It is

recommended that a specialized fixture be made for this style of disk for production inspection. During inspection, small indications were observed that corresponded to a rubber coating that was very difficult to remove (figure 89). After some effort at removal, the test was repeated and fewer indications were observed. No crack-like indications were observed on this disk.

Figure 88. The P&W First Stage Compressor Fan Disk (side A on left and side B on right)

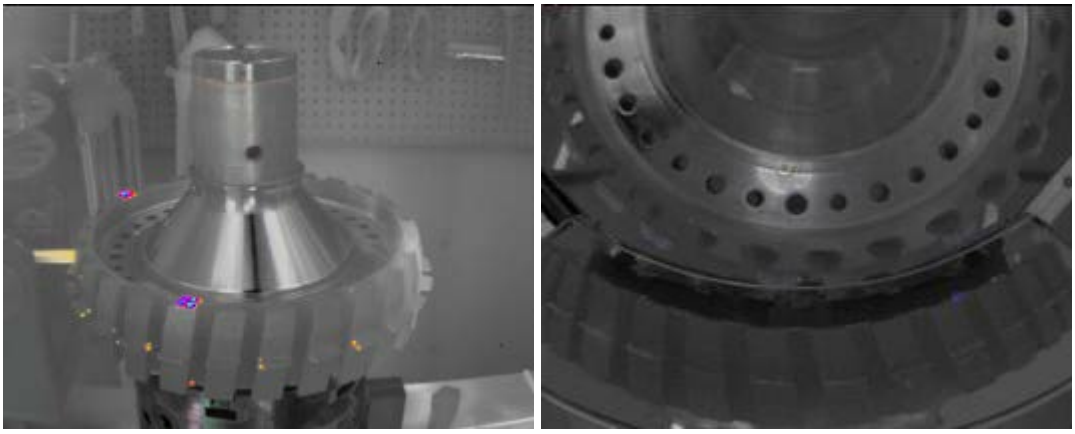

Figure 89. Representative Acoustic Thermography Results for Disk SN: M8320

7.3.2.9 Disk - SN: T04834.

Disk SN: T04834 is a P&W seventh-stage compressor fan disk (figure 90). Representative acoustic thermography results for disk serial number M8320 are shown in figure 91. No indications were observed on this disk.

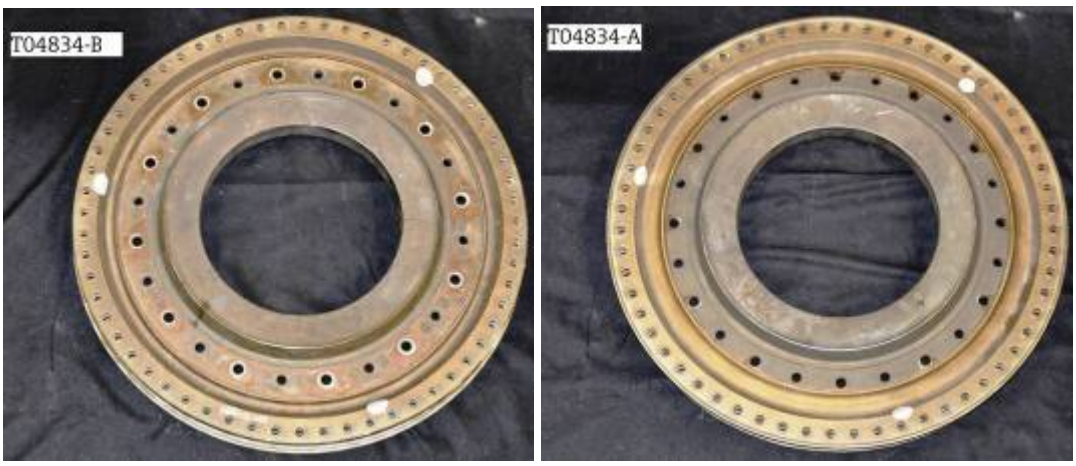

Figure 90. The P&W Seventh Stage Compressor Fan Disk Stage Compressor Disk (side A on left and side B on right)

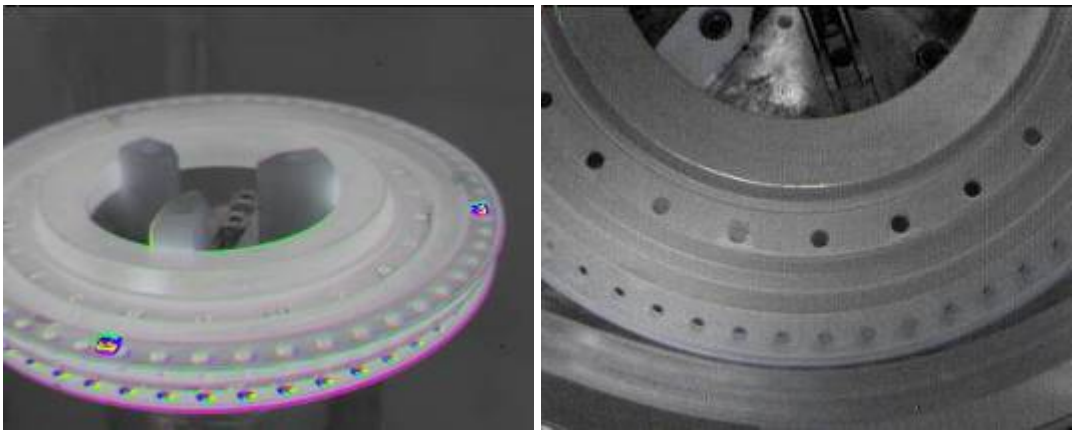

Figure 91. Representative Acoustic Thermography Results for Disk SN: T04834

7.3.2.10 Summary of Acquired Disk Inspection.

Of the nine disks inspected, four acoustic thermography indications and 19 FPI indications were observed (table 11). Fourteen of the FPI indications observed were not related to indications that acoustic thermography would be expected to detect. Two of the indications detected by acoustic thermography measure 16 mm and 10 mm. The third grew during the testing and was not measured before testing. The last indication was observed by liquid penetrant to be about 8 mm. One indication on the Rolls-Royce solid head disk that measured about 7 mm was missed by acoustic thermography. This was attributed to the depth of the indication and the rigidity of the disk.

Table 11. Summary of the Observed Indications and Methods by Which They Were Detected

Disk Serial Number	Acoustic Thermography Indications	Penetrant Indications	Microscope Verification	Visual Verifications
Rolls-Royce Solid Head Disk	1	13	8	0
BENCAL3598	2	2	2	2
BENCAR 9734	1	2	2	2
BBDUAR7726	0	0	0	0
BENCAK4671	0	1	1	1
BENCAK4805	0	1	1	1
BENCAK6446	0	0	0	0
TO4834	0	0	0	0
M8320	0	0	0	0

Red = Reportable indications
Orange = Reported, but not all cracklike
Green = No indications observed

7.4 DEMONSTRATION OF THE SIEMAT SYSTEM AT THE AIRWORTHINESS ASSURANCE NONDESTRUCTIVE INSPECTION VALIDATION CENTER.

As part of the FAA-funded development of acoustic thermography for aerospace jet engine disk inspections, Sandia National Laboratories was tasked with providing an independent third-party evaluation of the Siemens' SIEMAT system capability and reliability. Sandia operates the Airworthiness Assurance Nondestructive Inspection Validation Center (AANC) for the FAA William J. Hughes Technical Center, which is the sponsor of this project. Sandia National Laboratories is a multiprogram laboratory managed and operated by Sandia Corporation, a wholly owned subsidiary of Lockheed Martin Corporation, for the U.S. Department of Energy's National Nuclear Security Administration under contract DE-AC04-94AL85000.

The AANC personnel were trained in the use of the system and, in conjunction with Siemens personnel, performed inspections of four different types of aerospace gas turbine engine disks. Qualitative evaluations were conducted to assess the capability of the AT system to perform initial screening inspections of entire disks. Quantitative evaluations were conducted to determine the POD for defects typically found in jet engine turbine disks. Actual engine parts were used to support this evaluation. Delta Air Lines provided P&W JT8D engine turbine disks and Honeywell (HW) APU turbine disks that had been retired for life limits. The USAF Research Lab provided jet engine turbine disks with manually induced fatigue cracks. A retired TFE731 fan disk with characterized defects was provided by HW.

During November 2011, the AANC evaluated the Siemens SIEMAT acoustic thermography inspection system for jet engine disk inspection reliability. The evaluation occurred at the AANC Albuquerque International Airport Hangar facility from November 7-18, 2011. The evaluation consisted of basic assessments, such as ease of setup and basic use of the SIEMAT

inspection system; training on the use of the system (which included a review of IR inspection theory and practice); specific inspection procedure development and optimization of parameters for a given procedure; and, finally, inspection of a large number of aviation gas turbine engine disks with known and characterized defects for the purpose of generating reliability data. A total of four different part numbers was inspected, including enough individual pieces of one part number with sufficient characterized defects present to generate a POD curve and an estimate of false call rates. In this particular case, the turbine disks were from APU gas turbine engines. Overall detection sensitivity was nearly the goal stated by Siemens (POD_{90} less than or equal to 0.030 inch) at POD_{90} = 0.038 inch. However, false call rates were high because of generated heat that was characteristic of vibrational heating at known crack locations. Namely, the heating showed a peak-and-decay characteristic during chaotic ultrasonic excitation that exceeded the threshold determined during inspection process optimization. It should be noted that the inspection procedure development occurred during the 2-week evaluation period with fewer parts than would be available when developing and implementing the inspections in a production environment.

7.4.1 Equipment Setup and Operation.

Siemens and AANC staff worked together in the lab, setting up the system to perform initial verification inspection on a disk with known cracks. Logistics associated with equipment operation dictated an industrial lab or light shop setting. Utility requirements consisted of compressed air up to 100 psi and electrical power in the form of 220 VAC with a single-pole 20-amp supply. Safety and health concerns dictated the use of safety glasses and hearing protection during equipment operation. However, overall, the system arrived in appropriate shipping containers; included all tools and support equipment as part of the system; was relatively straightforward to assemble; and was operationally ready within the first half day.

The disk inspection order of precedence was finalized after a review of the available disk characterization data. Two sets of disks were determined to hold the highest potential of providing quantitative data for evaluation. The P&W JT8D second-stage turbine disks were found to have enough cracks with a reasonable size distribution to be used as the initial inspection articles. The team conducted an extensive review and discussion of the disk characterization data. The disks contained 19 individual cracks ranging in size from 0.020" to approximately 0.400" in length along the slots of the fir tree tangs. While all but one crack was on a single disk, their locations could be considered individual inspection sites. A second disk had an in-service, or natural crack, that was identified with FPI and verified with visual microscopic review. Other smaller cracks may occur on this disk that were not found with FPI, but none were found with subsequent eddy current inspections. The HW APU turbine disks were selected because they contain a large number of in-service cracks found with FPI. Six disks were selected that provide a uniform size distribution with an appropriate range, the smallest being 0.008" long along the blade slot root. Both sets of disks provide ample opportunities to collect false call rate data.

Siemens provided fixtures for the radial excitation of the JT8D disks and axial excitation of the APU disks (described in section 6.1). Fixtures for other disks had to be built for each unique disk type not supported by the provided fixturing, and was completed with basic shop materials

and tools. Disk hold-downs were configured each time with the disk lying flat on the cross section. Excitation configuration by ultrasonic horn placement was either horizontal or vertical to effect either radial or axial excitation, respectively. Any flat spot approximately the size of the horn tip or larger was a candidate area for excitation, but, in one case, the excitation horn was modified to fit the part so that it could be radially excited. Searching for an initial excitation location consisted of listening to the part ring when struck at several different locations with a nonmetal object. Any flat spot that gave a robust ring when struck was a candidate for UT excitation, provided the part and the welding horn could be configured to achieve such contact at the required pressures (usually between 30 and 50 lbs total). For any given part, there were only a limited number of ways it could be excited repeatedly, quickly, and with similar energization each time. A decision had been made to modify expensive UT welding horns, specifically to accommodate radial excitation of JT8D turbine disks. Several horn tips were ground into a shallow V shape to accept the slightly raised outer face of the fir tree tangs (figure 92). Cracks were thought to occur in the slots of these tangs. Experimentation conducted during this program (section 5.3) led to the need to perform radial excitation on this particular part, but no convenient flat spot existed. As part of the final horn-to-disk alignment procedure, extra setup testing was done to ensure the tip met the part faces within very tight alignment tolerances. This alignment was conducted to maximize the ultrasonic coupling efficiency between the horn and the part and minimize the potential for damaging the part. Card-stock (90-lb) paper was used to protect the parts from the horn (as a result of experiments conducted in section 6.2) and great care was taken during inspection parameter optimization after aligning the horn to the disk so that uneven or excessive pressure did not burn through the cardstock and damage the part. Competing interests needed to be balanced when using interface materials because they attenuate ultrasonic energy transmission, which can reduce thermal signal. Highest energy input into the part and, thus, theoretically greatest defect signal come from direct horn-to-part contact. The use of a calibration reference standard part with a known defect (preferably a relatively small defect) greatly facilitates the optimization of the inspection parameters.

Figure 92. Modified Horn for Radial Excitation (left) and SIEMAT System Configuration (right) for Inspecting JT8D Disks

Setup and inspection parameters for the JT8D disks were developed first, but they were done without the benefit of a calibration reference standard or test part. Determination of call thresholds is in units of average thermal signal counts from a manually placed 8 by 8 pixel

cursor. Counts were maximized while visually aligning the cursor on the computer screen image with the hottest portion of the indication or power strip. The time-temperature plot was also examined to determine if a peak and decay process was evident, indicating a cracklike signal.

7.4.2 Inspections of P&W JT8D Second-Stage Turbine Disks.

Inspections of three P&W JT8D second-stage turbine disks were performed with SIEMAT acoustic thermography. All disks were life-limited and were retired because of age, so no prior inspections had been done at Delta Air Lines' facilities. These disks were made of steel, according to the manufacturer's illustrated parts catalog. Two disks had single, natural discontinuities and the third contained several engineered flaws grown by low-cycle fatigue and torsional bending loading at Florida Turbine Technologies, Inc. The crack growth device and loading bar are shown in figure 93. The fir tree attachment was installed onto the disk using a bolt and loading pin. The loading pin pressed against the bottom lug to preload the fir tree into the disk. The outer shell of the load bar was then threaded onto the fir tree attachment, and the disk hub cycled axially at a few hundred hertz to cause "oil canning" of the central portion of the disk and torsional bending loading on the fir tree lugs because of the weight of the load bar. The disk was monitored by listening to the vibrational frequency, and with an IR camera during loading. If a change in frequency was heard, or a heat signature was noticed on the IR camera, loading was stopped and the disk was inspected for cracks by solvent removable FPI. Typical crack orientation is shown in figures 94 through 96, where cracks propagate at a corner and grow across the tang and down the slot on the opposite side. It was difficult to obtain small cracks because of the tendency of the cracks to open and propagate relatively quickly at the loads being developed in the tough steel.

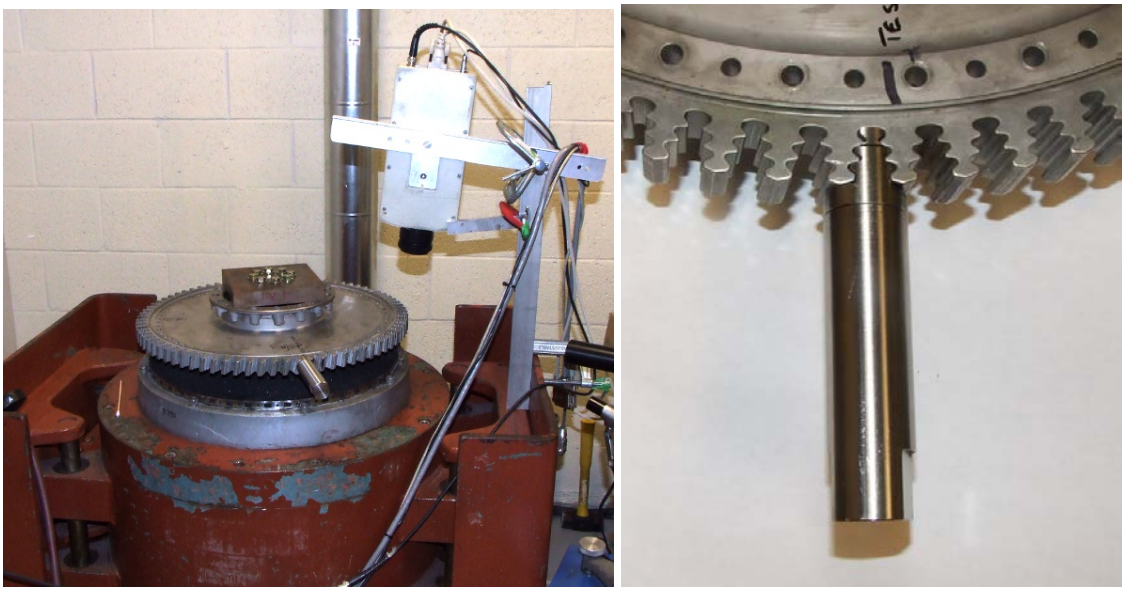

Figure 93. Loading Device and Apparatus Used to Grow Cracks in P&W JT8D Second-Stage Turbine Disks

Figure 94. Natural Discontinuity on Disk BLDLA34987 Tang 54 Slot 1 Viewed During FPI From the Top (B) Side

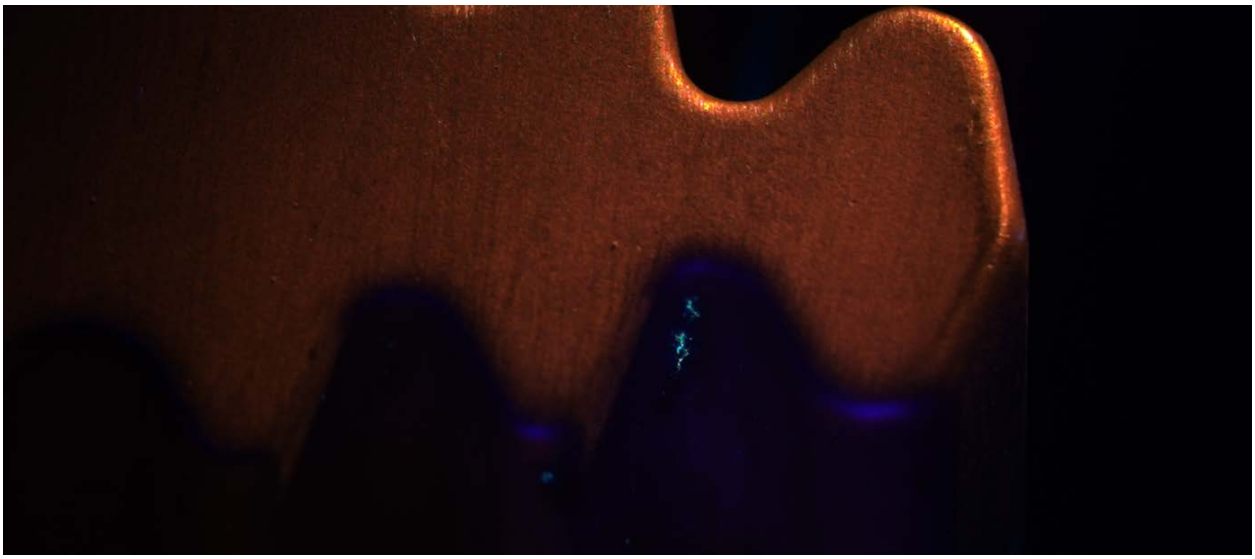

Figure 95. Natural Discontinuity on Disk BLDLA34341 Tang 47 Slot 1 Viewed During FPI From the Top (B) Side

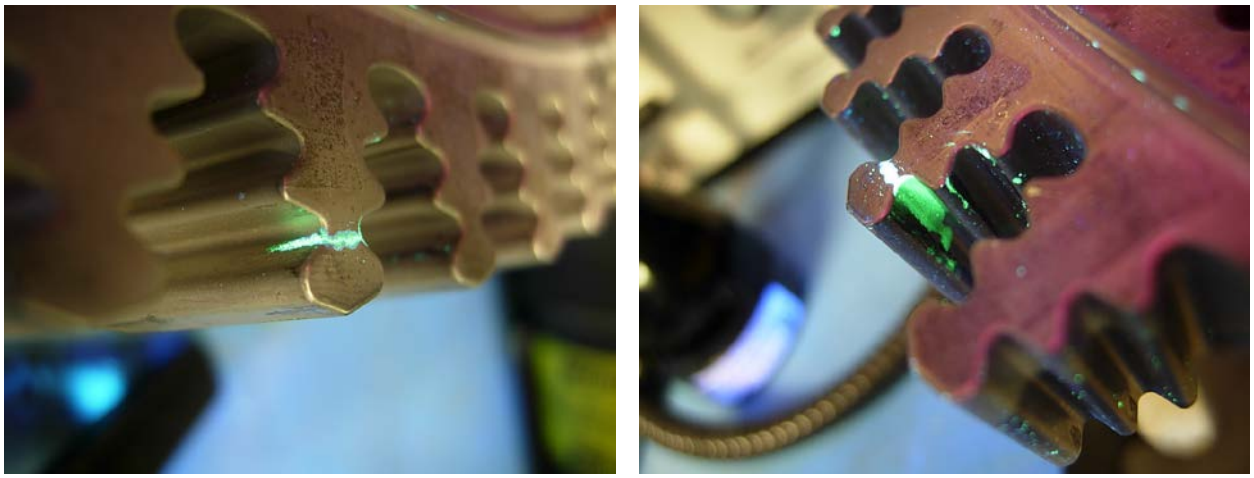

Figure 96. Engineered Discontinuity on Disk BLDLA34598 Tang 5 Slot 1 Viewed During FPI From the Top (B) Side in the Leading and Trailing Directions

Flaws in all disks were characterized for size at the AANC by using Method B, level 4, high-sensitivity postemulsifiable FPI. As part of the inspection process, these disks were cleaned at Delta Air Lines in accordance with their standard inspection procedures. Calibrated images were made of each discontinuity and measurements were derived from the images. Discontinuity measurement values are shown in table 12.

Table 12. Discontinuity Characterization for Three P&W JT8D Second-Stage Turbine Disks

Disk SN	Disk Side	Tang	Slot	FPI Top (in.)	FPI Leading (in.)	FPI Trailing (in.)	Note
BLDLA34987	B	54	1		0.100		Naturally Occurring Discontinuity
BLDLA34341	B	47	1		0.070		Naturally Occurring Discontinuity
BLDLA34598	B	5	1	0.160	0.160	0.270	All Engineered Discontinuities
BLDLA34598	A	7	2	0.118	0.305		
BLDLA34598	B	8	2	0.141		0.202	
BLDLA34598	B	11	1	0.085		0.194	
BLDLA34598	B	12	1	0.080		0.136	
BLDLA34598	B	13	2	0.103		0.154	
BLDLA34598	A	15	1	0.154	0.446	0.267	
BLDLA34598	B	16	3	0.155		0.111	
BLDLA34598	A	26	1	0.051		0.148	
BLDLA34598	A	26	2	0.137		0.197	
BLDLA34598	B	27	2	0.044		0.052	
BLDLA34598	A	27	1	0.067	0.104		
BLDLA34598	A	27	2	0.082	0.151		
BLDLA34598	B	28	2	0.102	0.147		
BLDLA34598	A	28	1	0.020	0.062		
BLDLA34598	B	29	2	0.217	0.308		
BLDLA34598	B	50	1	0.190	0.020	0.342	
BLDLA34598	B	57	1	0.160	0.244	0.438	
BLDLA34598	B	70	1	0.139	0.108		

A POD curve was calculated (figure 97) using Spencer's multiflaw model (which takes into account the possibility of more than one defect at each independent inspection location), with a two-parameter probit model fit of hit/miss data (although call threshold was set at 50 counts). Although the number of defects is fewer than what is considered optimal according to Military Handbook (MIL HDBK) 1823, it was still sufficient to yield a very good fit to the model, as was the defect size distribution, including the desired minimum crack size of less than 0.030 inch, and the associated hit/miss calls. Using FPI (as shown in table 13) as the referee inspection method appears to be sufficient for a basic capability analysis by identifying all known defects on the disk with engineered cracks, as well as finding two small natural discontinuities on the other two disks. Additionally, eddy current inspection of the disks did not reveal any additional defects, especially in the disk that was used for engineered cracks. Results from this data set

provide a 90th percentile value of POD_{90} = 0.114 inch. However, the POD_{90} value should be used as a rough order-of-magnitude indication only, and considered not fully developed because of the lack of a true independent referee method, a defect set that meets MIL HDBK 1823 guidelines, and a specimen set with more than one disk containing engineered defects. Likewise, the false call rates (as shown in table 4) should be considered as not fully developed because no final destructive evaluation was conducted to verify the presence or absence of defects at each location.

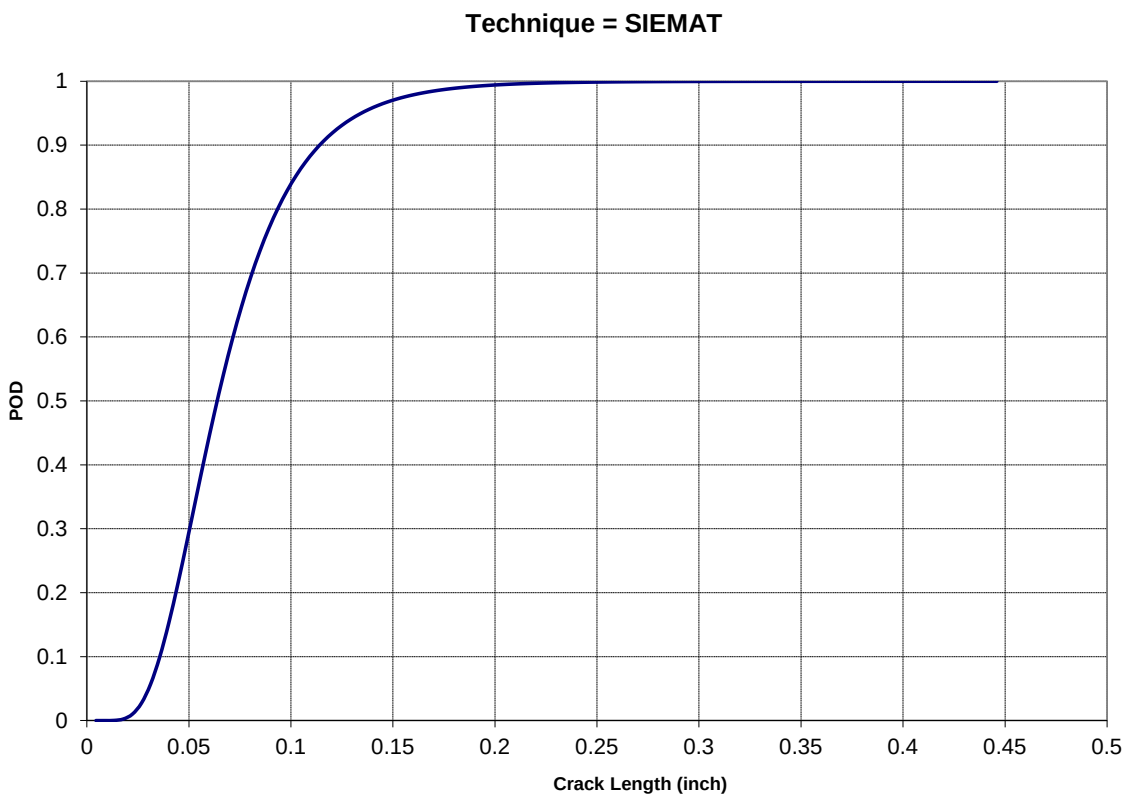

Figure 97. A POD Curve for SIEMAT Inspection of P&W JT8D Second-Stage Turbine Disks for Grown Cracks in Fir Tree Slots (flaw length in inches)

Table 13. SIEMAT Inspection Results Sorted by Hit/Miss Value, Then FPI Size of Leading and Top Discontinuities

Disk SN	Disk Side	Tang	Slot	FPI Top (in.)	FPI Leading (in.)	FPI Trailing (in.)	Sonic IR Counts	Sonic IR Energy (J)	Sonic IR Hit/Miss
BLDLA34598	A	15	1	0.154	0.446	0.267	1689	893	1
BLDLA34598	B	29	2	0.217	0.308		1687	988	1
BLDLA34598	A	7	2	0.118	0.305		520	960	1
BLDLA34598	B	57	1	0.160	0.244	0.438	11550	1128	1
BLDLA34598	B	5	1	0.160	0.160	0.270	9126	1090	1
BLDLA34598	A	27	2	0.082	0.151		155	963	1
BLDLA34598	B	28	2	0.102	0.147		NA	NA	1
BLDLA34598	B	70	1	0.139	0.108		909	1073	1
BLDLA34598	A	27	1	0.067	0.104		97	963	1
BLDLA34987	B	54	1		0.100		373	1104	1
BLDLA34598	B	50	1	0.190	0.020	0.342	86	1227	1
BLDLA34598	B	16	3	0.155		0.111	80	870	1
BLDLA34598	B	8	2	0.141		0.202	140	960	1
BLDLA34598	A	26	2	0.137		0.197	363	963	1
BLDLA34598	B	13	2	0.103		0.154	95	893	1
BLDLA34598	B	11	1	0.085		0.194	495	874	1
BLDLA34598	B	12	1	0.080		0.136	430	874	1
BLDLA34598	A	26	1	0.051		0.148	273	963	1
BLDLA34598	B	27	2	0.044		0.052	NA	NA	1
BLDLA34341	B	47	1		0.070				0
BLDLA34598	A	28	1	0.020	0.062		34	NA	0

NA = Signal data not available/crack called by inspector on review

Table 14. False Call Data for SIEMAT Inspections of P&W JT8D Second-Stage Turbine Disks—Also Showing Examples of Natural and Engineered Crack Locations

Disk SN	Disk Side	Tang	Slot	FPI Top (in.)	FPI Leading (in.)	FPI Trailing (in.)	Note	Disk False Call/Opportunity
BLDLA34341	B	47	1		0.070		Naturally Occurring Discontinuity	50/935
BLDLA34987	B	54	1		0.100		Naturally Occurring Discontinuity	11/935
BLDLA34598	B	5	1	0.160	0.160	0.270	All Engineered Discontinuities	0/917

Note that high false-call rates plagued the inspections of the two disks that have only one natural discontinuity in each. Meanwhile, the disk that underwent engineered cracking shows no false calls and high rates of discontinuity detection. It exhibits cracks that initiate at the top or bottom corner of the fir tree lug and propagate in both directions. Life-limited parts, such as retired disks, are reasonably expected to have higher potential for in-service defects, such as microcracking or changes in material structure causing a thermal response that may be detectable by SIEMAT. However, in this case, the disk with postretirement fatigue cycling did not exhibit any false calls. The question arises: could the repeated low-cycle fatigue loading that disk BLDLA34598 underwent change the response characteristics, such that it could remove stress risers that would otherwise cause heating signals during acoustic thermography? Is there some other reason disks that were not subjected to the fatigue cycling to grow cracks exhibit significantly higher rates of signals that break the call threshold? More importantly, are certain individual parts more prone to false calls because of some characteristic of the material or the part itself? The acoustic thermography technique clearly documents a thermal response at the location of false calls. However, the exact cause of heating has not been identified by the referee inspection methods applied. Extensive metallurgical evaluation would be required to determine the source of the heating causing the false calls. To become a viable industrial aerospace inspection method, the SIEMAT system acoustic thermography inspection must be tuned to exclude the bulk of the false calls. This will require a large number of parts because of potential variability in response between disks. For each disk, every call must be further evaluated by a complementary method as part of a final disposition of the part. A similar false call trend was observed for the HW APU disk inspections.

7.4.3 Inspections of HW APU Second-Stage Turbine Disks.

Individual fir tree slot inspections for POD data generation were performed on six disks that each contained 36 fir tree slots. Inspections were performed without the inspector having any knowledge of the defect condition of each disk. Images were generated with a field of view appropriate to detect heat blooms in the size range of 0.030 in. length, based on the instantiations field-of-view calculations. Thus, four slots on a side of a disk were inspected for each IR image

generated. Both sides of the disk were inspected separately, but occasionally a call was made for the far side of the disk when a heat bloom was clearly detected. For the practical purposes of this POD experiment, data from the front and back sides of the disks were kept separate. Results from each inspection site were listed as hit or miss data, but signal values in counts and energy input into the disk by the ultrasonic horn were recorded whenever a defect was called (i.e., signal values were recorded for each heat bloom that exceeded the threshold value of 34 counts). The pattern of heating and cooling was also used as a qualitative characteristic of the heating to help the inspector make a defect call decision. If the 8 by 8 pixel block from which the time temperature data was obtained showed a characteristic peak and decay pattern, then a defect call was made. The threshold value was set based on known cracks in a similar disk, which had been etched to reveal crack lengths, from prior work at Wayne State University with their acoustic thermography system earlier in the year. Since there was no predetermined location from which to take signal values from for nondefect sites, it was not recorded if no defect was called. With the system set up specifically to inspect these parts, each shot took approximately 2 minutes to prepare, record, and evaluate. Thus, the inspections were relatively quick. However, the number of times the ultrasonic horn had to excite the part was a concern, with a minimum of 18 shots per disk required to inspect both sides.

7.4.3.1 Characterization of Defects by Independent Method: Postinspection Etching.

Truth data for each disk was determined after all acoustic thermography inspections had been completed. This was done by etching each disk in an appropriate acid solution to remove metal that may have been smeared by a grit blasting step prior to FPI. The acid etch was very effective at opening the cracks to the surface so that they could then be clearly seen and measured by a 50x optical microscope, as shown in figure 98. The back side of each disk underwent a second etch procedure because the etch rate appeared to be slower than for the front sides, and also because there was a much higher apparent rate of false calls on the back sides. It was initially thought that the etch was not bringing out many cracks on the back sides, but after re-etch it was determined that most of the false calls appeared to be occurring on the back sides. There may be a metallurgical reason related to thermoelastic movement in the metal lattice, but more research is needed. However, it is clear that some disks appear more prone to high false calls than others. The etch and optical microscope evaluation was deemed a reasonable referee method for determining true defect condition because even very small cracks of only a few thousandths of an inch in length were observed in many locations, and all larger cracks were readily apparent. This trend was also observed in the JT8D disk inspections.

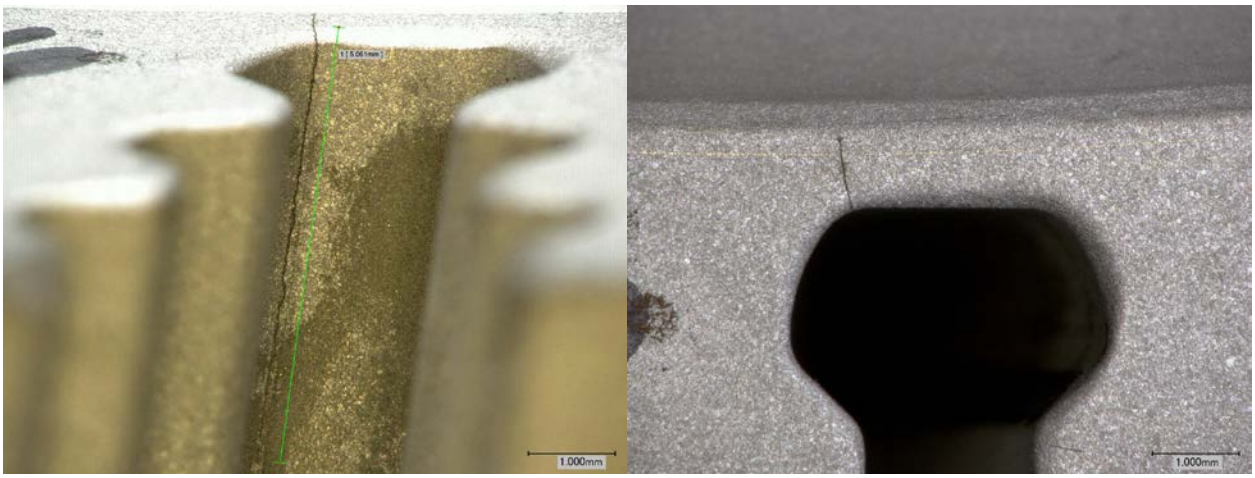

Figure 98. Example of a Large Crack and Its Measurement in an HW APU Fir Tree Slot After Etch Taken With 50x Optical Microscope

7.4.3.2 The SIEMAT Inspection Results of HW APU Disks.

The results of SIEMAT inspections of HW APU disks are shown in figure 99 and, for more information, in appendix C. Generated POD curves are shown in figure 100. A 90th percentile value of POD_{90} = 0.038 inch was obtained.

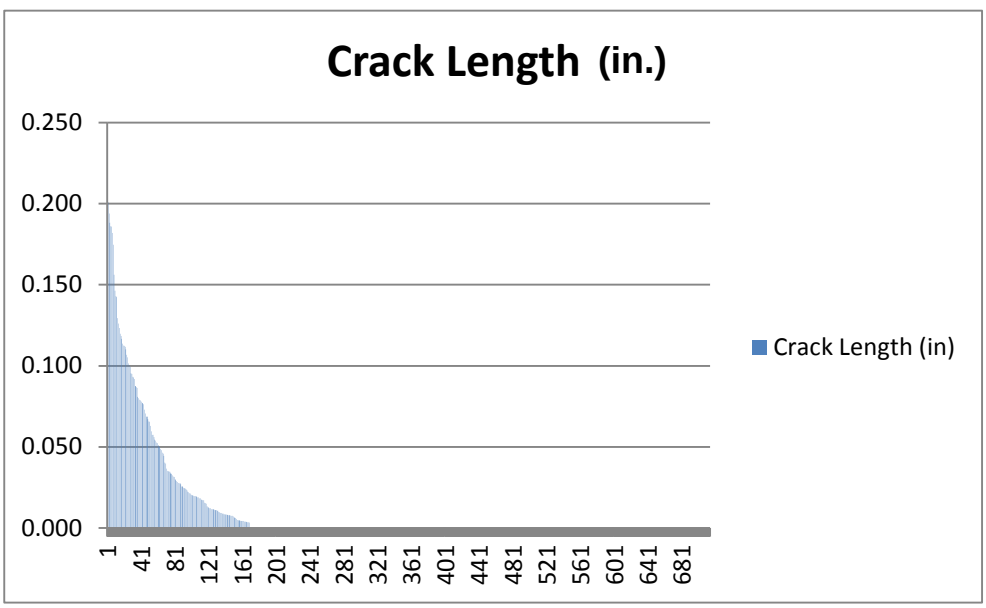

Figure 99. Crack Length Distribution for HW APU Disks as Determined by Etching and 50x Optimal Microscopy

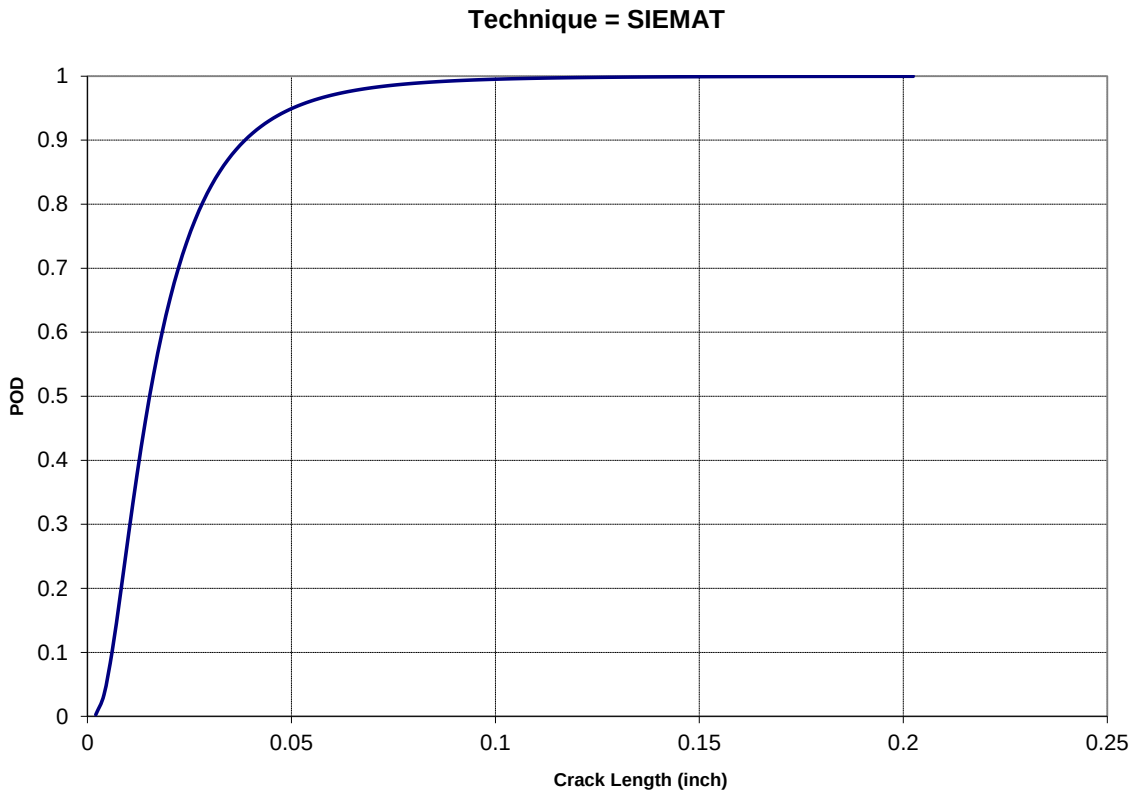

Figure 100. The POD Curve for SIEMAT Acoustic Thermography Detection of Cracks in Fir Tree Slots of HW APU Disks on Front Side Only

High false call rates also plagued the inspections of the HW APU disks. This was particularly true on the back sides of the disks, where there were relatively few actual cracks found in postinspection etching characterization. Again, the question arises as to whether stress risers or some other thermoelastic response is occurring that would cause heating signals during acoustic thermography. Just as with the P&W JT8D disks, certain individual parts appear more prone to false calls than others. To be considered a viable industrial aerospace inspection method, the SIEMAT system inspection must exclude the bulk of the false calls. In actual inspection usage, each call must be further evaluated by a complementary method as part of a final disposition of the part. False call rate data for all six disks are shown in table 15.

Table 15. False Call Rates on the Back Side of HW APU Disks

Disk Number	Number of Opportunities	Number of False Calls	False Call Rate	Number of Back Side Misses
0592	32	0	0%	3
2743	32	24	75%	2
1146	25	10	40%	2
2328	27	1	4%	8
2666	34	14	44%	1
1435	34	32	94%	0

7.4.3.3 Whole-Disk Inspections for Initial Screening of APU Disks.

Whole-disk inspections with SIEMAT for screening parts is a potentially viable technique as a preliminary method to detect those that are badly cracked. This method could greatly reduce the full inspection burden of operators with significant numbers of parts to inspect. This was demonstrated by inspecting the remaining 40 disks in the AANC specimen set. An example is shown in figure 101 and table 16 for disk number 2743, where a cluster of large defects that were evident in the characterization inspections is also evident in the SIEMAT pulse-phased IR image. Clearly, this particular disk would not require any further inspection to properly disposition it to the scrap bin. Because of the POD value obtained for APU disk inspections, and even with the relatively high false-call rates, there is much potential for screening out defective disks with high confidence. Even if initial screening of a particular part did not show the presence of any defects, further examination with complimentary techniques is still warranted. Particular attention must be paid to those sites that do show potential defects because of the propensity for false calls on some parts. Disks that show very few defective locations would also warrant further examination by complimentary methods so as to not scrap potentially good parts because one or a few false calls. The break point at which indications from screening can be used to scrap a part will become evident to the operator with continued inspection use and refinement, but is not readily evident in this study.

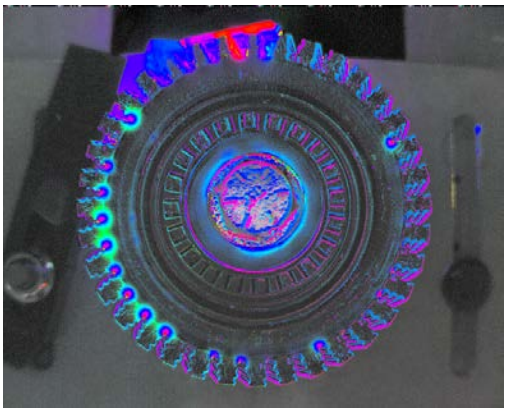

Figure 101. The SIEMAT IR Image for a Screening Inspection of an Entire Disk

Table 16. Crack Truth Data for Screening Inspection of an Entire Disk

SN	Disk Root No.	Sonic IR Hit/Miss	Crack Length (in.) FPI	Crack Length (in.) Etch TOP 1	Crack Length (in.) Etch TOP 2	Crack Length (in.) Etch TOP 3
2743	8	1	0.075	0.080	0	0
2743	10	1		0.010	0	0
2743	11	1		0.020	0	0
2743	12	1		0.016	0	0
2743	13	1		0.044	0	0
2743	14	1		0.053	0.018	0
2743	15	1		0.023	0	0
2743	16	1		0.077	0	0
2743	17	1		0.033	0.054	0
2743	18	1		0.008	0.009	0
2743	19	1		0.024	0.025	0.017
2743	20	1		0.022	0.034	0
2743	21	1	0.096	0.087	0	0
2743	23	1	0.09	0.117	0	0
2743	24	1	0.141	0.129	0	0
2743	25	1	0.11	0.102	0	0
2743	26	1	0.125	0.107	0	0
2743	27	1	0.139	0.120	0	0
2743	28	1	0.141	0.123	0	0
2743	29	1	0.087	0.099	0	0
2743	30	1	0.082	0.069	0	0
2743	32	1	0.132	0.112	0	0
2743	33	1		0.008	0	0
2743	35	1		0.006	0	0
2743	36	1		0.008	0	0

7.4.4 Inspections of USAF Turbine Disk Anti-Rotation Tangs.

Inspections of five USAF turbine disks were performed with SIEMAT acoustic thermography. All disks were retired from service and had cracks manually placed in anti-rotation tangs by the USAF for crack detection purposes. Characterization data were written on each disk. These disks are made of nickel-based alloys, according to the USAF. All disks had at least two cracked tangs, but other cracks were also identified by SIEMAT inspection. A typical anti-rotation tang and the resulting SIEMAT inspection image are shown in figure 102. Inspection results are

shown in table 17. It should be noted that all USAF-identified defects were found, but there were also seven potential false calls that could not be verified one way or the other. Some of the potential false calls were in areas suspected of being cracked and, in some cases, subsurface heat blooms appeared to be emanating from the material.

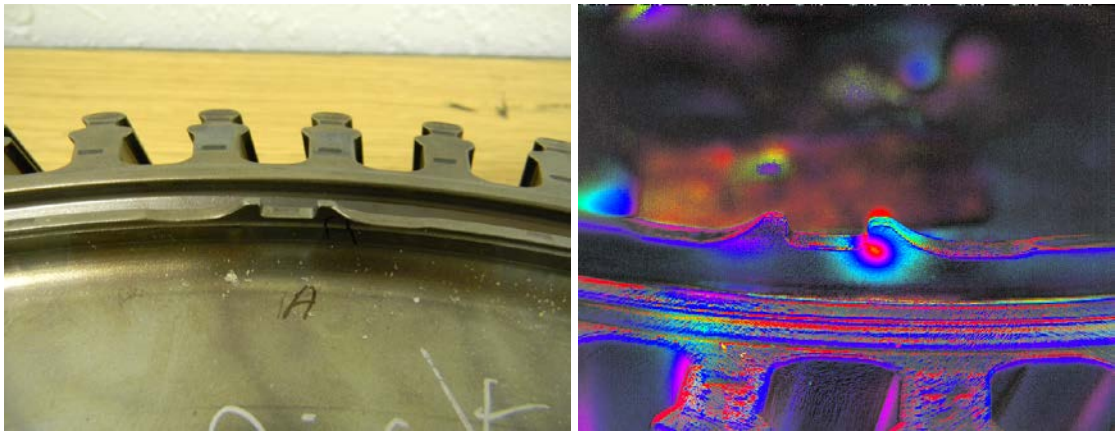

Figure 102. Anti-Rotation Tang (left) and Associated SIEMAT Acoustic Thermography Inspection (right)

Table 17. The SIEMAT Acoustic Thermography Inspection Results Showing Hits, Misses, and False Calls on USAF Nickel-Based Turbine Disk Anti-Rotation Tangs

AF Disk #	S/N	AF Tang Label	Siemens Inspection Label	Counts	E (J)	Crack Length (in.)	Hit/Miss	False Call	Note
1	R40	A	A	63	306	0.013	1		pictures DSCN 0670-0681
			B	51	527			FC	
		B	C	58	941	0.04	1		
			D	234	498			FC	large visible crack, but small heat bloo
2	R73		A	45	483			FC	pictures DSCN 0635-0645
		B	B	60	522	0.015	1		
			C	107	695			FC	
		A	D	165	678	0.009	1		
3	P47	B	1	45	570	0.029	1		
			2	62	641			FC	
		A	3	18	527	0.021	1		
			4		494				
4	R04	A	A	23	409	0.011	1		pictures DSCN 0657-0669
			B		508				
		B	C	84	441	0.026	1		
			D		634				
5	P34		A	85	580			FC	pictures DSCN 0646-0656
		B	B	120	518	0.017	1		
			C	50	508			FC	
		A	D	161	531	0.036	1		

7.4.5 Inspections of Allied Signal TFE731 Fan Disk.

SIEMAT was used to perform inspections for known and characterized cracks in a titanium alloy fan disk from the former Allied Signal TFE731 jet engine. Only one or two cracks were known on this disk, and they were of a small length. The crack was located in a thick area at the top of a slot where the web material was also thick. During acoustic thermography testing, the crack was not heating enough to cause an IR signal, so power and pressure were increased to try and cause more frictional heating and, thus, a better IR signal. When this higher energy excitation occurred, the crack did heat enough for detection. However, one of the thin tangs on the bottom side of the disk unexpectedly sparked and appeared to propagate a crack as shown in the black circle in figure 102. On three subsequent shots with the camera repositioned to view the thin tangs, they continued to heat dramatically, and the tang next to it also sparked and propagated a crack, as shown in the IR image in figure 103. It is not known if the tangs were already cracked and merely reacted to the strong energy input, or if cracks were initiated because of this higher energy input. This test demonstrates that excitation by the relatively high amounts of ultrasonic energy imparted by the plastic welding system has the potential to cause unacceptable damage to critical rotating engine parts. Thus, care must be taken to develop inspection procedures that use only the lowest amounts of excitation energy needed to excite the defects of interest. Once developed, strict adherence to the inspection procedure is equally critical or the risk of accidental part damage increases considerably.

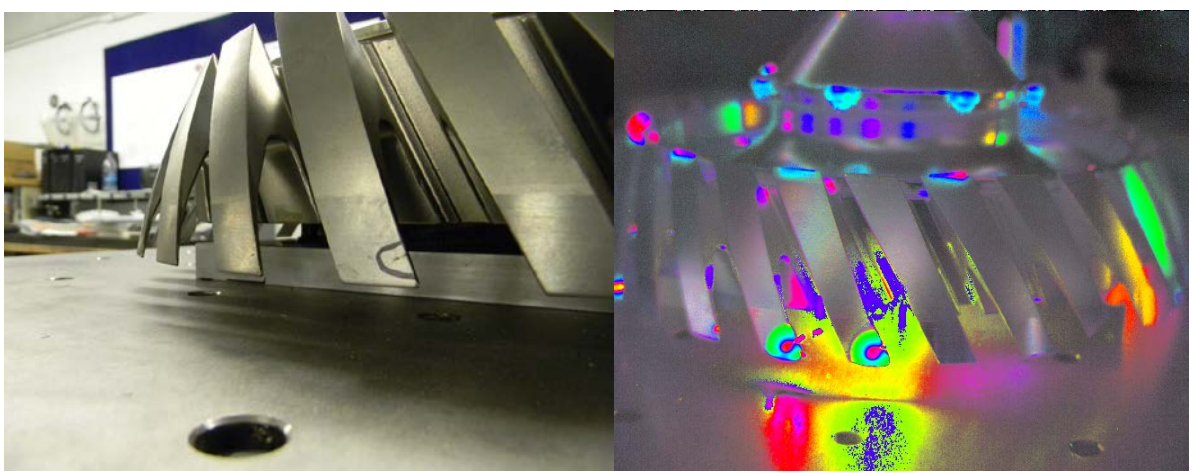

Figure 103. An HW TFE731 Titanium Engine Fan Disk With Cracks That Propagated During Extreme Ultrasonic Excitation (left) and the SIEMAT IR Inspection Image (right)

7.4.6 Conclusions.

The Siemens SIEMAT inspection system was used to inspect a significant number of aerospace jet engine disks made of all commonly used materials.

The SIEMAT system was easy to set up and operate, and requires minimal utilities and space to operate.

Determining the correct detection threshold values, horn-to-part pressure, and excitation energy

levels all require access to a significant number of parts that can be fully characterized for defects. Basic design of experiment principles can be used effectively to determine the best values for any particular inspection. As with all inspection processes, a skilled, high-level inspector is needed to create a final effective inspection process, and it may require continual refinement as it is used.

Training on the use of the system was completed in approximately 8 hours and included a review of IR inspection methods and details of the data and image analysis methods specific to the SIEMAT system. Specifically included was the use of the pulse phase analysis and time temperature plot methods.

Detection of cracks in full-sized jet engine disks was achieved for all known cracks installed on P&W JT8D steel turbine disks. A POD_{90} = 0.114 inch was obtained, although this is only a preliminary number due to inadequate MIL HDBK 1823 guidelines for the specimen set.

Detection of cracks in smaller aerospace APU nickel alloy turbine disks was achieved for six disks over a size range and number of defects that meet MIL HDBK 1823 guidelines. A POD_{90} = 0.038 inch was obtained, which can be considered a final detection reliability value on this particular part.

High false call rates were observed in both JT8D and APU disk inspections, yet some individual parts exhibited almost none. Further development of pulse phase analysis and more appropriate detection threshold values are required in order to reduce the false call rates to acceptable levels. The discrimination between crack vibrational heating and other heating mechanisms (such as thermoelastic movement of crystal lattices) was not possible in this study.

Detection of all known cracks in USAF nickel alloy turbine disks was achieved, although false calls were also evident.

Detection of one small known crack in an HW TFE731 titanium alloy fan disk was achieved. In this particular case, crack propagation was observed when the part was undergoing very high degrees of ultrasonic excitation to excite the small known crack. It should be noted that some part features appear to be prone to cracking because they are relatively thin, and it was not determined whether cracks were initiated or just grew from pre-existing defects. The need for very strict part handling and excitation process controls when using acoustic thermography for inspection of critical aerospace engine parts are also highlighted.

Inspections of whole disks in a single image per side were demonstrated on the APU disks, illustrating the potential for SIEMAT use as an initial screening inspection as part of a more involved inspection process.

The potential for disk damage from metal-to-metal contact of the ultrasonic excitation horn and the part was high, especially when using only the paper card stock interface material. More research is required to identify an appropriate interface material that will protect the part, yet transfer sufficient energy into it to adequately excite it and cause vibrational crack heating.

8. DEVELOPMENT AND COMMERCIALIZATION PLAN.

This section of the report describes the development and commercialization plan proposed by SIEMENS Energy. This plan is based on past experience with the commercialization of the acoustic thermography internally and on input from participating commercial partners. The plan is meant to be an outlined guide that can be added to or taken from as requirements change.

The successful implementation of acoustic thermography will require the cooperation of several parties who are funded according to their involvement in the implementation. These parties should work closely to manage the development of the new inspection process so that the final product is economically and technologically sound. The parties and their roles in the process are as follows:

1. An industry partner who has proprietary rights over the current inspection process will be responsible for the business case. The industry partner will be responsible for ensuring that the new inspection process meets or exceeds the required inspection criteria and makes good business sense.

2. A technology provider will work directly with the industry partner to adapt and apply the new technology (acoustic thermography) to the selected application. The technology provider will be responsible for creating an inspection system within the guidelines provided by the industry partner and notifying the industry partner of technological challenges that may affect the business case or the sensitivity of the technology with respect to the provided application.

3. A stakeholder who can approve the new inspection process for the parts of interest will be in control of documents relating to the inspection of the parts of interest and be able to amend them if necessary.

The general 11-step commercialization plan for implementation is listed below. During the first step in the commercialization plan, applications are identified for the implementation of the acoustic thermography technique. The successful use of this technique will be unique in nature, difficult for existing techniques to solve, and it will be related to a problem that, if solved, will have a significant economic benefit. During this step, the three parties involved will brainstorm for potential applications of acoustic thermography. Then, those selections will be further narrowed down and will be agreed on by all partners.

The commercialization plan consists of the following steps:

1. Select set of potential applications for acoustic thermography.

2. Determine approximate business case for each application.

3. Down select primary application.

4. Develop and fabricate inspection system for the application.

5. Conduct detailed risk assessment on part to ensure that the technique does not damage parts.

6. Conduct initial implementation trials to assess capability against other techniques in a laboratory environment.

7. Train industry personnel.

8. Implement acoustic thermography inspection in series with current inspection technique.

9. Obtain Alternative Means of Compliance FAA approval for acoustic thermography.

10. Assess real-world performance of acoustic thermography compared with existing method.

11. Transition to full acoustic thermography inspection.

The approximate business case for each of the down-selected applications will be created by the industry partner and reviewed by all parties in the second step of the commercialization plan. The cost of replacing current equipment should be considered separate from the costs of operation of the two inspection systems. The business case being implemented should be considered as follows:

- The potential cost savings related to the speed of inspection.
- The potential for increased life of parts because of indications being detected earlier.
- A reduction in environmental cost because parts do not need to be cleaned or stripped with hazardous chemicals.
- Benefits of digital documentation of parts throughout their life cycles.

The third step in the commercialization plan is for a primary application to be selected by the industry partner and reviewed by the technology provider and process documentation stakeholder. It is important to select the primary application of the acoustic thermography technique in such a way that the business case is sustainable and the potential inspection capability is improved. Some of the most successful applications of acoustic thermography are those in which traditional inspections struggle to identify defects. For example, acoustic thermography works well for the inspection of rough or porous surfaces. The fewer competing technologies and the higher the risk that missing a defect poses, the better chance acoustic thermography has at being successfully implemented.

After a primary application has been selected, plans for a production system can begin. This system should be designed by the technology provider and include input from the industry partner to ensure compatibility with currently employed processes and standards at the implementation location. The following are some details to consider during the design of the system:

- Size of the system
- Compatibility with part delivery systems
- Environmental conditions
- IR shielding
- Acoustic insulation
- Power requirements
- Data management

A detailed risk assessment should be conducted in order to prove that the acoustic thermography technique does not damage the life of the part. It is important that the risk assessment experiments be designed and carried out with the involvement of the part owner or engineering authority. The risk assessment typically uses strain gauges to assess the approximate stresses at different locations on the part during the test and should show that these stresses are not serious enough to damage the part.

Next, an initial implementation trial should be conducted to optimize and test the system against the existing inspection process. This implementation trial can take place in the laboratory environment and should be repeated when the system is set up in the depot environment to ensure that the system is operating with the same sensitivity. This step in the commercialization plan is important in determining if the system is capable of meeting the inspection criteria set forth by the business case. If the system performs well during this trial implementation, the next step should be taken.

Industry personnel should be trained just after the acoustic thermography system arrives at the inspection facility, so the depot personnel can be trained on the actual equipment to be used. Training will be provided by the technology developer and personnel will be provided by the industry partner. Minimum training requirements for acoustic thermography consist first of American Society of Nondestructive Testing IR level 1 training and Siemens-approved acoustic thermography training. This includes several hours of on-the-job training to allow the inspectors time to work with the system and learn to call relevant indications.

Once training has been completed, it is suggested that the developed acoustic thermography system be implemented in series with the current inspection technique. This will allow a side-by-side comparison of the two inspection techniques on the same parts. This comparison can be used to determine more accurately the inspection system's capability as compared to the existing inspection technique in the eighth step of the commercialization plan.

In the tenth step of the commercialization plan, the real world performance of the acoustic thermography system will be compared to the performance of the existing inspection technique. Data collected from the two inspection techniques over a significant period of time (approximately 6 months) will be analyzed to determine the capability of both the existing and acoustic thermography inspection techniques. It is at this point that a final business case can be developed to confirm the transition to the acoustic thermography inspection.

After the business case for the full implementation has been confirmed, a transition period will begin with the intermittent use of the existing inspection technique to check that the acoustic

thermography process is still performing at a level above the existing process. These evaluation periods will be spaced further apart as more confidence is placed in the acoustic thermography method. Toward the end of this step in the commercialization plan, the existing inspection equipment will cease to be used.

The full acoustic thermography inspection step of the commercialization plan will consist of confirming that the acoustic thermography inspection system is providing an adequate inspection capability and business benefit. It is at this point that the industry partner should begin fully relying on the acoustic thermography method for the specified inspection; equipment used for the previous inspection will be removed from the process.

These steps in the commercialization plan chart the path from research and development acoustic thermography systems to the commercial implementation of acoustic thermography. It is not expected that this process will be completed in the short term, but rather that the commercialization plan will provide guidance for the acoustic thermography community and industry partners to achieve a long-term goal of commercial implementation.

9. TRAINING OF INDUSTRY PARTNERS.

On November 8, 2011, Siemens conducted training at the AANC in Albuquerque, New Mexico with the FAA, AANC staff, and contract researchers for the FAA on the fundamental physics of acoustic thermography inspection and its application to jet engine inspections for crack detection. The training title was "Acoustic Thermography First Principles, Methods and Practice," and was developed by Christian Homma, Paul Zombo, and Forrest Ruhge of SPG, Inc. The training was presented by Forrest Ruhge and was delivered using a PowerPoint™ presentation and written training manual. The general topics covered included a review of vibration physics; IR energy and its measurement via IR cameras; SIEMAT system hardware components and operation; and details of $SInE^2$ software developed by Siemens specifically for the SIEMAT system operation data collection and analysis. The training outline and presentation notes specifically covered an overview of acoustic thermography, ultrasonic excitation modes, vibration modes, thermal propagation, IR emission, IR cameras, IR data analysis, and interpretation of IR inspection results (both raw signal and pulse phase analysis). Additional items covered during training discussions included avoidance of excessive energization of parts; use of laser vibrometry to detect movement and measure energy input into parts; parameter optimization schemes; selection characteristics for calibration test parts; inspection coverage; and detection sensitivity. The end of the training was spent discussing prior POD work at the AANC that compared acoustic thermography against FPIs of titanium and Inconel® bars with grown cracks, and verifying the goals of the evaluation event. The prior work with acoustic thermography demonstrated very good crack detection of small defects in the bars relative to FPI, but was unable to generate a POD because all defects were detected in the specimen set. Thus, much discussion and review of available specimens went into the final work planning done in the training session. The basic requirements for achieving a valid POD were reviewed and the available specimens canvased to select the parts and defects that were most likely to facilitate a fully quantitative evaluation. Thus, the final goals for the evaluation event were developed and agreed on by the involved staff and are as follows:

- Document an inspection procedure development and optimization process for a part that has not been previously inspected. This process is defined as determining the best excitation mode for optimal thermal signal in the part, based on engineering experience. The values of the important parameters of contact pressure, excitation amplitude, and excitation time are determined by simple testing using basic design of experiment principles.

- Train AANC staff to be proficient in the use of the SIEMAT system to inspect jet engine disks. Proficiency is defined as demonstrating the ability to start with a new part number requiring inspection and, using all the fundamental principles discussed in training along with the assembled SIEMAT system, develop a basic inspection process that can detect known defects of interest.

- Perform a quantitative capability assessment of crack detection in jet engine disks, including the proportion of grown cracks detected, smallest crack detected, largest crack missed, and the proportion of nondefect sites falsely called cracked. The JT8D second-stage turbine disks with grown and natural cracks are designated as appropriate for this task since there are only a limited number of cracks in the specimens. Crack growth in this specimen set proved more difficult than indicated in the initial trial cracking on softer material parts. A limited number, and size distribution, of defects made this specimen set less likely to provide a POD that would meet MIL HDBK 1823 guidelines. Since only one disk had grown cracks, and two others each had a single natural defect, there was little reason to inspect more than those three disks in a blind inspection. Ample nondefect sites were present to determine false call tendencies.

- Estimate the POD for cracks in blade slots of HW APU turbine disks. Even though the parts are not specifically from a propulsion turbine engine, they exhibit all the main features of larger turbine engines. Among the known defects presented, there are ample numbers of defects across the size distribution thought to extend below the detectable size for acoustic thermography. By selecting six disks with cracks characterized by FPI, the required number of nondefect sites is also achieved.

10. CONCLUSION.

During this program, the Siemens acoustic thermography system (SIEMAT) was evaluated for application to aircraft engine disks. Candidate parts were surveyed, acquired, and analyzed for inspection by acoustic thermography. Artificial discontinuities were investigated for use with the acoustic thermography method. The SIEMAT system was modified to inspect a variety of aircraft engine disks. A test procedure was developed for the inspection of disks and the test parameters determined for several disk styles. Disks were inspected at Siemens' Casselberry laboratories facility and the nondestructive inspection (NDI) testing and validation center where training on the system took place and the inspection process capability was evaluated. Finally, a commercialization plan was outlined for the introduction of the inspection method to industry.

A survey of aircraft engine disks conducted by Florida Turbine Technologies Inc. found that there is a wide range of aircraft engine disks. For the most part, this project used traditional flat

disks, but flexibility was a key attribute when evaluating fixtures for the inspection of the aircraft engine disks. It was also determined by this study that the Pratt & Whitney JT8D and General Electric CFM56 disks were most frequently used in the commercial aviation market, which resulted in a special effort to make the prototype system capable of handling these disks.

There was also an effort to develop artificial defects for the acoustic thermography. Current state-of-the-art technology uses power strips for the evaluation of acoustic thermography. Power strips do not reproduce the signal from in-service indications. During this project, several methods for the fabrication and application of artificial defects to parts were investigated. A process for the evaluation of artificial defects was presented for future evaluation of artificial defects.

To determine the best methods for the excitation and fixturing of parts for acoustic thermography evaluation, finite element modeling (FEM) analysis and experimental evaluations were carried out. The FEM methods for the determination of fixturing and excitation were observed not to agree, which could be because of the amount of generalization needed to get timely and cost-effective results from the FEM process or because better models were needed for the introduction of acoustic energy by acoustic thermography. It was finally determined that the experimental results would be carried out to determine which fixturing and excitation method would be used for aircraft engine disks. These results indicated that a radial excitation with three grip points 120 degrees apart on the inner diameter (ID) would result in the most efficient energy input to the disk.

The modification of the SIEMAT system was accomplished in three ways. First, new fixtures were developed to hold onto the disks. These were made in two ways. One fixture was made for axial excitation, which sandwiched the disk between two plates or bars, while the horn excited the disk in the axial direction from one side of the disk. A second fixture was made for the radial excitation of the disks. This fixture used a three-jaw lathe chuck to hold the ID of the disk while the ultrasonic horn excited the disk from the outer diameter (OD) in the radial direction. Both of these fixtures were used to inspect a variety of disk types. Also, The SIEMAT system was modified to better protect the parts being inspected. This was accomplished with the introduction of an interface material between the part and ultrasonic horn. An investigation was performed to determine which interface material would provide the best protection to the part while allowing the most acoustic energy to be transmitted to the part. In this investigation, 16 potential interface materials were evaluated. The 20-lb Wausau card stock was found to provide the most part protection and transmit the most energy into the part. Finally, the acoustic thermography software was modified to provide electronic documentation of indications. This documentation can be used to train automatic defect-detection algorithms in the future to reduce the variation in defect identification. These changes to the SIEMAT system equipped it for the inspection of aircraft engine disks.

This program resulted in the inspection of several disks acquired from industry partners. An inspection process was developed and documented, which included system setup, inspection, and shutdown procedures. Design of experiment evaluations were carried out to determine the relation of each independent inspection variable to the indication signal and optimum disk-inspection parameters. All inspections of disks were documented in *.sec files and a

representative set of inspections were documented in appendix C of this report.

The acoustic thermography system was demonstrated at the NDI Testing and Validation Center at Sandia National Laboratories. During this demonstration, industry partners were invited to attend one-day training on acoustic thermography covering basic principles and application of the technique. A double-blind evaluation using sonic infrared was conducted at the NDI Testing and Validation Center. The system was observed to be easy to set up and operate. It was also observed that the system required a design-of-experiments approach to determine the best excitation parameters for a particular part. These parameters may need to be adjusted during the testing to maintain consistent inspection. A preliminary inspection capability of the SIEMAT method on JT8D disks was determined to be probability of detection $(POD)_{90}$ = 0.114 inch. It should be noted that this value was determined without the full Military Handbook (MIL HDBK) 1823 guidelines in the specimen set. A POD_{90} = 0.038 inch was obtained for the inspection of auxiliary power unit disks. This can be considered a final detection reliability value on this particular part as the inspection set did meet the requirements of MIL HDBK 1823. High false-call rates were observed in both sets of data. These high false-call rates could be attributed to noncrack discontinuities in the part that may also generate heat when excited by ultrasonic energy. Further investigation is needed to determine what is generating heat in these regions and how to discriminate against it if necessary. One way to reduce false calls would be to increase the inspection threshold. This may also increase the POD_{90} value. It was also observed that care should be taken when applying the technique to parts. There is a danger of overenergization and the propagation of cracks if the technique is applied without the appropriate inspection design. It is recommended that the inspection design be created and certified for a specific technique and part by a knowledgeable level III inspector.

Several of the potential benefits of acoustic thermography were observed and realized during this program for aircraft engine disks. The acoustic thermography technique was observed to be useful for triage inspection of disks in their entirety. The inspection was fast and could be used to conduct either full field or local evaluation of the part under test. The resulting data was intuitive and simple to interpret. This program has successfully conducted a preliminary evaluation for acoustic thermography on engine disks, both qualitatively and quantitatively.

11. REFERENCES.

1. Henneke, E.G., Reifsnider, K.L., and Stinchcomb, W.W., "Thermography—an NDI Method for Damage Detection," *Journal of Metals*, Vol. 31, No. 9, 1979, pp. 11-15.

2. Rothenfusser, M. and Homma, C., "Acoustic Thermography: Vibrational Modes of Cracks and the Mechanisms of Heat Generation," *Review of Quantitative Nondestructive Evaluation*, Vol. 24, 2005, pp. 624-631.

3. Homma, C., Rothenfusser, M., Baumann, J., and Shannon, R.E., "Study of Heat Generation Mechanisms in Acoustic Thermography," *Review of Quantitative Nondestructive Evaluation*, Vol. 25, 2006, pp. 566-573.

4. Hassan, W., Homma, C., Wen, Z., Vensel, F., and Hogan, B., "Detection of Tight Fatigue Cracks at the Root of Dampers in Fan Blades Using Sonic IR Inspection: A Feasibility Demonstration," *Review of Quantitative Nondestructive Evaluation*, Vol. 26, 2007, pp. 455-462.

5. Homma, C., *Untersuchungen zu Mechanismus und technischer Umsetzung der akustischen Thermographie*, Ph.D. Thesis, Saarbrücken, Germany, 2007, http://scidok.sulb.uni-saarland.de/volltexte/2007/1257/

APPENDIX A—INSPECTION PROCEDURE FLOWCHARTS

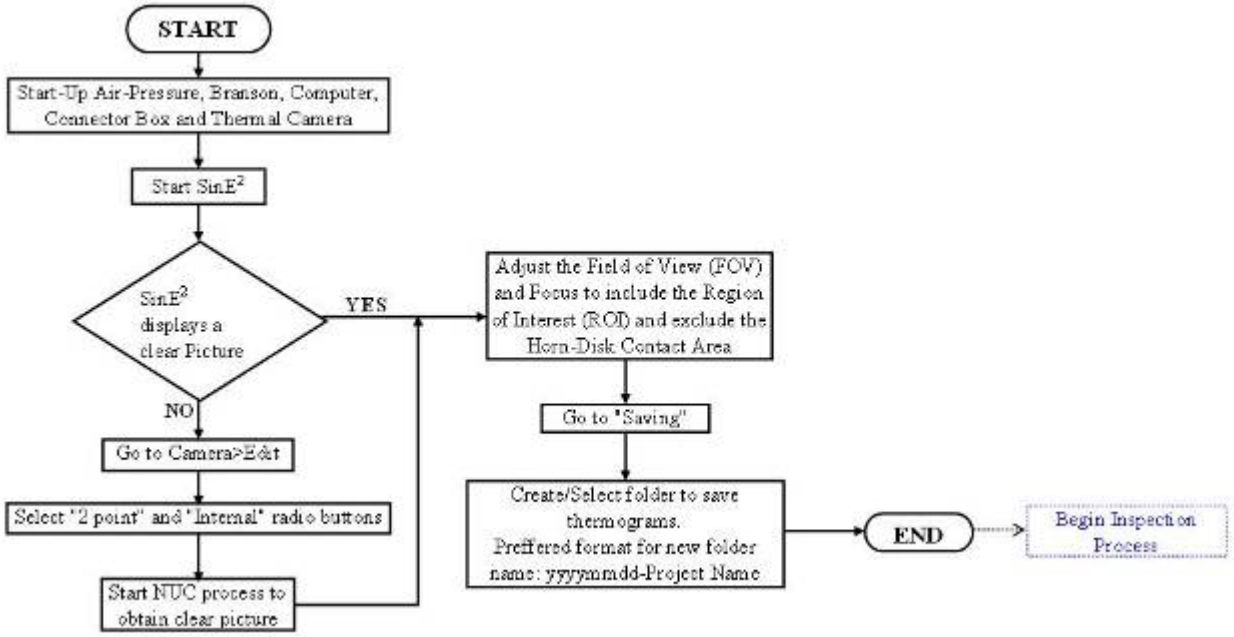

Figure A-1. The SIEMAT Start-Up Procedure Flowchart

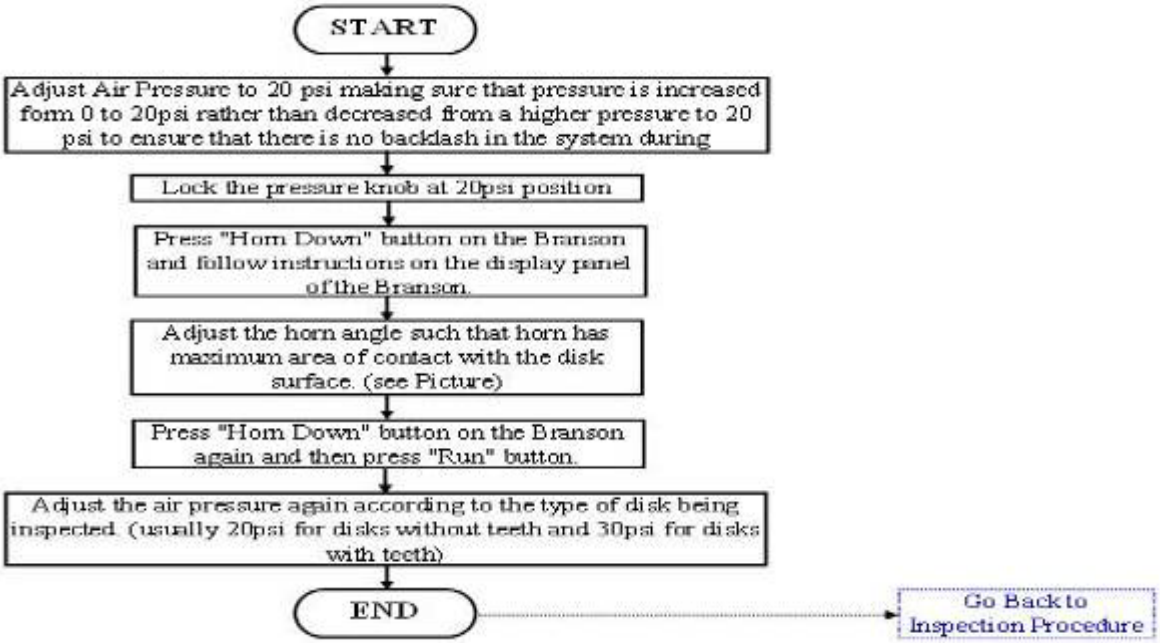

Figure A-2. The SIEMAT Horn-Down Procedure Flowchart

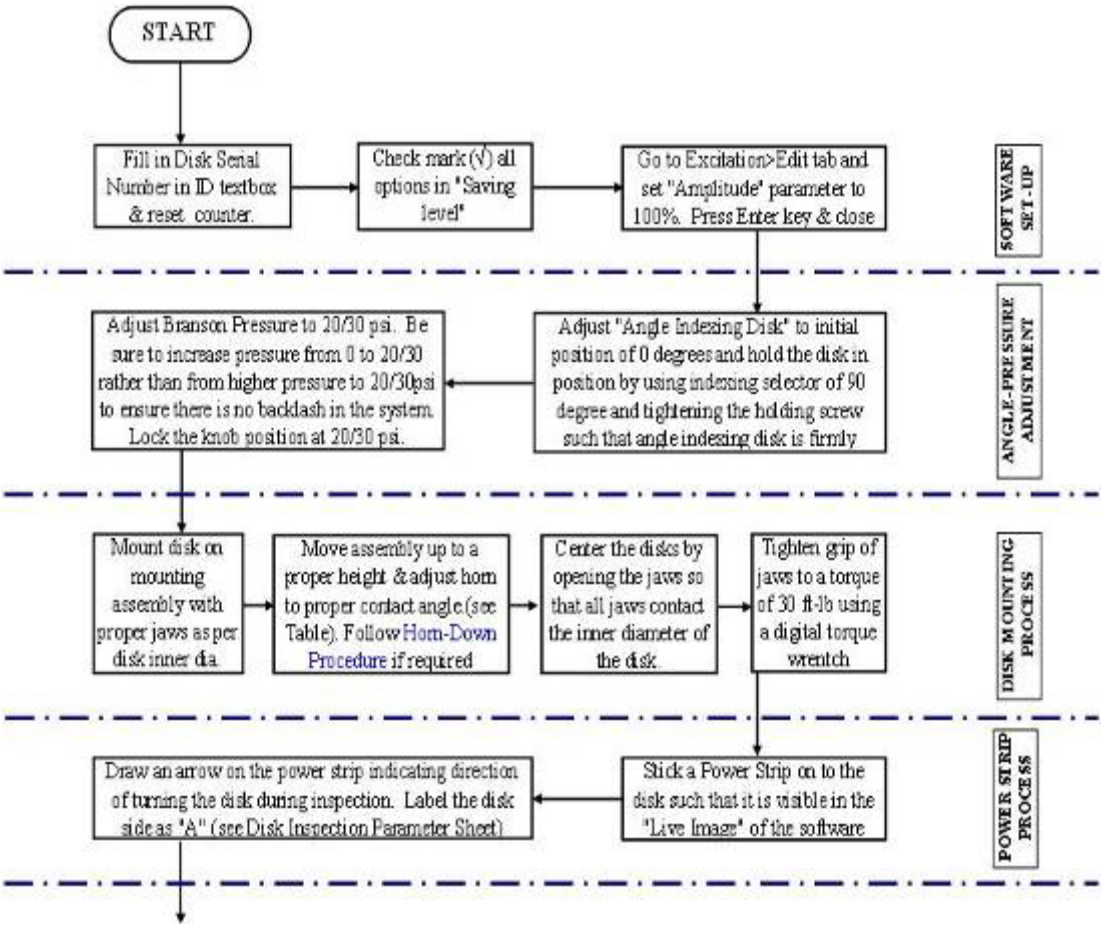

Figure A-3. The SIEMAT Inspection Procedure Flowchart

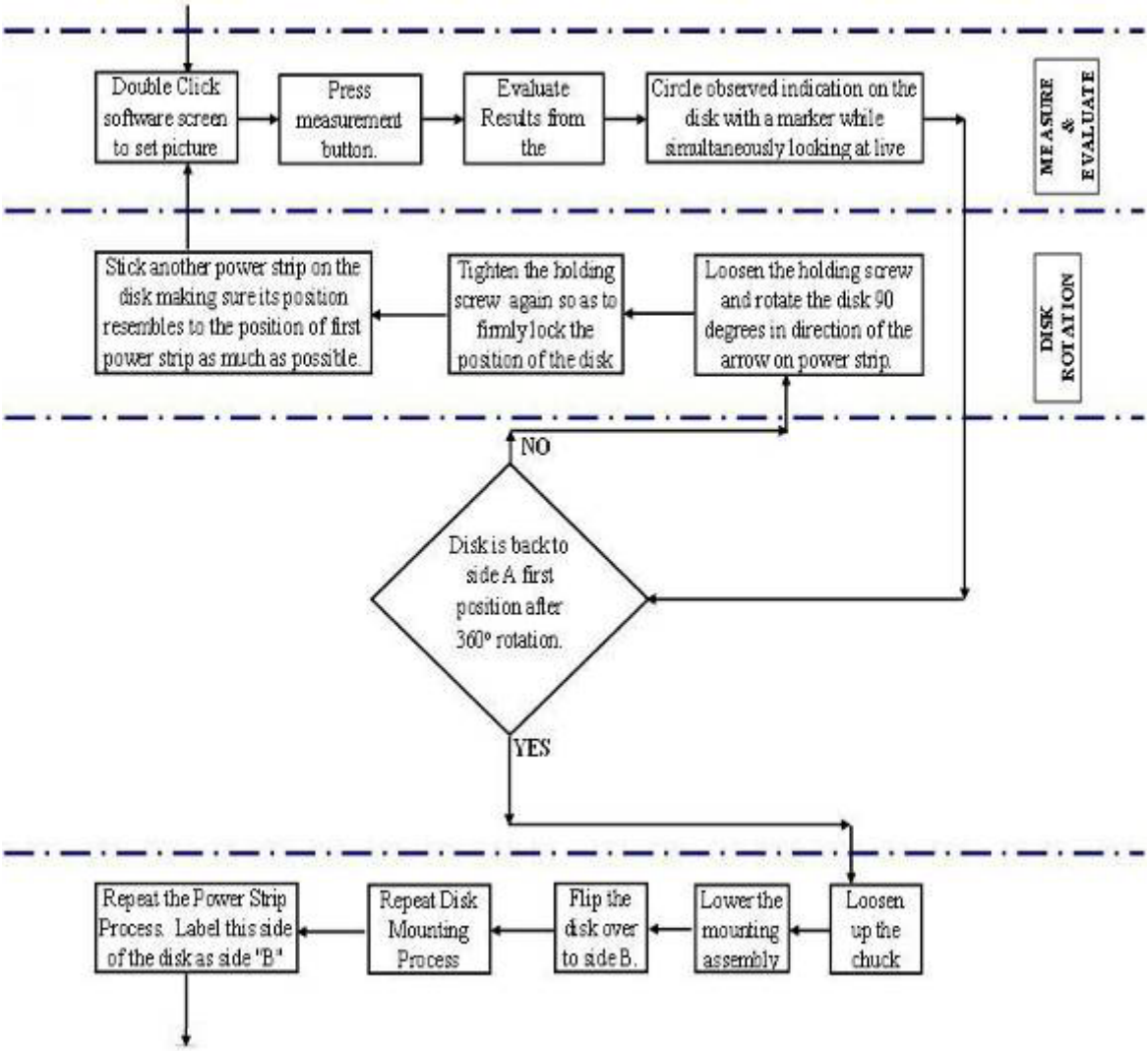

Figure A-3. The SIEMAT Inspection Procedure Flowchart (continued)

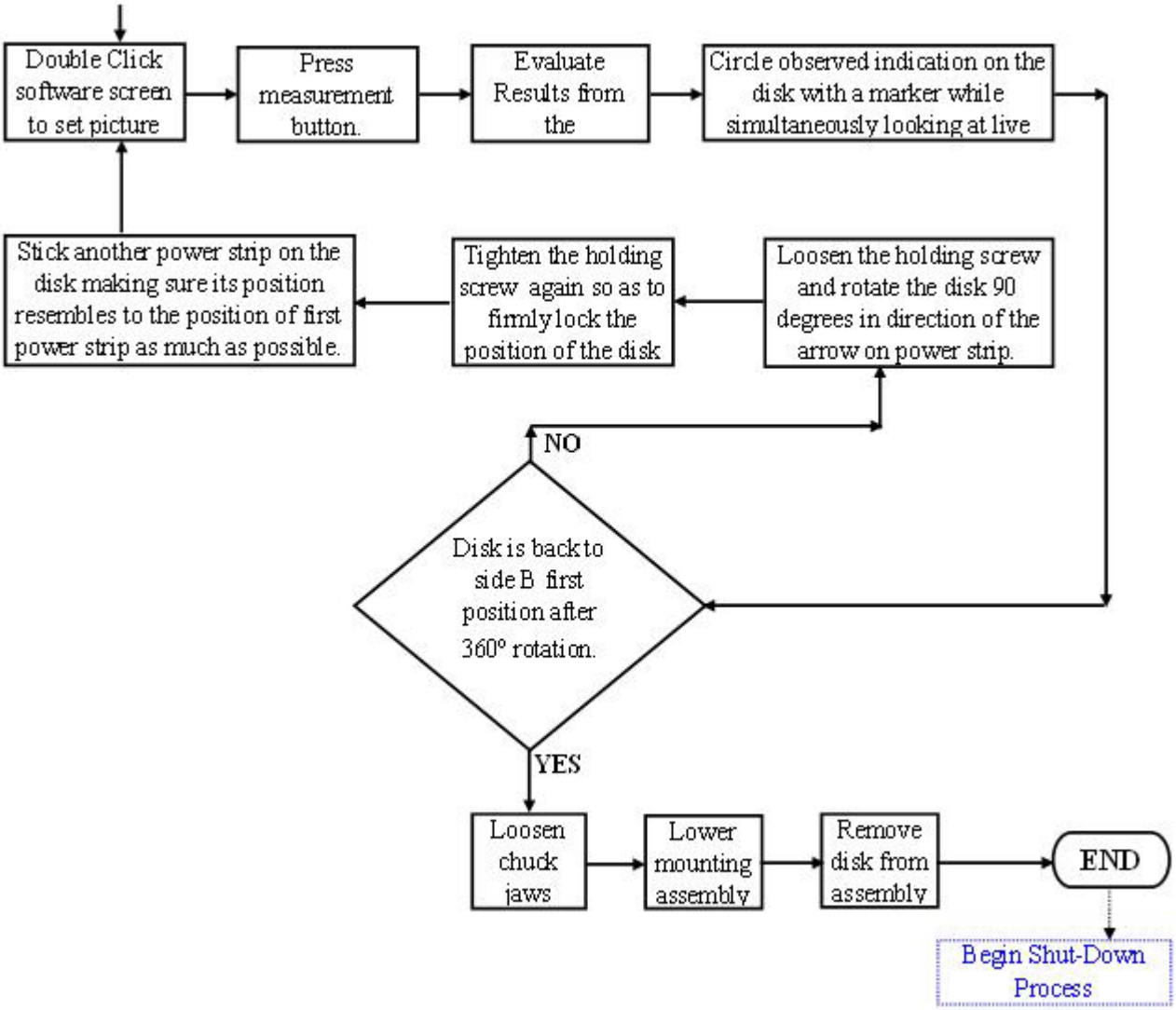

Figure A-3. The SIEMAT Inspection Procedure Flowchart (continued)

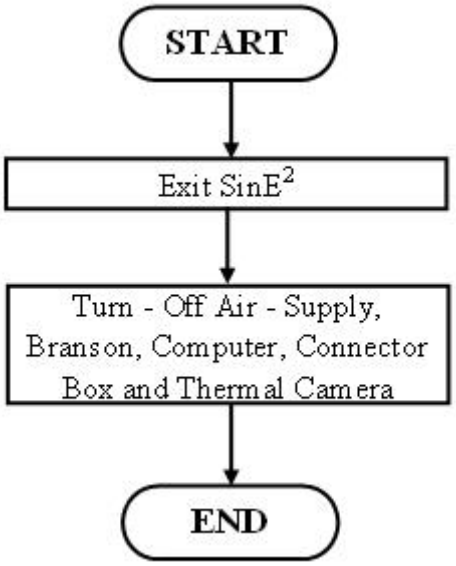

Figure A-4. The SIEMAT Shut-Down Procedure Flowchart

APPENDIX B—HORN CONTACT-ANGLE TEST RESULTS

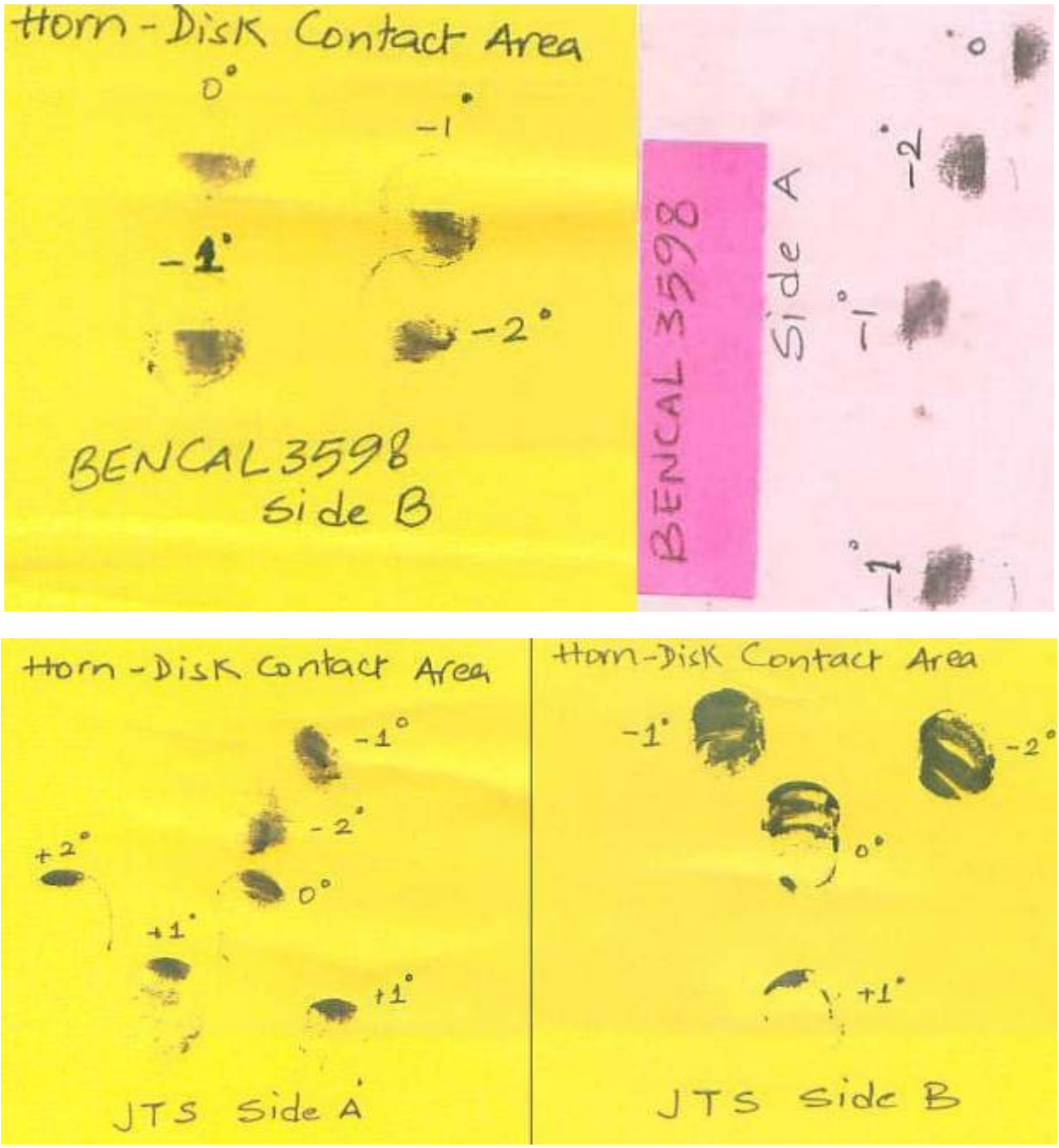

Figure B-1. Contact Area Between the Horn and the Disk at Different Contact Angles

APPENDIX C—AUXILIARY POWER UNIT DISK-INSPECTION RESULTS

Table C-1. Auxiliary Power Unit Disk Inspection Results

Disk Number	Disk Root No.	Sonic IR Hit/Miss	Crack Length (in.) Etch TOP 1	Crack Length (in.) Etch TOP 2	Crack Length (in.) Etch TOP 3	Crack Length (in.) Etch TOP 4	Crack Length (in.) Etch TOP 5	Crack Length (in.) FPI
592	6	1	0.202	0	0	0	0	0.113
2328	14	1	0.201	0.005	0	0	0	0.202
2328	34	1	0.194	0	0	0	0	0.207
2328	33	1	0.188	0	0	0	0	0.172
2328	36	1	0.186	0	0	0	0	0.196
592	5	1	0.186	0	0	0	0	
2328	15	1	0.182	0	0	0	0	0.173
2328	1	1	0.175	0	0	0	0	0.187
2328	18	1	0.156	0	0	0	0	0.161
2328	35	1	0.146	0.012	0	0	0	0.167
1435	2	1	0.142	0	0	0	0	0.137
2743	24	1	0.129	0	0	0	0	0.141
2328	19	1	0.126	0	0	0	0	0.137
2743	28	1	0.123	0	0	0	0	0.141
2743	27	1	0.120	0	0	0	0	0.139
1146	29	1	0.118	0	0	0	0	0.125
2743	23	1	0.117	0	0	0	0	0.09
2666	1	1	0.114	0	0	0	0	0.056
592	25	1	0.112	0	0	0	0	
1146	5	1	0.112	0	0	0	0	0.06
2743	32	1	0.112	0	0	0	0	0.132
1146	20	1	0.110	0	0	0	0	
2743	26	1	0.107	0	0	0	0	0.125
1146	1	1	0.105	0	0	0	0	0.077
2743	25	1	0.102	0	0	0	0	0.11
1146	23	1	0.100	0.012	0	0	0	
2743	29	1	0.099	0	0	0	0	0.087
2328	13	1	0.095	0	0	0	0	0.099
1146	14	1	0.095	0	0	0	0	

Table C-1. Auxiliary Power Unit Disk-Inspection Results (continued)

Disk Number	Disk Root No.	Sonic IR Hit/Miss	Crack Length (in.) Etch TOP 1	Crack Length (in.) Etch TOP 2	Crack Length (in.) Etch TOP 3	Crack Length (in.) Etch TOP 4	Crack Length (in.) Etch TOP 5	Crack Length (in.) FPI
1146	18	1	0.093	0	0	0	0	0.076
1146	3	1	0.093	0	0	0	0	
1146	32	1	0.092	0	0	0	0	0.095
1146	4	1	0.088	0	0	0	0	0.028
2743	21	1	0.087	0	0	0	0	0.096
1146	6	1	0.086	0	0	0	0	
1146	8	1	0.081	0	0	0	0	
2743	8	1	0.080	0	0	0	0	0.075
2328	28	1	0.079	0	0	0	0	0.067
1146	2	1	0.079	0	0	0	0	0.079
2328	27	1	0.078	0.008	0	0	0	0.088
2743	16	1	0.077	0	0	0	0	
1146	31	1	0.077	0	0	0	0	0.078
1146	11	1	0.076	0	0	0	0	0.094
1435	7	1	0.073	0	0	0	0	
1435	9	1	0.071	0	0	0	0	
2743	30	1	0.069	0	0	0	0	0.082
1146	34	1	0.069	0	0	0	0	0.072
1146	28	1	0.067	0.035	0.012	0.006	0	0.088
2328	2	1	0.066	0	0	0	0	0.069
1146	24	1	0.066	0.028	0	0	0	0.105
1435	14	1	0.063	0	0	0	0	
1146	26	1	0.060	0.030	0.008	0	0	0.072
1146	13	1	0.057	0.035	0	0	0	0.049
1146	9	1	0.057	0	0	0	0	0.062
1146	17	1	0.056	0	0	0	0	0.061
1146	12	1	0.054	0	0	0	0	0.081
2743	17	1	0.054	0.033	0	0	0	
2743	14	1	0.053	0.018	0	0	0	
1146	30	1	0.052	0.009	0	0	0	
1146	36	1	0.051	0.035	0	0	0	0.036

Table C-1. Auxiliary Power Unit Disk-Inspection Results (continued)

Disk Number	Disk Root No.	Sonic IR Hit/Miss	Crack Length (in.) Etch TOP 1	Crack Length (in.) Etch TOP 2	Crack Length (in.) Etch TOP 3	Crack Length (in.) Etch TOP 4	Crack Length (in.) Etch TOP 5	Crack Length (in.) FPI
1146	35	1	0.050	0	0	0	0	0.06
1146	33	1	0.050	0.033	0.004	0	0	0.024
1146	27	1	0.049	0.019	0.004	0.005	0.004	0.04
1146	22	1	0.048	0.007	0.008	0	0	
1146	7	1	0.047	0	0	0	0	
1146	16	1	0.046	0	0	0	0	0.05
2743	13	1	0.044	0	0	0	0	
1435	29	1	0.040	0	0	0	0	
2328	3	1	0.040	0.011	0	0	0	0.065
2328	20	0	0.037	0	0	0	0	0.043
1435	6	1	0.035	0	0	0	0	
2743	20	1	0.034	0.022	0	0	0	
1435	3	1	0.032	0	0	0	0	
1435	18	1	0.032	0	0	0	0	
2328	17	1	0.030	0.011	0	0	0	0.086
1435	21	1	0.029	0.018	0	0	0	
1146	15	1	0.028	0.028	0.017	0	0	0.095
1435	10	1	0.028	0.019	0	0	0	
1435	8	1	0.027	0	0	0	0	
1435	11	1	0.026	0.013	0	0	0	
1435	34	1	0.026	0	0	0	0	
2743	19	1	0.025	0.024	0.017	0	0	
1146	19	1	0.025	0.019	0.008	0.004	0.008	
2328	12	0	0.023	0	0	0	0	0.109
2743	15	1	0.023	0	0	0	0	
1435	36	0	0.022	0	0	0	0	
2666	36	0	0.021	0.013	0	0	0	
1435	24	0	0.021	0	0	0	0	
1435	30	1	0.020	0	0	0	0	
1146	25	1	0.020	0.017	0.012	0.009	0.008	
592	23	0	0.020	0	0	0	0	

Table C-1. Auxiliary Power Unit Disk-Inspection Results (continued)

Disk Number	Disk Root No.	Sonic IR Hit/Miss	Crack Length (in.) Etch TOP 1	Crack Length (in.) Etch TOP 2	Crack Length (in.) Etch TOP 3	Crack Length (in.) Etch TOP 4	Crack Length (in.) Etch TOP 5	Crack Length (in.) FPI
1146	21	0	0.020	0	0	0	0	
2743	11	1	0.020	0	0	0	0	
1146	10	1	0.019	0	0	0	0	0.025
2328	29	0	0.018	0.011	0	0	0	0.036
2743	12	1	0.016	0	0	0	0	
592	10	0	0.015	0	0	0	0	
1435	31	1	0.015	0	0	0	0	
592	24	0	0.014	0.011	0	0	0	
592	32	0	0.012	0	0	0	0	
2666	20	0	0.012	0	0	0	0	
1435	15	1	0.011	0	0	0	0	
2743	10	1	0.010	0	0	0	0	
2666	23	0	0.010	0	0	0	0	
2743	18	1	0.009	0.008	0	0	0	
1435	12	0	0.009	0	0	0	0	
2743	33	1	0.008	0	0	0	0	
2328	6	0	0.008	0	0	0	0	0.008
2743	36	1	0.008	0	0	0	0	
2666	27	0	0.008	0	0	0	0	
2328	4	0	0.007	0	0	0	0	
2328	8	0	0.006	0	0	0	0	
2743	35	1	0.006	0	0	0	0	
592	26	0	0.005	0	0	0	0	
2328	22	0	0.005	0	0	0	0	
2666	28	0	0.004	0.004	0	0	0	
2328	16	0	0.004	0.003	0.004	0	0	
592	27	0	0.004	0.004	0	0	0	
2666	16	0	0	0	0	0	0	